

**COMPUTATION OF PLANE POTENTIAL FLOW IN MULTIPLE
CONNECTED DOMAINS USING SERIES METHODS AND CONFORMAL
MAPPING**

A Dissertation by

Justin L. Mears

Master of Science, Wichita State University, Spring 2016

Bachelor of Business Administration, Wichita State University, 2009

Submitted to the Department of Mathematics, Statistics, and Physics
and the faculty of the Graduate School of
Wichita State University
in partial fulfillment of
the requirements for the degree of
Doctor of Philosophy

December 2023

© Copyright 2023 by Justin L. Mears
All Rights Reserved

COMPUTATION OF PLANE POTENTIAL FLOW IN MULTIPLE CONNECTED
DOMAINS USING SERIES METHODS AND CONFORMAL MAPPING

The following faculty members have examined the final copy of this dissertation for form and content, and recommend that it be accepted in partial fulfillment of the requirement for the degree of Doctor of Philosophy with a major in Applied Mathematics.

Thomas K. DeLillo, Committee Chair

Christopher C. Green, Committee Member

Mohamed Nasser, Committee Member

Yuan Liu, Committee Member

Ikram Ahmed, Committee Member

ABSTRACT

This paper presents a method for calculating potential flow in the exterior of multiply-connected circle domains in the complex plane. The method employs a Laurent series expansion of the potential function on the circular boundaries, which can be easily written into a linear system for finding the Laurent coefficients. This system exhibits the form of “identity plus a low-rank matrix”, enabling efficient utilization of conjugate-gradient-like methods.

Through the use of conformal mapping, the method is extended to calculate the potential flow in multiply-connected domains exterior to any closed curves. This is achieved by computing the potential flow over an appropriate circle domain and mapping this result to the desired physical domain using an approximation of the Laurent series for the conformal map. Circulations around each boundary can be specified or calculated, with a specific focus on multi-element airfoils where the circulations are determined to satisfy the Kutta condition at trailing edges.

Comparisons with alternative methods for computing flow in circle domains, namely reflection and least-squares methods, are included to demonstrate the accuracy and efficiency of the new method. Finally, there are many examples of flow calculations over multiply-connected regions with smooth boundaries and multi-element airfoils.

ACKNOWLEDGEMENTS

I would like to thank Lloyd Trefethen for the ideas presented in “Series solution of Laplace Problems” which led to the pursuit of our new method.

I would like to thank my adviser, Tom DeLillo, for his continued dedication to mathematics and the success of his graduate students. The patience and guidance he has afforded me over these many years has been pivotal to the completion of this work and my own personal success.

I would like to thank my wife, Arelis, who’s patience, encouragement, and mathematical expertise, have made this process a lot easier than it could have been.

Finally, I would like to thank the rest of my family, friends, professors, and colleagues both inside the Department of Mathematics, Statistics, and Physics, and outside, for their continued support and encouragement. I would not be the person I am today without the many influences you have made over the years, and I am truly grateful.

TABLE OF CONTENTS

Chapter	Page
1. INTRODUCTION	1
2. BACKGROUND	3
2.1. The Complex Velocity Potential	3
2.2. Two Alternative Methods for Computing Potential Flow.....	5
2.2.1. The Method of Images	6
2.2.1.1. Successive Reflections in m Circles	6
2.2.1.2. Method of Images for Potential Streaming Flow Over m Disks	7
2.2.1.3. Method of Images for Potential Vortex Flow Over m Disks.....	9
2.2.2. The Least Squares Solution.....	12
2.3. Conformal Mapping	15
2.3.1. Fornberg's Method for Mapping the Exterior of a Single Smooth Closed Curve.....	19
2.3.2. Extension of Fornberg's Method to the Exterior of Multiply Connected Domains	20
2.3.3. Parameterizing the Boundary.....	22
2.3.4. The Karman-Trefftz Transformations for Airfoils.....	23
3. NEW SERIES SOLUTION	25
3.1. Computing The Velocity Potential for a Single Disk	26
3.1.1. Streaming Flow for a Single Disk.....	26
3.1.2. Circulating Flow or Vortex Flow for a Single Disk.....	28
3.1.3. Total Flow for a Single Disk.....	30
3.2. Computing the Velocity Potential for Multiple Disks	31
3.2.1. Streaming Flow for Multiple Disks	32
3.2.2. Circulating or Vortex Flow for Multiple Disks.....	35
3.2.3. Total Flow for Multiple Disks	38
3.2.4. Applying the Kutta Condition to Solve for the Γ_k 's.....	41
3.3. Some Numerical Observations.....	44
3.4. Accuracy Estimates	46
3.5. Convergence.....	49
4. EXAMPLES OF FLOW CALCULATIONS	52
4.1. Potential Flow in the Circle Domain.....	52
4.1.1. Example 1: Single Circle Example from Acheson	52
4.1.2. Example 2: Flow Over a Set of Three Circles	53
4.1.3. Example 3: Flow Over a Set of Eight Circles.....	56

TABLE OF CONTENTS (continued)

Chapter	Page
4.1.4. Example 4: Efficiency for High Connectivity	59
4.2. Flow Over Multiply Connected Smooth Domains.....	61
4.2.1. Example 5: Flow Over Two Smooth Boundaries	61
4.2.2. Example 6: Flow Over Four Smooth Boundaries	62
4.2.3. Example 7: Flow Over Five Smooth Boundaries	63
4.2.4. Example 8: Flow Over Regions of Increasing Multiplicity with Smooth Boundaries	64
4.3. Flow Over Multi-Element Airfoils.....	66
4.3.1. Mapping from the Airfoil Domain to the Circle Domain	66
4.3.2. Calculating Pressures	68
4.3.3. Example 9: Three Cosine Airfoils.....	69
4.3.4. Example 10: Two-Airfoils from Williams.....	71
4.3.5. Example 11: Three-Airfoils from Suddhoo and Hall.....	73
4.3.6. Example 12: Four-Airfoils from Suddhoo and Hall	75
5. CONCLUSIONS AND FUTURE WORK.....	78
REFERENCES	79

LIST OF TABLES

Table	Page
2.1	Timings for connectivity m increase like $(m - 1)^{N_{refl}}$, as seen above for $m = 3$. The decrease in the errors follows the decrease in the sum of the radii at level N_{refl} , as shown in Figure 2.211
4.1	Comparison of typical timings in seconds on a laptop running MATLAB version R2012a, for $m = 3$ example, radius = [0.9, 0.35, 0.3], center = [0 1.4 + 0.6i, -1 + 1i], $U = 1$, $\Gamma_i = 0$. We stop the cgls iterations at k_ϵ , a few iterations after the error stops decreasing. The spectral accuracy with increasing N is clearly seen on each circle54
4.2	Comparison of typical timings in seconds on a laptop running MATLAB version R2012a, for $m = 16$ example, using least squares/backslash (left) and cgls (right). cgls is iterated iter. steps-slightly more than the number of steps needed to achieve the minimum error.60
4.3	Average values of $\text{Im}\{w(z)\}$, $z \in C_1, C_2$, for $m = 2$ smooth boundaries and overall accuracy of conformal map in Figure 4.12.62
4.4	Sample timing for domains in Figure 4.15.65
4.5	Accuracy of Γ_1 , $\text{Im}\{w(z)\}$, $z \in C_1$, and ϕ_1 for middle circle and overall accuracy ϵ In Figure 4.17, $m = 3$, $Ns = 8000$, $J = N/2 - 1$. The accuracies for C_2 and C_3 are similar. $\sigma_{min}(AS) \approx 10^{-2}$ for all N.70
4.6	Computed circulation comparisons from [Wil73] between the reflection method and our new method using $N = 128$ Fourier points on the boundary.71
4.7	Sample timings (sec), circulations, Γ_i , and accuracy of the MATLAB code on a laptop for a set of airfoils from [SH85] for $m = 3$ configuration B with angle of attack $\alpha = 20^\circ$73
4.8	Sample timings (sec), circulations, Γ_i , and accuracy of the MATLAB code on a laptop for a set of airfoils from [SH85] for $m = 4$ configuration A with angle of attack $\alpha = 0^\circ$76

LIST OF FIGURES

Figure	Page
2.1 Streaming flow around three cylinders by method of images with $U = 1$ and $N_{refl} = 10$ with reflections of circle centers plotted.	9
2.2 The error (o), given by ϵ , defined in Section 3.4, for streaming flow around three cylinders using the method of images with $U = 1$ and $N_{refl} = 10$, is well estimated by the rate of decrease of the sum of radii (\cdot) of the reflected circles at each level.	12
2.3 Flow over $m=3$ disks with centers $1, i, -1$, and radii $0.6, 0.6, 0.5$, using least squares approach with $N = 33, J = 16$	15
2.4 On the left we have the singular values which are not as well-grouped as our new method. On the right we have the decay of the Laurent coefficients on three circles indicates the accuracy achieved on the two larger circles is about 10^{-5}	16
3.1 Contour plot of the streaming flow past a single disk, computed using our new method, with $U = 1 + i$	27
3.2 Contour plot of the circulating flow around a single disk computed using our new method.	30
3.3 Contour plot of the combined flow past a single disk computed using our new method.	31
3.4 Counter plot of the streaming flow past $m = 20$ disks computed by our new method.	35
3.5 Singular values from a system computing the flow over $m=3$ disks using our new series method with $N = 128$ and $J = 63$	36
3.6 Contour plot of the circulating flow past $m = 10$ disks as computed using our new method.	38
3.7 Contour lines for the “total” potential flow for three disks with no circulation.	40
3.8 Singular values of A_s for the set of disks in Figure 3.7 from our new method.	40
3.9 Singular values for a system with discretization of $J = N/2$ chosen.	45
3.10 Singular values for a system with discretization of $J = N/2 - 1$ chosen.	46
4.1 Test of I_1 calculation using series method and new system for $m = 1$	53

LIST OF FIGURES (continued)

Figure	Page
4.2 Flow over $m = 3$ disks using the new combined method solving for the Kutta condition using MATLAB contour plot.	54
4.3 Singular values for system describing the flow shown in Figure 4.2.	55
4.4 Boundary value error for successive cgls iterates.	55
4.5 Log plot of the decay of the Laurent coefficients.	56
4.6 Contour plot of the flow over $m = 8$ disks using the new combined method solving for the Kutta condition using MATLAB contour plot.	57
4.7 Singular values of the system for $m = 8$ circles.	57
4.8 Boundary error ϵ of the system for $m = 8$ circles.	58
4.9 Log plot of the decay of the Laurent coefficients for each of the $m = 8$ circles.	58
4.10 Flow over $m = 16$ disks using the new method with $N = 64, J = 31$	59
4.11 Errors and residuals for 200 cgls iterations of flow in Figure 4.10.	60
4.12 Streamlines for flow exterior to $m = 2$ ellipses with $N = 6, \Gamma_1 = \Gamma_2 = 2, U = 1$	61
4.13 Potential flow over $m = 4$ smooth boundaries with $N = 256$	63
4.14 Potential flow over $m = 5$ smooth boundaries with $N = 128$	64
4.15 Potential flow over $m = 2, 4, 8$ smooth boundaries with $N = 64$ for timings in Table 4.4. The circulations are given.	65
4.16 Conformal map $f = k^{-1} \circ h$, where composition of Karman-Trefftz maps $k = k_1 \circ k_2 \circ k_3 \circ k_4$ successively, smoothing corners (left), Laurent series map h maps from circle (right) to the smooth domain (center), and potential flow with Kutta condition at the trailing edges (X) is computed in circle domain by Laurent series and $N = 128$ Fourier points on each circle.	67
4.17 Conformal map between airfoil domain and circle domain along with potential flow. Pressures on the upper and lower portion of each airfoil are plotted in the lower figure. The horizontal axis is the real part of the points on the airfoil.	69

LIST OF FIGURES (continued)

Figure	Page
4.18 Flow for configuration A from [Wil73] using the full series with $N = 129$	71
4.19 Pressure curves for configuration A from [Wil73] using the full series with $N = 128$	72
4.20 Flow for configuration B from [SH85] using the full series method with $N = 128$ and angle of attack $\alpha = 20^\circ$ using $k_{steps} = 35$ cg iterations. Opration counts for the flow and the map are $O((mN)^2 \times k_{steps})$	73
4.21 Pressure curves for the airfoils in configuration B from [SH85] computed using our methods demonstrated in Figure 4.20	74
4.22 Exact map given by successive Karman-Trefftz transformations applied to four circles to produce the four-airfoil setup.	75
4.23 Flow for configuration A from [SH85] using the full series with $N = 128$ and angle of attack $\alpha = 0$ and $k_{steps} = 40$ cg iterations. Operation counts for the flow and the map are $O((mN)^2 \times k_{steps})$	76
4.24 Pressure curves for the airfoils in configuration A from [SH85] computed using our methods demonstrated in Figure 4.23.	77

CHAPTER 1

INTRODUCTION

Potential flow problems are an essential and historical part of fluid dynamics research. As S. Childress stated in [Child09], potential flow theory is a “fundamental concept” in this field. He gave two reasons for this claim. First, he said that the development of mathematical tools for this kind of fluid flows was closely related to the historical evolution of this theory. Second, he said that many practical situations in nature are either exactly or approximately described by potential flow. They offer a fundamental mathematical framework for solving many types of fluid problems that involve irrotational flows such as flows around solid bodies, which we will discuss in this dissertation. In fact, there has been an increase in recent years of interest towards solving potential flow problems in finitely connected circle domains. In 2018, D. Crowdy addressed solving such problems in [Crow18] using methods associated with the Schottky-Klein Prime function. In 2018, L. Trefethen discussed the effectiveness of using series solutions for solving potential theory problems in [Tref18]. We will continue these investigations with a topic that lies within a specific subset of these previous works, namely, we will describe a novel way for computing solutions to potential flow problems in multiply connected circle domains using Laurent-series based methods. The linear systems resulting from our construction have a special “identity plus low rank matrix” form which can be exploited through the use of conjugate-gradient like methods for solving the systems similar to work done by DeLillo and Balu in [BD16]. Once our method is developed, we can apply it toward solving potential flow problems over several forms of multiply connected domains. That is, we will explore some examples that link both of Childress’ reasons, namely, a novel method for calculating potential flow and some “real-world” applications of that technique.

Rather than use conformal mapping to solve the potential flow problem directly, we will leverage the power of conformal mapping in a different way. Since some of the “real-world” problems we will consider involve domains containing multiple airfoils, a conventional

way for computing potential flow over multi-element airfoils is to conformally map a problem in the physical domain onto a domain with circular boundaries where the potential flow problem can be solved efficiently, such as in [DS18] by DeLillo and Sahraei or [Pros87] where Prosnak treats several problems using Laurent Series formulations similar to ours. Also, because the velocity potential is harmonic, it transplants under conformal mapping. This approach will work for our purposes as we will rely on a composition of Karman-Trefftz and Fornberg-like methods to map the potential flow, which we will compute in the circle domain, to the physical domain containing the airfoils.

We conclude by giving a brief overview of this dissertation. In Chapter 2 we will cover the necessary background information from complex potential theory, one classic and one modern method for computing the velocity potential, and provide an overview of the conformal mapping techniques we used to compute some of our examples. Chapter 3 contains the construction for our new Laurent-series based method along with addressing how we measured accuracy and proved convergence. In Chapter 4 we address examples of solving the potential flow using our new method in various types of domains. Finally, in Chapter 5 we conclude our paper and offer potential avenues for future work.

CHAPTER 2

BACKGROUND

We begin by covering some necessary background information related to our method. This includes a review of the basic concepts from two-dimensional potential flow theory, two alternative methods for computing the potential flow over circular domains, and a review of the conformal mapping techniques that we will use in later examples.

2.1 The Complex Velocity Potential

As we mentioned in the previous chapter, potential flow is an important concept in many fields including aerodynamics and hydrodynamics. In fluid dynamics it helps to describe the flow of an ideal, inviscid, and incompressible fluid. One of the most useful properties, which we will exploit later, is that one can construct complicated flows by adding simple flows together, a property known as superposition. Another property that is relevant for our purposes is that it enables the application of complex analysis for finding solutions of the Laplace equation, $\nabla^2 f(x) = 0$, the governing equation of the potential function. For our formulation of the complex velocity potential, we follow the well known texts of Childress [Child09] and Acheson [Ach05].

Let us assume that we have an ideal, incompressible, and irrotational fluid flow exterior to m disks. We can then represent the complex velocity potential of that flow as

$$w(z) = \phi(x, y) + i\psi(x, y) \tag{2.1}$$

for a complex-valued $z = x + iy$. Our goal is to find the analytic function $w(z)$ such that the velocity, $\nu(z)$, is given by

$$\nu(z) = w'(z) = u - iv \tag{2.2}$$

where

$$u = \phi_x = \psi_y \quad \text{and} \quad v = \phi_y = -\psi_x$$

by the Cauchy-Riemann equations. Additionally, our flow must satisfy the physical condition that the circular boundaries, given by $C_k : z = c_k + r_k e^{i\theta}$, are streamlines, that is $\psi = \text{constant}$ on the C_k 's. Once computed, we can use the velocity potential to calculate some fundamental quantities for flow around a body with boundary given by a closed curve, C , such as lift in the case of the solid body being an airfoil.

Next we consider some important results from potential theory.

Theorem 1. *The circulation Γ of flow around C and the flux, F , of the flow through C are given by*

$$\Gamma + iF = \int_C w'(z) dz. \quad (2.3)$$

Proof. Following Ablowitz and Fokas in [AF97, p. 77], consider the circulation of the flow around C ,

$$\Gamma = \int_C (\phi_x dx + \phi_y dy) = \int_C \vec{v} \cdot \hat{t} ds \quad (2.4)$$

and the flux of the flow through C ,

$$F = \int_C (\phi_x dy - \phi_y dx) = \int_C \vec{v} \cdot \hat{n} ds \quad (2.5)$$

where $\nu = (\phi_x, \phi_y)$, $\hat{t} = (\frac{dx}{ds}, \frac{dy}{ds})$, and $\hat{n} = (\frac{dy}{ds}, -\frac{dx}{ds})$. Then

$$\begin{aligned} \Gamma + iF &= \int_C (\phi_x dx + \phi_y dy) + i \int_C (\phi_x dy - \phi_y dx) \\ &= \int_C \phi_x(dx + idy) + \phi_y(dy - idx) \\ &= \int_C \phi_x(dx + idy) - i\phi_y(dx + idy) \\ &= \int_C (\phi_x - i\phi_y)(dx + idy) \\ &= \int_C (\phi_x + i\phi_y)dz \\ &= \int_C w'(z)dz \end{aligned}$$

□

Next, we recall that the *reflection* of a point z through a circle C with center c and radius r is given by

$$z^* = \rho_C(z) := c + \frac{r^2}{\bar{z} - \bar{c}}, \quad (2.6)$$

where z and z^* are symmetric points with respect to the circle C .

Finally, we include the Milne-Thomson Circle Theorem, as stated by Childress in [Child09, Theorem 4.1], as it is an essential theorem for the reflection method, which we will discuss in the next section.

Theorem 2 (Milne-Thomson Circle Theorem). *Let a harmonic flow have complex potential $f(z)$, analytic in the disk $D : |z - c| \leq r$ with boundary C . If a circular cylinder of radius r is placed at center c , then the new complex potential is*

$$w(z) = f(z) + \overline{f(\rho_C(z))} \quad (2.7)$$

Proof. By Schwarz reflection, $w(z)$ is clearly analytic at z , if $f(z)$ is analytic at z . We note that on the circle $C : z = c + re^{i\theta}$

$$\rho_C(z) = c + \frac{r^2}{\bar{c} + re^{-i\theta} - \bar{c}} = c + \frac{r^2}{re^{-i\theta}} = c = re^{i\theta} = z. \quad (2.8)$$

Therefore, $w(z) = f(z) + \overline{f(z)} = 2\text{Re}f(z)$, so the stream function $\text{Im}f(z)$ is constant on C and therefore C is a streamline. \square

Now that we have addressed the relevant concepts and theorems in the study of complex velocity potentials, we will next provide an overview of the method of reflections, a traditional approach for solving the potential flow problem in a multiply connected circle domain.

2.2 Two Alternative Methods for Computing Potential Flow

In this section we will cover two possible methods for computing potential flow alternative to our new series solution so that we may make comparisons later.

2.2.1 The Method of Images

One of the historical approaches to solving potential flow problems in the exterior of multiply connected circle domains involves a process of reflecting singularities repeatedly across the circular boundaries. This process is equivalent to the idea of introducing disks into an existing uniform flow by means of the Milne-Thomson Circle Theorem. A basic application of the reflection method was used to compute the streaming flow by Acheson in [Ach05]. DeLillo and Sahraei implemented the methods in [DS18], and extend the approach for calculating the circulating flow. Using reflections, in [Wil73], Williams constructs series expressions for the velocity potentials of both the streaming and circulating flows for the doubly-connected case and proves convergence with no restrictions on the separation of the circles. Velocity potentials for vortex flows are derived using reflections for flows over a finite assembly of disks by Zemlyanova, Manly, and Handley in [ZMH18]. In [AS07], Antipov and Silvestrov solve the flows Riemann-Hilbert problems for automorphic functions.

We will provide an overview for the method of images in order to later make meaningful comparisons between our new method and previously utilized processes for computing the streaming and circulating flows in circle domains. Our discussion here follows that which was detailed and implemented by DeLillo and Sahraei in [DS18] and again covered by DeLillo, Mears, and Silva-Trujillo in [DMS21].

2.2.1.1 Successive Reflections in m Circles

Consider a finitely connected domain in the plane exterior to m non-overlapping disks. Since our space contains m circles, we will use τ to denote the index of the circle we are considering, that is, we will use notation such as C_τ and denote ρ_{C_τ} by ρ_τ .

Now, let this general m -connected unbounded circular domain be D with boundary components C_1, C_2, \dots, C_m . We fix an index $\nu_i \in \{1, 2, \dots, m\}$, and reflect the center of the circle, $s_i = c_i$, through the circle C_j to form

$$s_{ji} = \rho_j(s_i), \quad i \neq j.$$

In general, the reflections of the centers are labeled with multi-indices of the form,

$$\nu = \nu_1\nu_2 \cdots \nu_n$$

where $\nu_j \in \{1, 2, \dots, m\}$ and $\nu_k \neq \nu_{k+1}$ for $k = 1, 2, \dots, n - 1$.

Next, we will discuss a few important concepts to this procedure. Firstly, we will denote the *length of ν* by $|\nu|$, giving us $|\nu| = n$. Second, it is also important to acknowledge that reflecting through the same circular boundary twice in succession maps the space back to how it was before the first reflection, that is, ρ_j^2 is an identity operation, and therefore repeated indices will never be used. Then, it is important for one to keep in mind that the reflections of the centers of the circles and the centers of the reflected circles are not the same, that is, $s_\nu \neq c_\nu$. Lastly, the radii of the reflected circles are denoted by r_ν and the ultimate convergence of the series depends on the rate of decrease of the r_ν 's.

Finally, when stating the convergence results and error estimates for this method, it is essential to have the separation of the m boundary circles C_j 's expressed analytically. For this purpose we have the *non-overlap inequalities* defined by

$$\mu_{jk}^{sep} := \frac{r_j + r_k}{|c_j - c_k|} < 1, \quad j \neq k, \quad 1 \leq j, k \leq m. \quad (2.9)$$

Finally, the *separation modulus* for the region is defined by

$$\Delta := \max_{i,j;i \neq j} \mu_{ij}^{sep} \quad (2.10)$$

for the m boundary circles.

2.2.1.2 Method of Images for Potential Streaming Flow Over m Disks

Given m non-overlapping disks, we want to find the streaming flow over the assemblage. Theorem 2.1 can be used to solve for the flow as was done by Halsey in [Hal79], Suddhoo and Hall in [SH85], and Williams in [Wil73]. In fact, this case was even treated by Burnside in 1891 in [Burn91]. In our discussion, we will begin with the streaming flow, then work with the complex velocity potential, and then finish by giving some convergence results.

Suppose again that we have m - non-overlapping disks in the complex plane. The velocity potential $w(z)$ for streaming flow around an assembly of disks D_j must satisfy three conditions: (1) The flow must be uniform at infinity, (2) the boundary circles must be streamlines, and (3) the circulation around each disk is zero. We write these conditions explicitly as follows,

Conditions on $w(z)$ for streaming flow:

- (1) $w(z) \approx Uz$ as $z \rightarrow \infty$,
- (2) $\text{Im } w(z) = \text{constant}$ for $z \in C_i$, with $i = 1, 2, \dots, m$ (2.11)
- (3) $\Gamma_i = 0$, for all $i = 1, 2, \dots, m$.

Applying these conditions, and noting in this case we have $\text{Im } w_{N_{\text{refl}}}(z) \approx \text{constant}$ for $z \in C_j$, the velocity potential for streaming flow, $w_{\text{stream}}(z)$, is approximated by

$$w_{\text{stream}}(z) \approx w_{N_{\text{refl}}}(z) := Uz + \sum_{|v|=1}^{N_{\text{refl}}+1} \frac{U_\nu}{z - s_\nu} \quad (2.12)$$

using $N_{\text{refl}}+1$ levels of reflection, where the indices ν are as given as in the previous chapter. The coefficients for the series, that is the U_ν 's, are generated recursively from $U_j = r_j^2 \bar{U}$ with $j = 1, 2, \dots, m$ by

$$U_{j\nu} = - \left(\frac{r_j}{\bar{s}_\nu - \bar{c}_j} \right)^2 \bar{U}_\nu \quad (2.13)$$

This can be seen from the fact that for $z \in C_j$, the terms

$$\frac{U_\nu}{z - s_\nu} + \frac{U_{j\nu}}{z - s_{j\nu}} = \frac{U_\nu}{z - s_\nu} - \left(\frac{r_j}{\bar{s}_\nu - \bar{c}_j} \right)^2 \frac{\bar{U}_\nu}{z - s_{j\nu}} \quad (2.14)$$

in 2.12 are the sum of two complex conjugates and are therefore real. One important thing to note is that whenever an index is written like $j\nu$, it is implicitly assumed that the indices do not repeat, that is, for something like $j\nu = j\nu_1\nu_2 \dots$, j cannot be ν_1 . The s_ν are computed in a similar way for $w(z)$. Finally, the convergence of the series in 2.12 is proven in [DS18] as long as the circles are sufficiently separated. Figure 2.1 shows the contour lines for $\text{Re}(w(z))$ and $\text{Im}(w(z))$ for flow over three circles using the MATLAB `contour` function.

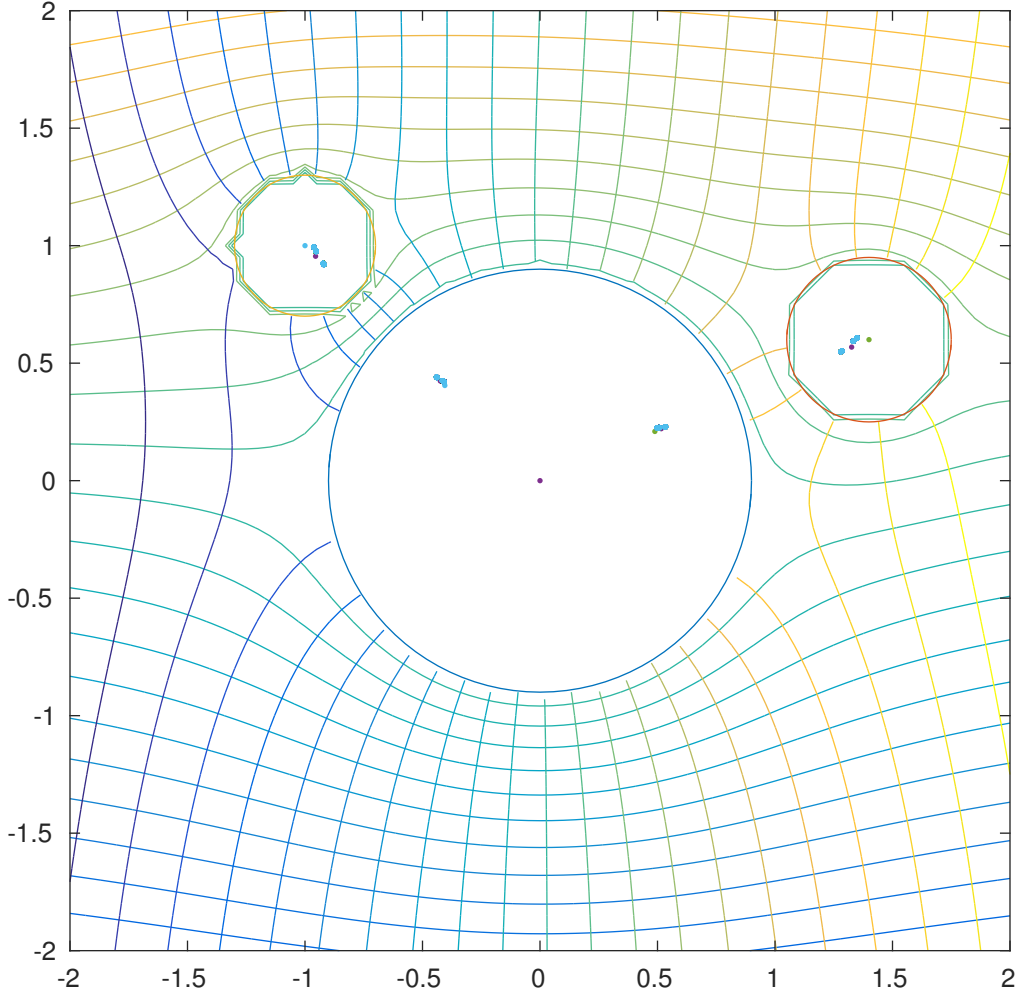


Figure 2.1: Streaming flow around three cylinders by method of images with $U = 1$ and $N_{refl} = 10$ with reflections of circle centers plotted.

2.2.1.3 Method of Images for Potential Vortex Flow Over m Disks

In order to construct what we will later call the *total flow*, we must now consider the vortex, or circulating velocity potential, $w_{\Gamma_i}(z)$, around the m disks, where Γ_i is used to denote the circulation around the i -th disk. This vortex flow must satisfy three conditions: (1) The circulation is zero around all disks except D_i and $\Gamma_i \neq 0$ is given, (2) the circular boundaries are streamlines, and (3) the velocity is zero at infinity. We write these conditions explicitly as follows:

Conditions on $w(z)$ for vortex flow:

- (1) $\Gamma_i =$ a given constant $\neq 0$ and $\Gamma_j = 0$ for $j = 1, 2, \dots, m$ when $j \neq i$,
- (2) $\text{Im } w(z) = \text{constant}$ for $z \in C_i$, with $i = 1, 2, \dots, m$ (2.15)
- (3) $\lim_{z \rightarrow \infty} w'_{\Gamma_j}(z) \rightarrow 0$.

Satisfying these conditions, it is shown in [DS18] that w_{Γ_i} has the form

$$-\frac{2\pi}{i\Gamma_i} w_{\Gamma_i}(z) = \ln(z - s_i) + \sum_{\nu \in \sigma_n(i), n=1}^{n=\infty} (-1)^{n+1} (\ln(z - s_\nu) - \ln(z - s_{\nu i})). \quad (2.16)$$

Solving for these circulations, we ultimately have that flows with given constant velocity at infinity and specified vorticity around each disk can be given as the linear combination of the velocity potentials,

$$w(z) = w_{\text{stream}}(z) + \sum_{i=1}^m w_{\Gamma_i}(z). \quad (2.17)$$

Now, before we move on we are going to investigate the convergence of the series for the circulating velocity, truncated at the N_{refl} levels of reflection, given by

$$i \frac{2\pi}{\Gamma_i} w'_{\Gamma_i, N_{\text{refl}}}(z) = \frac{1}{z - s_i} + \sum_{\nu \in \sigma_n(i), n=1}^{n=N_{\text{refl}}} (-1)^{n+1} \left(\frac{1}{z - s_\nu} - \frac{1}{z - s_{\nu i}} \right).$$

We include the next theorem and proof from [DS18] to illustrate a useful error estimate for the reflection method.

Theorem 3. *If $\Delta < (m - 1)^{1/4}$, then $w'_{\Gamma_i, N_{\text{refl}}}(z)$ converges absolutely as $N \rightarrow \infty$ for $z \in \Omega$, exterior to the D_j 's.*

Proof. We begin by observing that

$$\begin{aligned} \left| \frac{2\pi}{\Gamma_i} w'_{\Gamma_i, N_{\text{refl}}}(z) \right| &\leq \left| \frac{1}{z - s_i} \right| + \left| \sum_{\nu \in \sigma_n(i), n=1}^{n=N_{\text{refl}}} (-1)^{n+1} \left(\frac{1}{z - s_\nu} - \frac{1}{z - s_{\nu i}} \right) \right| \\ &\leq \left| \frac{1}{z - s_i} \right| + \sum_{\nu \in \sigma_n(i), n=1}^{n=N_{\text{refl}}} \left| \left(\frac{1}{z - s_\nu} - \frac{1}{z - s_{\nu i}} \right) \right| \\ &\leq \left| \frac{1}{z - s_i} \right| + \sum_{\nu \in \sigma_n(i), n=1}^{n=N_{\text{refl}}} \left| \frac{s_\nu - s_{\nu i}}{(z - s_\nu)(z - s_{\nu i})} \right| \end{aligned}$$

Since $s_\nu, s_{\nu i} \in C_\nu$, where $C_\nu = \rho_{\nu_1}, \rho_{\nu_2}, \dots, \rho_{\nu_{n-1}}(C_{\nu_n})$, the repeated reflection of the circle C_{ν_n} , and for $z \in \Omega$ there exists a $\delta > 0$ such that $|z - s_\nu|, |z - s_{\nu i}| > \delta$, using $|s_\nu - s_{\nu i}| \leq 2r_\nu$, the radius of C_ν , we have

$$\begin{aligned}
\sum_{\nu \in \sigma_n(i)} \frac{|s_{\nu n} - s_{\nu i}|}{|z - s_\nu| |z - s_{\nu i}|} &\leq \frac{2}{\delta^2} \sum_{\nu \in \sigma_n(i)} r_\nu \\
&\leq \frac{2}{\delta^2} \left(\sum_{\nu \in \sigma_n(i)} r_\nu \right)^{1/2} \left(\sum_{\nu \in \sigma_n(i)} 1 \right)^{1/2} \\
&\leq \frac{2}{\delta^2} \left(\sum_{\nu \in \sigma_n(i)} r_\nu \right)^{1/2} (m-1)^{n/2} \\
&\leq \frac{2}{\delta^2} \Delta^{2n} \left(\sum_{i=1}^m r_i^2 \right)^{1/2} (m-1)^{n/2} \\
&\leq C \Delta^{2n} (m-1)^{n/2}
\end{aligned}$$

by Lemma 2 from [DS18] where $\delta = \delta_\Omega$. Therefore the series converges if $\Delta^2 \sqrt{m-1} < 1$. \square

Table 2.1, given below, shows some timings and levels of error in the boundary conditions on each circle for $m = 3$ at various levels of reflection. Comparison with error levels and timings for the series method in Chapter 4 show that the reflection method is considerably slower and less accurate. Additionally, the timings would be much worse for higher connectivity m . Having briefly discussed the method of images, we will now consider a more

Table 2.1: Timings for connectivity m increase like $(m-1)^{N_{refl}}$, as seen above for $m = 3$. The decrease in the errors follows the decrease in the sum of the radii at level N_{refl} , as shown in Figure 2.2.

N_{refl}	sec	C_1 error	C_2 error	C_3 error
7	1.85	$.28 \cdot 10^{-4}$	$.10 \cdot 10^{-4}$	$.11 \cdot 10^{-4}$
8	3.50	$.38 \cdot 10^{-5}$	$.41 \cdot 10^{-5}$	$.64 \cdot 10^{-5}$
9	7.43	$.22 \cdot 10^{-5}$	$.87 \cdot 10^{-6}$	$.96 \cdot 10^{-6}$
10	13.71	$.32 \cdot 10^{-6}$	$.32 \cdot 10^{-6}$	$.51 \cdot 10^{-6}$

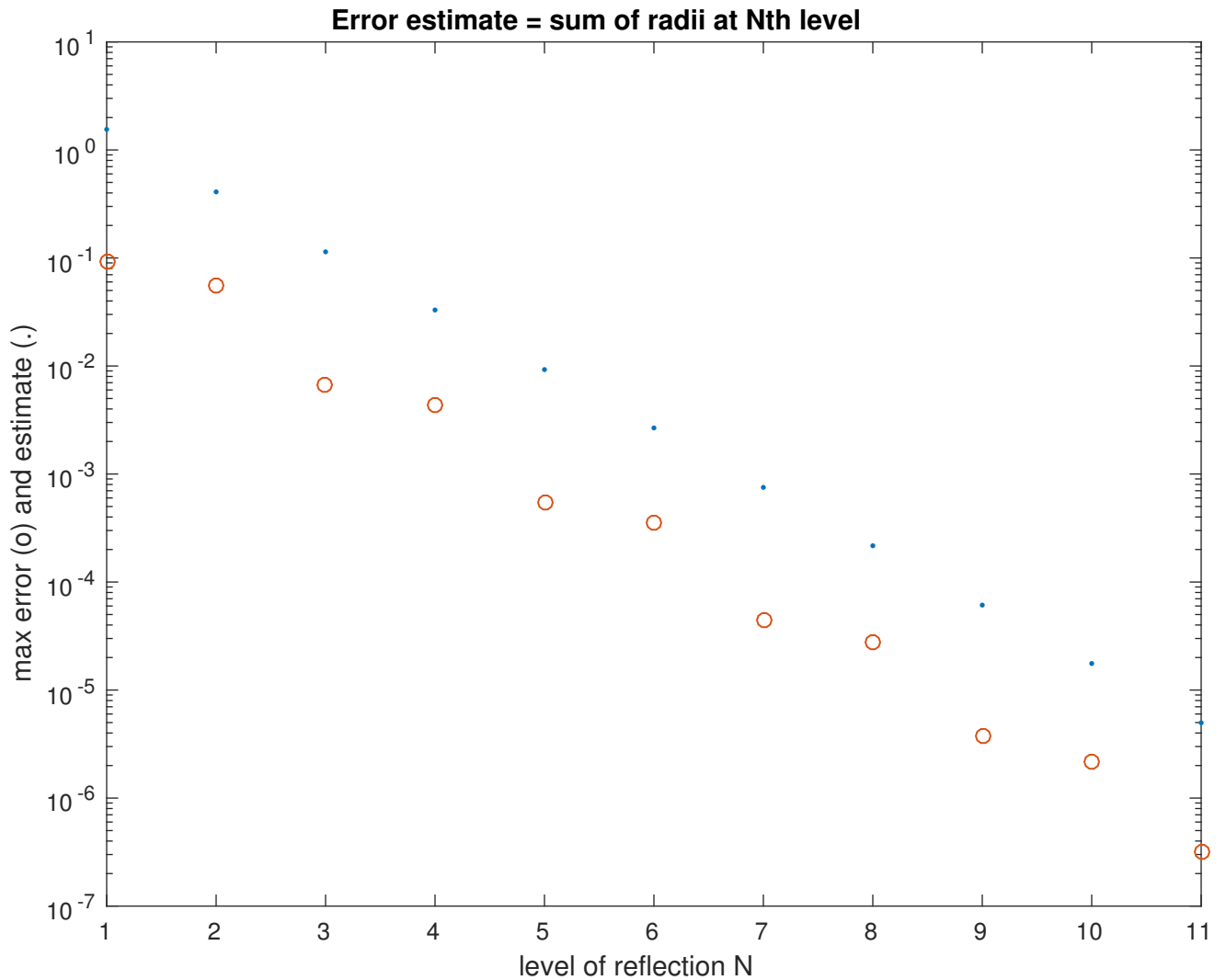


Figure 2.2: The error (o), given by ε defined in Section 3.4, below, for streaming flow around three cylinders using the method of images with $U = 1$ and $N_{refl} = 10$, is well-estimated by the rate of decrease of the sum of radii (.) of the reflected circles at each level.

modern approach for computing the potential flow over multiply connected circle domains using a method based on least-squares.

2.2.2 The Least Squares Solution

The next technique we will discuss for computing potential flow solves a least squares problem for the coefficients of the series using the MATLAB `backslash` operator as was presented by Trefethen in [Tref05] and [Tref18] along with DeLillo, Driscoll, Elcrat [DDEP08]. Unlike those applications mentioned above, we have chosen to include the radii in our for-

mulation, to avoid highly ill-conditioned systems resulting from large N . This decision also mirrors the approach we will take when developing our new method. Additionally, it was the presentation of this least-squares based approach by Trefethen in [Tref18] that led us to propose our new method, and hence we include it here for later comparison. We will be following the discussion of this method presented in [DMS21].

We begin by noting that the velocity potential $w(z)$ is given by

$$w(z) = Uz + \sum_{k=1}^m \frac{i\Gamma_k}{2\pi} \log(z - c_k) + g(z), \quad (2.18)$$

for a function g that is analytic in a region Ω , exterior to the D_j 's. The function $g(z)$ is then expanded in the form

$$g(z) \approx \sum_{k=1}^m \sum_{j=1}^J \left(\frac{r_k}{z - c_k} \right)^j a_{k,j}, \quad (2.19)$$

which allows singularities in each of the circles. In practice we discretize the boundaries of the circles by placing N equally spaced points on each of the circles, and express the double sum in 2.19 as a matrix-vector product Ax , where each column of the matrix A is the discretization of some $(r_k/(z - c_k))^j$ and $x = [a_{k,j}]$.

The unknown coefficients in x are determined by the fact that $\text{Im}\{w(z)\}$ is constant on the circles. We can impose these conditions linearly. We break both A and x into their real and imaginary parts. Letting $A = A_R + iA_I$ and $x = x_R + ix_I$, we get

$$\begin{aligned} Ax &= (A_R + iA_I)(x_R + ix_I) \\ &= A_R x_R + iA_R x_I + iA_I x_R - A_I x_I \\ &= (A_R x_R - A_I x_I) + i(A_R x_I + A_I x_R) \end{aligned}$$

giving us,

$$[\text{Re}\{g\}] = A_R x_R - A_I x_I \quad \text{and} \quad [\text{Im}\{g\}] = A_I x_R + A_R x_I. \quad (2.20)$$

For the circles to be streamlines, we want $\text{Im}\{w(z)\}$ to be constant on each circle. These constant values are not known in advance, so we ask that pairwise difference of $\text{Im}\{w(z)\}$

be zero around each circle. Defining the $N \times N$ matrix D by

$$D = \begin{bmatrix} 1 & & & & -1 \\ -1 & 1 & & & \\ & -1 & 1 & & \\ & & & \ddots & \ddots \\ & & & & -1 & 1 \end{bmatrix} \quad (2.21)$$

and the $mN \times mN$ matrix E by,

$$E = \begin{bmatrix} D & & & \\ & D & & \\ & & \ddots & \\ & & & D \end{bmatrix} \quad (2.22)$$

with the blank space assumed to be zero, we arrive at the expression

$$E \begin{bmatrix} A_I & A_R \end{bmatrix} \begin{bmatrix} x_R \\ x_I \end{bmatrix} \approx -E \left[\operatorname{Im} \{U(c_i + r_i e^{-i\theta_n})\} + \operatorname{Im} \left\{ \sum_{k=1}^m \frac{i\Gamma_k}{2\pi} \log ((c_i + r_i e^{-i\theta_n}) - c_k) \right\} \right],$$

where the right-hand side has been discretized for each circle C_i , with $i = 1, 2, \dots, m$ at $\theta = \theta_n := 2\pi n/N$ with $n = 0, 1, \dots, N - 1$. We see that this equation is an ordinary least-squares problem for the unknown coefficients. This problem can be solved quickly, even for fairly large discretizations. If we do not include the radii, using instead just $(1/(z - c_k))^j$ to form the matrix A , the method often still works. However, A becomes very ill-conditioned and fails in many cases. Furthermore, although we do not do it here, the least squares approach could be extended to compute the Γ_k 's. However, we will cover this case in the next chapter. In Figure 2.3 we show the contour plot of the potential flow over three disks as computed using this least-squares method in Figure 2.4 we plot the associated singular values on the left and the absolute values of the Laurent coefficients from $g(z)$, on the right. Next, we will cover the conformal mapping techniques vital to later applications, examples, and comparisons presented in Chapter 4.

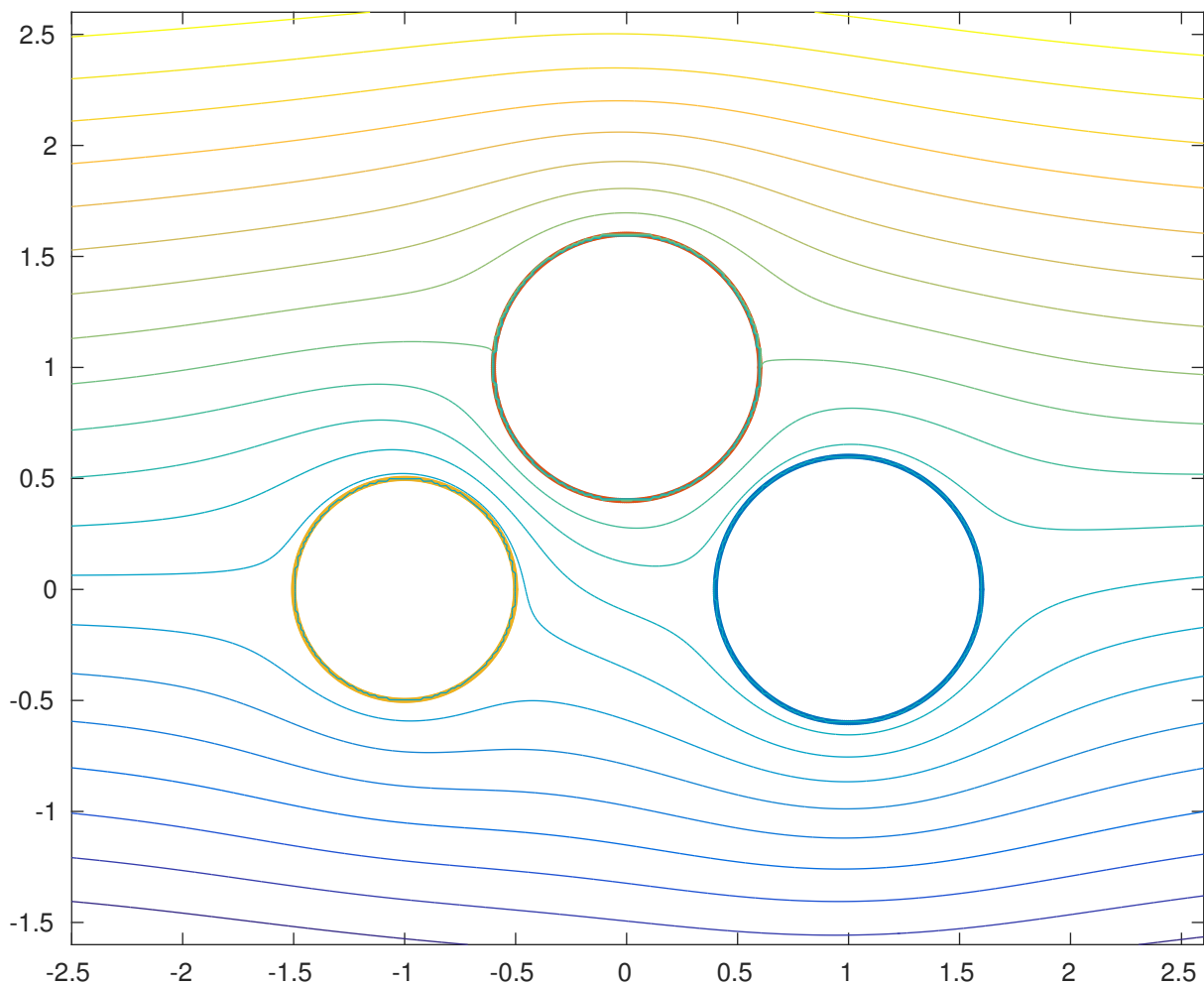


Figure 2.3: Flow over $m = 3$ disks with centers $1, i, -1$, and radii $0.6, 0.6, 0.5$, using least squares approach with $N = 33, J = 16$.

2.3 Conformal Mapping

As we will see in the next chapter, our new method computes the potential flow over multiply-connected circle domains accurately and efficiently. However, the most interesting problems are not necessarily over circle domains. So, we will need methods allowing us to map between multiply-connected, non-circular “physical” domains and the canonical circle domain. These maps must preserve the geometry of the space and allow the solutions of Laplace’s equation to transplant, that is, we need conformal maps.

Recall that a conformal map is a biholomorphic function mapping between two re-

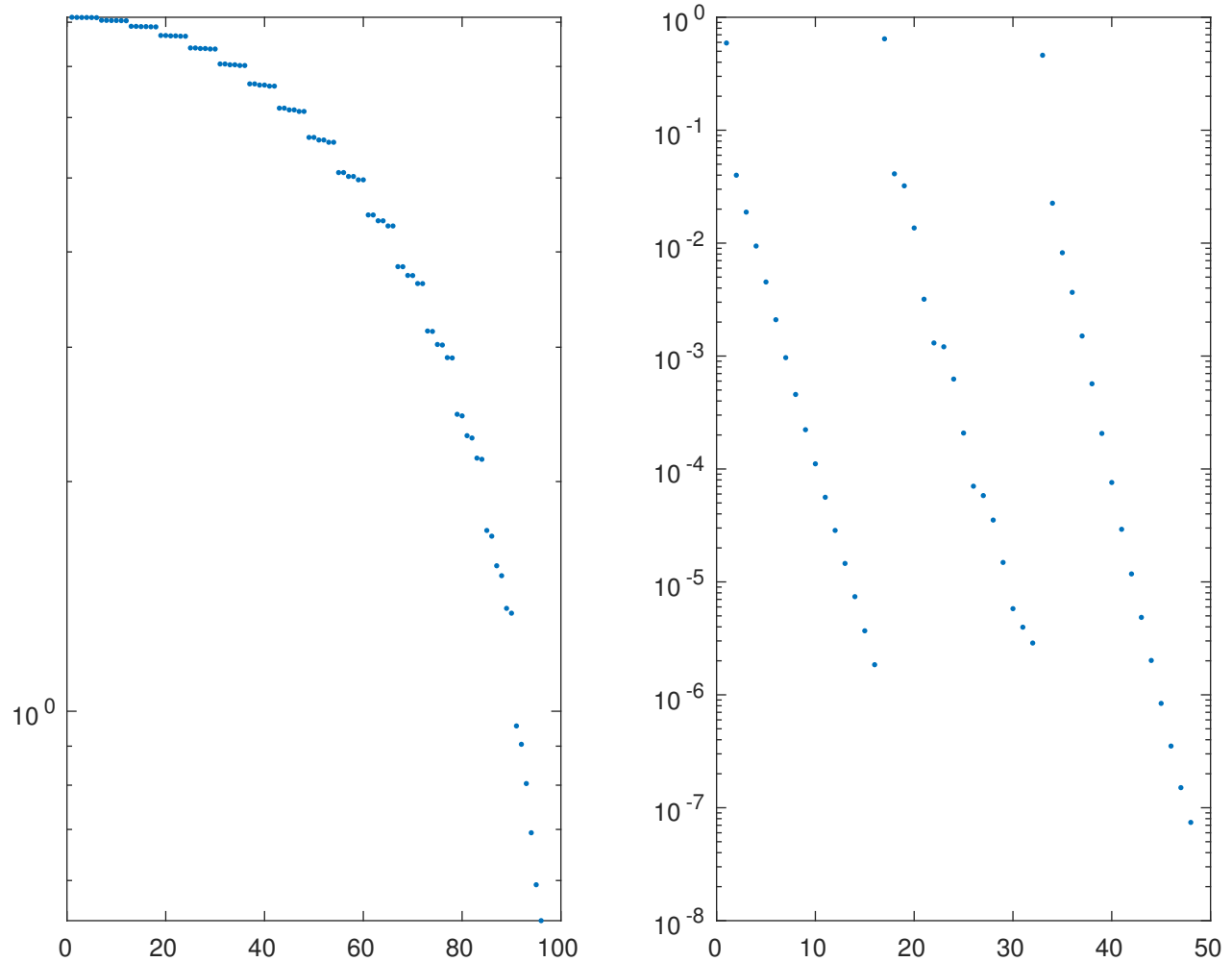


Figure 2.4: On the left we have the singular values which are not as well-grouped as our new method. On the right we have the decay of Laurent coefficients on three circles indicates the accuracy achieved on the two larger circles is about 10^{-5} .

regions in the complex plane that preserves angles. Ahlfors explains in [Ahl79] that this special geometric property allows conformal maps to play an important and influential role in the geometric theory of analytic functions. He additionally notes in that book that some existence and uniqueness theorems allows us to be able to determine analytic functions without necessarily expressing them explicitly and also gain insight on analytic properties about the mapping function by considering the geometric properties of the regions that are being mapped. Another important benefit of conformal maps related to potential theory is that

the Laplacian is invariant under such maps, and therefore, the velocity potential, which is harmonic, transplants between the spaces.

One of the aforementioned theorems, the Riemann Mapping Theorem guarantees the existence and uniqueness of a conformal map between the open unit disk and a simply connected region in the complex plane. The theorem, as stated in by Ahlfors in [Ahl79] follows here without proof.

Theorem 4 (The Riemann Mapping Theorem). *Given any simply connected region Ω which is not the whole plane, and a point $z_0 \in \Omega$, there exists a unique analytic function $f(z)$ in Ω , normalized by the conditions $f(z_0) = 0$, $f'(z_0) > 0$, such that $f(z)$ defines a one-to-one mapping of Ω onto the disk $|w| < 1$.*

We will also need a way to guarantee existence and uniqueness for conformal maps between multiply-connected domains. This is given from the following theorem from [Hen86, Theorem 17.6a] which we state without proof.

Theorem 5. *Let R be a region of connectivity $n \geq 2$ in the extended complex plane such that $\infty \in R$. Then there exists a unique circular region C of connectivity n and a unique one-to-one analytic function f in R satisfying $f(z) = z + O(1/z)$, such that $f(R) = C$.*

One might notice that although these theorems establish existence and uniqueness, they do not describe a way for finding the mapping functions. Many explicit maps exist, and we will utilize one later, but for most of the regions we are considering, numerical methods for computing conformal maps will be essential. Indeed, for applications such as those involving computing potential flow over single and multi-element airfoils, by Halsey in [Hal79], numerical conformal mapping techniques play a pivotal role in mapping between circle domains and domains containing airfoils. In Chapter 4 we will perform calculations similar to Halsey, using more recently developed methods by Benchama, DeLillo, Hrycak, and Wang in [BDHW07] for the conformal mapping of multiply connected domains with smooth boundaries. Specifically, we will use an extension fo Fornberg's original method for

simply connected regions in [For80], to exterior multiply connected domains. The problem of computing the conformal map from the circle domain to the target (physical) domain is nonlinear. Fornberg’s original method is a Newton-like method that converges more rapidly than methods such as Theodorsen’s and Timman/James’, available from Henrici in [Hen86], which are linearly convergent methods of successive approximation. Halsey and others used the simply connected exterior method of Timman/James and applied Koebe’s method as described in [Hen86, Sec.17.7] to successfully map domains to the exterior of a disk. The latest techniques for computing the conformal map of multiply connected domains produce the map directly to the domain. For regions with sharp corners, such as airfoils, it is sometimes necessary to apply explicit maps which remove corners, such as Karman-Trefftz to smooth out the boundary before using Fornberg’s method to compute the map between the circle domain and the smooth boundary domain.

Additionally, the extension of Fornberg’s method to the exterior of multiply connected domains and the series method we developed earlier both solve linear boundary value problems on the multiply connected circle domain using sums of Laurent series centered on the disks. Discretization of both systems is based on N -point trigonometric interpolation on each circle, and they are both solved for the Laurent coefficients and auxiliary parameters such as circulations or conformal moduli. In fact, both linear systems share the same special “Identity plus low rank matrix” property that we discussed above, allowing for conjugate-gradient like methods to solve the systems efficiently.

In the remainder of this chapter, we will provide a brief review of the conformal mapping methods used in these calculations following the discussions by Badreddine, DeLillo and Sahraei in [BDS19], by DeLillo and Sahraei in [DS18], and by DeLillo, Mears, and Sahraei in [DMS23].

2.3.1 Fornberg's Method for Mapping the Exterior of a Single Smooth Closed Curve

We begin by discussing Fornberg's method for finding the mapping function between the exterior of simply-connected domains. Although we will not use this method in our computations, the discussion provides insight on the numerical structure of the map. More details of the numerical method are given by DeLillo and Pfaltzgraff in [DP98] following the original discussion by Fornberg in [For80]. It should come as no surprise that computing the potential flow over a single airfoil or disk is identical whether using our new series method or the reflection method.

For $m = 1$, the existence and uniqueness of the conformal map $\zeta = f(z)$ from the exterior of the unit disk to the exterior of a smooth Jordan curve, $\partial\Omega : \gamma(S)$ with $\gamma'(S) \in C^0$ is given by Theorem 4. The mapping function has the form

$$f(z) = a_1 z + a_0 + \sum_{j=1}^{\infty} \frac{a_j}{z^j}. \quad (2.23)$$

Fornberg's method for approximating the discretized and truncated series for $f(z)$ is a Newton-like method for finding the boundary correspondence $S = S(\theta)$, such that

$$f(e^{i\theta}) = \gamma(S(\theta)). \quad (2.24)$$

At the k th Newton step, if $S^k(\theta)$ describes the approximation of $S(\theta)$, a correction, $U^{(k)}(\theta)$, is computed such that the boundary values of the linearization

$$\gamma(S^{(k)}(\theta)) + U^{(k)}(\theta) \approx \gamma(S^{(k)}(\theta)) + \gamma'(S^{(k)}(\theta)) U^{(k)}(\theta), \quad (2.25)$$

are boundary values of a function analytic in the exterior of the disk with a simple pole at infinity. Fixing the boundary point, $f(1) = \gamma(S(0)) = \gamma_0$, normalizes the map to the unit disk. Analytic extension of the mapping function to the exterior of the disk is achieved as long as the condition that the positive-indexed Fourier coefficients, a_j , are 0 for $j = 2, 3, \dots$. Using N -point trigonometric interpolation to truncate this condition produces a symmetric

positive semi-definite linear system for $U^{(k)}$, which can be solved efficiently by the conjugate gradient method using N -point `fft`. The Newton update is

$$S^{(k+1)}(\theta) = S^{(k)}(\theta) + U^{(k)}(\theta), \quad (2.26)$$

with $U^{(k)}(0) = 0$ to fix $f(1) = \gamma_0$. We note that the cost of the matrix-vector multiplication is $O(N \log N)$. Another important note which affects the potential flow calculations is that we could have normalized the map by $f(z) = z + O(1/z)$ for $z \rightarrow \infty$, resulting in the map satisfying $f'(z)$, as we will do for the $m > 1$ case. However, this would give us $a_1 = 1$ and $a_0 = 0$, requiring us to compute the center and radius of the mapped circle since it would no longer be fixed as the unit circle.

2.3.2 Extension of Fornberg's Method to the Exterior of Multiply Connected Domains

Now, following the discussions in [BDS19] and [DMS23], we discuss Fornberg's method for $m > 1$. The existence and uniqueness for the conformal map $\zeta = f(z)$ from the complement, D , of m non-overlapping disks, D_k in the complex z -plane, onto a region Ω in the complex ζ -plane which is exterior to m nonoverlapping smooth Jordan curves, $\partial\Omega_k$, with $1 \leq k \leq m$ is given Theorem 5. Given the region Ω and the normalization $f(z) = z + (1/z)$ for $z \approx \infty$, the circle domain D and the map f are uniquely determined. Let D_k be the m disks in D and their boundary circles be defined by $C_k : c_k(\theta) := c_k + r_k e^{i\theta}$. Then we can define the preimage boundary be $C = C_1 + C_2 + \dots + C_m$. The target boundary, the boundary of Ω , is $\partial\Omega = \partial\Omega_1 + \partial\Omega_2 + \dots + \partial\Omega_m$, where the $\partial\Omega_k$ are smooth Jordan curves parameterized by S , the arc length of each boundary, that is, $\partial\Omega_k : \gamma_k(S)$. The map f extends smoothly to the boundary so that $f(C_k) = \partial\Omega_k$. In order to compute f , we have to find the boundary correspondences $S = S_k(\theta)$ and conformal moduli c_k and r_k such that

$$f(c_k + r_k e^{i\theta}) = \gamma_k(S_k(\theta)), \quad 1 \leq k \leq m, \quad (2.27)$$

where f is analytic and $f(z) = z + O(1/z)$ when $z \approx \infty$. Thus,

$$f(z) = z + \sum_{k=1}^m \sum_{k=j}^{\infty} \left(\frac{r_k}{z - c_k} \right)^j a_{k,j}. \quad (2.28)$$

To ensure that the mapping function we define on the boundary extends analytically into the domain D , we use relations among the $a_{k,j}$'s developed in [BDHW07], rather than the condition on the Fourier coefficients, $a_j = 0$ for $j = 2, 3, \dots$ that we used for the exterior simply connected map.

Theorem 6. *Suppose $f \in Lip(C)$ has the Fourier series representation*

$$f(c_k + r_k e^{i\theta}) = \sum_{j=-\infty}^{\infty} a_{k,j} e^{ij\theta}, \quad 1 \leq k \leq m. \quad (2.29)$$

Then f extends analytically into D with $f(z) = z + O(1/z)$ for $z \approx \infty$ if and only if

$$a_{k,j} - \left(\frac{r_k}{c_l - c_k} \right)^j \sum_{l \neq k} \sum_{\nu=0}^{\infty} B_{j+1,\nu} \left(\frac{r_l}{c_k - c_l} \right)^{\nu+1} a_{l,-\nu-1} = r_{k,j}, \quad j \geq 0, \quad (2.30)$$

where $r_{k,0} = c_k$, $r_{k,1} = r_k$, $r_{k,j} = 0$ for $j \geq 2$ and $B_{k,j} =$ the binomial coefficients.

A quick note regarding the simply connected case; the conditions above would reduce to $a_j := a_{1,j} = 0$ for $j \geq 2$, which is what we should expect.

Next, just as we did in the simply connected case, we will linearize the problem about with respect to the current guesses for the boundary correspondences, circle centers, and radii, and then use a Newton-like iteration. For some initial guess $S_k(\theta)$ and 2π periodic correction $U_k(\theta)$, we use

$$\gamma_k(S_k(\theta) + U_k(\theta)) \approx \gamma_k(S_k(\theta)) U_k(\theta).$$

for the linearization for $U_k(\theta)$. For some initial guess c_k and r_k with corrections δc_k and δr_k , we use the linearization

$$(f + \delta f)(c_k + \delta c_k + (r_k + \delta r_k)e^{i\theta}) \approx (f + \delta f)(c_k + r_k e^{i\theta}) + f'(c_k + r_k e^{i\theta})(\delta c_k + \delta r_k e^{i\theta}).$$

Combining the two linearizations yields

$$(f + \delta f)(c_k + r_k e^{i\theta}) = \gamma_k(S_k(\theta)) U_k(\theta) - f'(c_k + r_k e^{i\theta})(\delta c_k + \delta r_k e^{i\theta}). \quad (2.31)$$

Theorem 6 from above can be used to force the functions to be boundary values of a function analytic in D . The conditions on the $a_{k,j}$'s are truncated and discretized at N Fourier points on each circle leading, to a linear system for the unknown Newton updates U_k , δc_k , and δr_k , denoted by \underline{U} , of the form

$$A\underline{U} = \underline{b}. \quad (2.32)$$

The matrix A is a symmetric positive definite matrix with the desirable form “identity plus a low-rank matrix,” where, specifically, that low-rank matrix has geometrically decaying singular values. As is the case in our series method, the eigenvalues of A are well-grouped around 1, allowing for the system to be efficiently solved by the conjugate gradient method, as in the simply connected case. The matrix-vector multiplication cost for this extension is $O((mN)^2)$.

Finally, we remark that the $i + 1$ st Newton updates for this method are,

$$\begin{aligned} S_k^{i+1} &= S_k^i + U_k^i \\ c_k^{i+1} &= c_k^i + \delta c_k^i \\ r_k^{i+1} &= r_k^i + \delta r_k^i \end{aligned}$$

for $k = 1, 2, \dots, m$.

2.3.3 Parameterizing the Boundary

Continuing along the discussion presented in [DMS23], the Karman-Trefftz maps, which we will discuss in the next section, are constructed by successively conformally transforming a large, finite set of given points along the boundary of a simply-connected region. In order to use Fornberg's method, the set of points resulting from this transformation must be interpolated by a smooth and differentiable function, that is, it cannot have corners. So, following a process based on [HK72] by Hoskins and King, we fit the points by two periodic cubic splines for the x and y coordinates parameterized by the chordal arclength,

$$s_k = \sqrt{(x_{k+1} - x_k)^2 + (y_{k+1} - y_k)^2},$$

between two successive points (x_k, y_k) for $k = 1, 2, \dots, N_s$, along the boundary, with $x_{N_{s+1}} = x_1$ and $y_{N_{s+1}} = y_1$. Using this parameterization for the boundary curve generally avoids introducing large oscillations into the interpolant, $\gamma(S) = x(S) + iy(S)$, since any large changes in the x_k 's or y_k 's give large changes in the s_k 's.

For some smooth boundaries, such as ellipses for example, analytic parameterizations exist where the map extends analytically across the boundary. In these cases the coefficients of the map decay geometrically resulting in spectral accuracy of the truncated series. Fitting these curves with cubic splines reduces the accuracy, however it reflects a more realistic situation as in practice most boundaries will not have analytic formulas to describe them. So, we will be fitting all boundaries in our later examples with cubic splines, which ultimately does not drastically affect accuracy for well-separated smooth domains.

2.3.4 The Karman-Trefftz Transformation for Airfoils

As discussed in [DMS23], a traditional approach for removing a corner at a point z_1 on a closed boundary curve of a domain exterior to that curve is the Karman-Trefftz transformation. This method has frequently been employed to calculate potential flow over the exterior of a multi-element airfoil such as by Halsey in [Hal79]. The Karman-Trefftz transformation, $\zeta = k(z)$, is given by

$$\frac{\zeta - \zeta_1}{\zeta - \zeta_2} = \left(\frac{z - z_1}{z - z_2} \right)^{1/\beta}, \quad (2.33)$$

smooths the exterior angle $\beta\pi$ at z_1 by mapping the corner point, z_1 , to ζ_1 and maps the point z_2 , which is some point interior to the curve, to ζ_2 . With a little bit of algebra, we solve for ζ in the transformation formula resulting in the following mapping function,

$$\zeta = k(z) = \frac{\zeta_1 - \zeta_2 \left(\frac{z - z_1}{z - z_2} \right)^{1/\beta}}{1 - \left(\frac{z - z_1}{z - z_2} \right)^{1/\beta}}. \quad (2.34)$$

If we are applying the Karman-Trefftz map to an airfoil, and z_2 is chosen near the leading edge, the map results in a nearly circular set of points which is then interpolated with the

periodic cubic spline routine described in the previous section. Additionally, as is pointed out in [Hal79], in practice a branch tracking procedure must be used to ensure that the arguments of the fractional powers vary continuously around the boundary curve.

In the case of multiply connected domains, the Karman-Trefftz transformations, k_i , are applied successively to the images of the m airfoils to produce a map

$$k = k_m \circ \cdots \circ k_2 \circ k_1,$$

from the domain Ω bounded by the airfoils to the domain bounded by nearly circular smooth curves. This composition process requires that each of the k_i for the simply connected domain exterior to $\partial\Omega_i$ be applied to all of the curves at each step. Once mapped to a region of m nearly circular boundaries, Fornberg's method for exterior multiply connected domains can be used to compute a Laurent series map $\zeta = h(z)$ from a conformally equivalent domain exterior to m disks to $k(\Omega)$. Additionally, we know that the Karman-Trefftz maps k_i can be explicitly inverted,

$$k^{-1}(\zeta) = \frac{z_1 - z_2 \left(\frac{\zeta - \zeta_1}{\zeta - \zeta_2} \right)^\beta}{1 - \left(\frac{\zeta - \zeta_1}{\zeta - \zeta_2} \right)^\beta}.$$

This allows us to consider the final conformal map f from the circle domain to the domain exterior to the m airfoils which we will use for our computations of potential flow,

$$f = k^{-1} \circ h = k_1^{-1} \circ k_2^{-1} \circ \cdots \circ k_m^{-1} \circ h.$$

With the most crucial background information covered, we will now focus our attention on introducing our new series method for computing potential flow over circular domains.

CHAPTER 3

NEW SERIES SOLUTION

As was mentioned in the previous chapter, the historical approach for computing potential flow was through a method of images. We saw that when computing the streaming flow, this process utilizes a successive sequence of reflections of singularities in circles leading to an infinite series, where convergence is proven as long as the circles are sufficiently well-separated. To find the circulation, a second system is solved to satisfy the Kutta condition. In contrast, our new method is closer to the least-squares approach discussed in the previous chapter. It is based on using sums of Laurent series to find the potential flow satisfying the Kutta condition. This method leads to a single well-conditioned linear system which can be solved efficiently using a conjugate-gradient like method. Our approach expands on the work done by Trefethen in [Tref18] and is quite similar to that done by Prosnak in [Pros87, Chap 3] where a Gauss-Seidel iteration is used, however there is little discussion of the numerics, nor is the structure of the system analyzed. Our primary contribution lies in the analysis and investigation of the structure of the linear system. Furthermore, solutions to problems using Laurent series formulations similar to ours are given by Wegmann in [Weg01] and [Weg05]. Finally, this method builds on the work done by Balu and DeLillo in [BD16] where Laurent series are computed for conformal maps from the exterior of disks to the exterior of multiple slits, and contains further results about similar systems.

In constructing a unified linear system, we will find it beneficial to consider the problem in two parts; (1) the problem of finding the potential streaming flow, and (2) the problem for finding the potential circulating flow. We can then use the property of superposition to add these solutions together to find a “total” flow function. We will consider the case where our circles represent conformally mapped airfoils, and therefore require the Kutta condition be enforced, as an extension of the circulating flow discussion. Finally, even though our method is for multiply-connected domains, we find it beneficial to include

a concise discussion of the constructions for the simply-connected cases as they will provide some insight for the multiply-connected cases.

3.1 Computing The Velocity Potential for a Single Disk

We present these constructions following similar discussions to those presented in [DMS21] and [DMS23], but limited to a domain with a single disk. Suppose we have an ideal, incompressible, and irrotational flow, and a single disk placed into that flow. For $z \in \mathbb{C}$, the complex velocity potential and velocity are given by Equations 2.1 and 2.2. The circular boundary is defined by

$$C_1 : z = c_1 + r_1 e^{i\theta}$$

centered at c_1 with radius r_1 , is a streamline, implying that $\psi = \text{constant}$ on the circle.

3.1.1 Streaming Flow for a Single Disk

We want to represent the streaming flow potential, $w_{\text{stream}}(z)$, in terms of a Laurent Series expansion. Letting $U = a + ib$ be the velocity of the uniform flow at infinity, our representation needs to satisfy the following boundary conditions.

- (1) $w_{\text{stream}}(z) \approx Uz$ as $z \rightarrow \infty$,
- (2) $\text{Im}\{w_{\text{stream}}(z)\} = \text{constant}$ for $z \in C_1$,
- (3) $\Gamma_1 = 0$.

Note that these conditions are similar to the ones given in 2. So, we can write our analytic representation in the following form.

$$w_{\text{stream}}(z) = Uz + \sum_{j=1}^{\infty} \left(\frac{r_1}{z - c_1} \right)^j a_j \quad (3.1)$$

Next, we need to setup a system describing $w_{\text{stream}}(z)$ so that we may apply the method of least-squares. Since C_1 is a streamline, we have that for $z = c_1 + r_1 e^{-i\theta} \in C_1$, $\text{Im}[w(z)] =$

constant. Thus, on C_1 we have

$$\begin{aligned} 0 &= \frac{\partial}{\partial \theta} \text{Im} [w_{stream}(c_1 + r_1 e^{-i\theta})] = \frac{\partial}{\partial \theta} \text{Im} \left[U(c_1 + r_1 e^{-i\theta}) + \sum_{j=1}^{\infty} \frac{a_j r_1^j}{(c_1 - c_1 + r_1 e^{-i\theta})^j} \right] \\ &= -\text{Re} [U r_1 e^{-i\theta}] + \text{Re} \left[\sum_{j=1}^{\infty} \frac{r_1^j r_1 e^{-i\theta}}{(r_1 e^{-i\theta})^{j+1}} (j a_j) \right]. \end{aligned}$$

Implying

$$\text{Re} [U r_1 e^{-i\theta}] = \text{Re} \left[\sum_{j=1}^{\infty} (e^{i\theta})^j (j a_j) \right]. \quad (3.2)$$

We then discretize the sum on the right, can construct a matrix of which we take the real and imaginary parts. Choosing the expression on the left of Equation 3.2 to be the “right-hand side” of our system, we can solve the system for the unknown coefficients, a_j ’s, using Conjugate Gradient Least Squares(CGLS) as in [Han98]. Figure 3.1 shows a the streaming flow past a single circle using this method with the flow lines given by the MATLAB contour function.

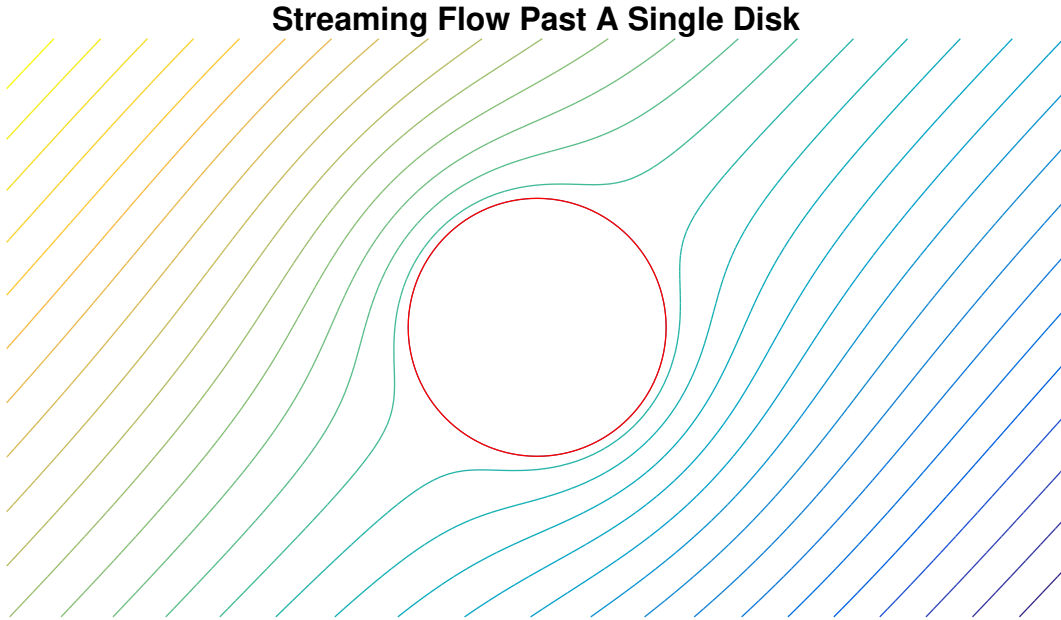


Figure 3.1: Contour plot of the streaming flow past a single disk computed using our method with $U = 1 + i$.

Alternatively, we could have just used the Circle Theorem(Theorem 2.1) to write the

velocity potential in a simpler form as,

$$w_{\text{stream}}(z) = Uz + U \overline{\left(c_1 + \frac{r_1^2}{\bar{z} - \bar{c}_1} \right)} = Uz + \bar{U}\bar{c}_1 + \frac{\bar{U}r_1^2}{z - c_1}.$$

However, we note that the solution of our system returns the Circle Theorem result, which can be seen from the following. Taking equation 3.2, we assume U is real, giving us

$$\begin{aligned} Ur_1 \cos(\theta) &= \operatorname{Re} \left[\sum_{j=1}^{\infty} (e^{i\theta})^j (ja_j) \right] \\ &= \operatorname{Re} \left[\sum_{j=1}^{\infty} j \left(\cos(j\theta) + i \sin(j\theta) \right) \left(\operatorname{Re}\{a_j\} + i \operatorname{Im}\{a_j\} \right) \right] \\ &= \sum_{j=1}^{\infty} j \operatorname{Re} \left[\left(\cos(j\theta) \operatorname{Re}\{a_j\} - \sin(j\theta) \operatorname{Im}\{a_j\} \right) + i \left(\cos(j\theta) \operatorname{Im}\{a_j\} + \sin(j\theta) \operatorname{Re}\{a_j\} \right) \right] \\ &= \sum_{j=1}^{\infty} j \left(\cos(j\theta) \operatorname{Re}\{a_j\} - \sin(j\theta) \operatorname{Im}\{a_j\} \right) \\ &= \cos(\theta) \operatorname{Re}\{a_1\} - \sin(\theta) \operatorname{Im}\{a_1\} + 2 \cos(2\theta) \operatorname{Re}\{a_2\} - 2 \sin(2\theta) \operatorname{Im}\{a_2\} + \dots \end{aligned}$$

Implying that

$$Ur_1 \cos(\theta) = \operatorname{Re}\{a_1\} \cos(\theta)$$

and consequently the result we expect from the Circle Theorem,

$$\operatorname{Re}\{a_1\} = Ur_1.$$

A similar calculation can be done for complex-valued U , showing that the solution to our system returns the Circle Theorem result.

3.1.2 Circulating or Vortex Flow for a Single Disk

We now consider the vortex flow around single disk, where we will represent the vortex flow, $w_{\text{circ}}(z)$ as a Laurent Series expansion. This representation must satisfy the following boundary conditions:

- (1) $\Gamma =$ a given constant $\neq 0$
- (2) $\operatorname{Im}\{w_{\text{circ}}(z)\} = \text{constant}$ for $z \in C_1$,
- (3) $\lim_{z \rightarrow \infty} w'_{\text{circ}}(z) \rightarrow 0$.

We can write our analytic representation in the following form

$$w_{\text{circ}}(z) = \frac{i\Gamma}{2\pi} \ln(z - c_1) + \sum_{j=1}^{\infty} \left(\frac{r_1}{z - c_1} \right)^j a_j. \quad (3.4)$$

Since the boundary C_1 is a streamline, we have that $\text{Im}[w_{\Gamma_1}(z)] = \text{constant}$. And differentiating as in the previous case yields the following.

$$\begin{aligned} 0 &= \frac{\partial}{\partial \theta} \text{Im} [w_{\text{circ}}(c_1 + r_1 e^{-i\theta})] = \frac{\partial}{\partial \theta} \text{Im} \left[\frac{i\Gamma}{2\pi} \ln(c_1 - c_1 + r_1 e^{-i\theta}) + \sum_{j=1}^{\infty} \frac{a_j r_1^j}{(c_1 - c_1 + r_1 e^{-i\theta})^j} \right] \\ &= \text{Im} \left[\frac{\Gamma}{2\pi} \frac{r_1 e^{-i\theta}}{(r_1 e^{-i\theta})} \right] + \text{Re} \left[\sum_{j=1}^{\infty} \frac{r_1^j r_1 e^{-i\theta}}{(r_1 e^{-i\theta})^{j+1}} (j a_j) \right]. \end{aligned}$$

Thus, on the boundary circle we have

$$-\text{Im} \left[\frac{\Gamma}{2\pi} \right] = \text{Re} \left[\sum_{j=1}^{\infty} (e^{i\theta})^j (j a_j) \right] \quad (3.5)$$

We easily see that the sum on the right in Equation 3.5 is a portion of the DFT allowing us to construct a matrix representing the system, as we did in the streaming case, and applying the method of CGLS to solve for the vortex velocity potential. Figure 3.2 shows the contour plot of the circulating flow around a single disk as computed by our method and drawn by the `contour` function in MATLAB.

We note that for this case the setup we described above is unnecessary since the natural logarithm sets the circle as a streamline since we have

$$w_{\text{circ}}(c_1 + r_1 e^{i\theta}) = \frac{i\Gamma}{2\pi} \ln(c_1 + r_1 e^{i\theta} - c_1) = \frac{i\Gamma}{2\pi} \ln(r_1 e^{i\theta}) = -\frac{\Gamma}{2\pi} \theta + \frac{i\Gamma}{2\pi} \ln(r_1)$$

showing that $\text{Im}\{w_{\text{circ}}(z)\} = \text{constant}$, which we expect. Additionally, rewriting Equation 3.5 yields

$$0 = \text{Im} \left[\frac{\Gamma}{2\pi} \right] + \text{Re} \left[\sum_{j=1}^{\infty} (e^{i\theta})^j (j a_j) \right]$$

which, since Γ is real, we have

$$0 = \text{Re} \left[\sum_{j=1}^{\infty} (e^{i\theta})^j (j a_j) \right]$$

implying that the $a_j = 0$. Again, the purpose of these sections are to show a simplified version of our new setup before we introduce the setup for regions of higher connectivity.

Circulating Flow Around a Single Disk

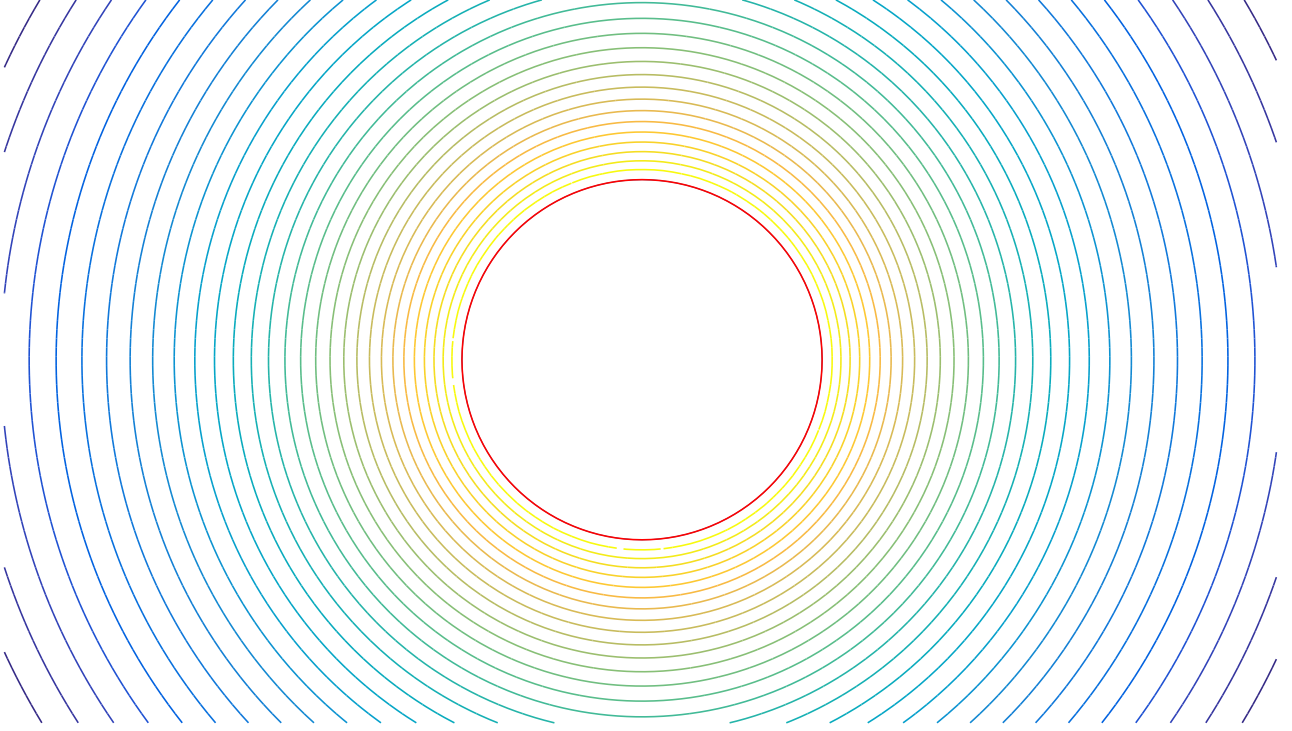


Figure 3.2: Contour plot of the circulating flow around a single disk computed using our new method.

3.1.3 Total Flow for a Single Disk

Combining the streaming and vortex flows, we can write the complex velocity potential, $w(z)$, for a single disk by

$$w(z) = w_{\text{stream}}(z) + w_{\text{circ}}(z) = Uz + \frac{i\Gamma_1}{2\pi} \ln(z - c) + \sum_{j=1}^{\infty} \left(\frac{r_1}{z - c_1} \right)^j a_j \quad (3.6)$$

It follows from before that on the boundary circle we have

$$\begin{aligned} 0 &= \frac{\partial}{\partial \theta} \text{Im} [w(c_1 + r_1 e^{-i\theta})] \\ &= \frac{\partial}{\partial \theta} \text{Im} \left[U(c_1 + r_1 e^{-i\theta}) + \frac{i\Gamma}{2\pi} \ln(c_1 - c_1 + r_1 e^{-i\theta}) + \sum_{j=1}^{\infty} \left(\frac{r_1}{c_1 - c_1 + r_1 e^{-i\theta}} \right)^j a_j \right] \\ &= -\text{Re} [U r_1 e^{-i\theta}] + \text{Im} \left[\frac{\Gamma}{2\pi} \frac{r_1 e^{-i\theta}}{(r_1 e^{-i\theta})} \right] + \text{Re} \left[\sum_{j=1}^{\infty} \frac{r_1^j r_1 e^{-i\theta}}{(r_1 e^{-i\theta})^{j+1}} (j a_j) \right]. \end{aligned}$$

Which gives us,

$$\operatorname{Re} [U r_1 e^{-i\theta}] - \operatorname{Im} \left[\frac{\Gamma}{2\pi} \right] = \operatorname{Re} \left[\sum_{j=1}^{\infty} (e^{i\theta})^j (j a_j) \right]. \quad (3.7)$$

Discretizing the sum, setting up the matrix, and establishing the correct structure for our system allows us to again use CGLS to solve for the coefficients. Figure 3.3 shows a contour plot of the potential flow computed using our new method and drawn using the `contour` function in MATLAB.

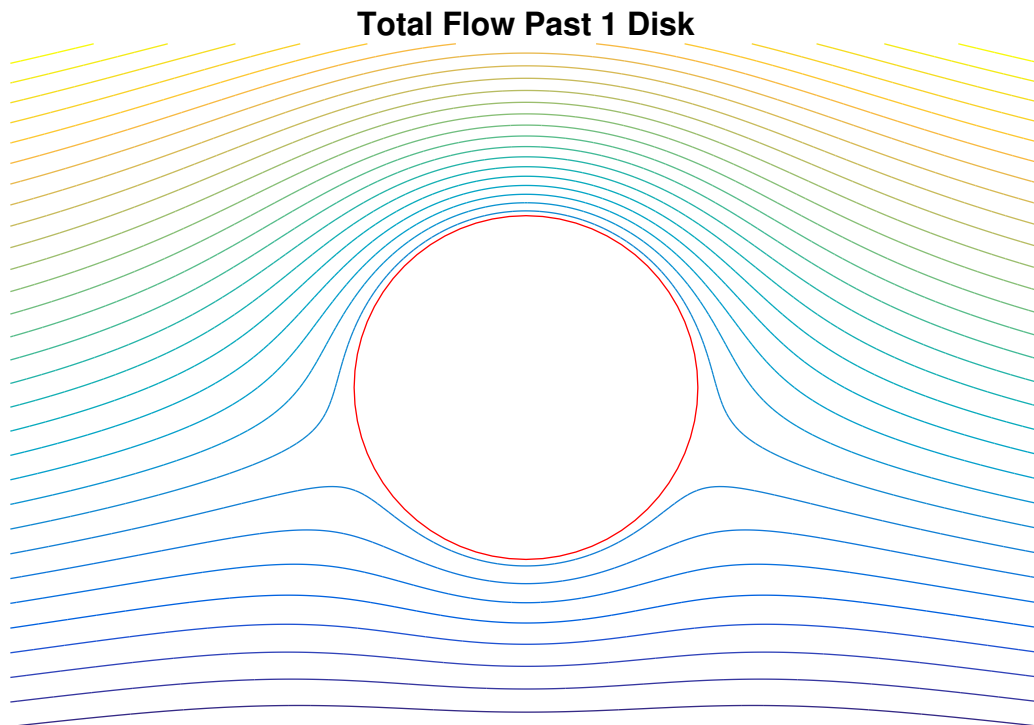


Figure 3.3: Contour plot of the combined flow past a single disk computed using our new method.

3.2 Computing the Velocity Potential for Multiple Disks

Building upon the single-disk cases, we will now present our method for computing the complex velocity potential over multiple disks. We will now follow a more complete discussion based on those presented in [DMS21] and [DMS23].

3.2.1 Streaming Flow for Multiple Disks

Suppose that we now have m non-overlapping disks with boundary circles C_i , centers c_i , and radii r_i , in the complex plane. We want to find the streaming flow potential over this assembly of disks. Just as we did in the single disk case, we can represent the velocity potential for streaming flow, $w_{\text{stream}}(z)$, as a Laurent series expansion which must satisfy the following boundary conditions:

$$\begin{aligned}
(1) \quad & w_{\text{stream}}(z) \approx Uz \quad \text{as } z \rightarrow \infty, \\
(2) \quad & \text{Im}\{w_{\text{stream}}(z)\} = \text{constant} \quad \text{for } z \in C_i, \text{ with } i = 1, 2, \dots, m \\
(3) \quad & \Gamma_i = 0, \quad \text{for all } i = 1, 2, \dots, m.
\end{aligned} \tag{3.8}$$

we can write our streaming flow in the following form.

$$w_{\text{stream}}(z) = Uz + \sum_{k=1}^m \sum_{j=1}^{\infty} \left(\frac{r_k}{z - c_k} \right)^j a_{kj}, \tag{3.9}$$

where the a_{kj} are the Laurent coefficients we want to find. Next, since $\text{Im}[w(z)]_{C_i} = \text{constant}$ for $z \in C_i$, $z = c_i + r_i e^{-i\theta}$ gives

$$\begin{aligned}
0 &= \frac{\partial}{\partial \theta} \text{Im} [w_{\text{stream}}(c_i + r_i e^{-i\theta})] \\
&= \frac{\partial}{\partial \theta} \text{Im} \left[U(c_i + r_i e^{-i\theta}) + \sum_{k=1}^m \sum_{j=1}^{\infty} \left(\frac{r_k}{c_i - c_k + r_i e^{-i\theta}} \right)^j a_{kj} \right] \\
&= \text{Im} \left[U \frac{\partial}{\partial \theta} (c_i + r_i e^{-i\theta}) + \frac{\partial}{\partial \theta} \sum_{k=1}^m \sum_{j=1}^{\infty} \left(\frac{r_k}{c_i - c_k + r_i e^{-i\theta}} \right)^j a_{kj} \right] \\
&= \text{Im} [-iUr_i e^{-i\theta}] + \text{Im} \left[\sum_{k=1}^m \sum_{j=1}^{\infty} i r_i e^{-\theta} \left(\frac{r_k}{c_i - c_k + r_i e^{-i\theta}} \right)^{j+1} \left(\frac{j a_{kj}}{r_k} \right) \right] \\
&= -\text{Re} [Ur_i e^{-i\theta}] + \text{Re} \left[\sum_{k=1}^m \sum_{j=1}^{\infty} r_i e^{-\theta} \left(\frac{r_k}{c_i - c_k + r_i e^{-i\theta}} \right)^{j+1} \left(\frac{j a_{kj}}{r_k} \right) \right]
\end{aligned}$$

Consequently, after canceling the r_i 's and moving one of the expressions over, we have

$$\text{Re} \left[\sum_{k=1}^m \sum_{j=1}^{\infty} r_i e^{-\theta} \left(\frac{r_k}{c_i - c_k + r_i e^{-i\theta}} \right)^{j+1} \left(\frac{j a_{kj}}{r_k} \right) \right] = \text{Re} [Ur_i e^{-i\theta}] \tag{3.10}$$

We discretize this equation for each circle C_i , with $i = 1, 2, \dots, m$ at $\theta = \theta_n := 2\pi n/N$ with $n = 0, 1, \dots, N-1$ and truncate generally at $J = N/2$ to get the resulting system of Nm

real equations for the Jm complex unknowns, ja_{kj}/r_k 's,

$$\operatorname{Re} \left[\sum_{k=1}^m \sum_{j=1}^J r_i e^{-i\theta_n} \left(\frac{r_k}{c_i - c_k + r_i e^{-i\theta_n}} \right)^{j+1} \left(\frac{ja_{kj}}{r_k} \right) \right] = \operatorname{Re} [U r_i e^{-i\theta_n}] \quad (3.11)$$

As in [BD16], we can write this system in block matrix form to reveal its structure. Let $b_{jk} := ja_{kj}/r_k$ and $c_{ik} := c_i - c_k$ and define the $N \times J$ matrix,

$$H_{ik} := E \begin{bmatrix} \left(\frac{r_k}{r_i e^{-i\theta_0} + c_{ik}} \right)^2 & \left(\frac{r_k}{r_i e^{-i\theta_0} + c_{ik}} \right)^3 & \cdots & \left(\frac{r_k}{r_i e^{-i\theta_0} + c_{ik}} \right)^{J+1} \\ \left(\frac{r_k}{r_i e^{-i\theta_1} + c_{ik}} \right)^2 & \left(\frac{r_k}{r_i e^{-i\theta_1} + c_{ik}} \right)^3 & \cdots & \left(\frac{r_k}{r_i e^{-i\theta_1} + c_{ik}} \right)^{J+1} \\ \vdots & \vdots & & \vdots \\ \left(\frac{r_k}{r_i e^{-i\theta_{N-1}} + c_{ik}} \right)^2 & \left(\frac{r_k}{r_i e^{-i\theta_{N-1}} + c_{ik}} \right)^3 & \cdots & \left(\frac{r_k}{r_i e^{-i\theta_{N-1}} + c_{ik}} \right)^{J+1} \end{bmatrix} \quad (3.12)$$

where

$$E = \begin{bmatrix} e^{-i\theta_0} & & & \\ & e^{-i\theta_1} & & \\ & & \ddots & \\ & & & e^{-i\theta_{N-1}} \end{bmatrix}$$

where the blank entries are assumed to be zero. Next, we define the $J \times 1$ vector of unknowns,

$$b_k := [b_{1,k} \quad b_{2,k} \quad \cdots \quad b_{J,k}]^T. \quad (3.13)$$

Then, the sum over k in Equation 3.11 is given in matrix-vector form as $H_{ik} b_k$. Now, define the $mN \times mJ$ matrix,

$$A = \begin{bmatrix} H_{11} & \cdots & H_{1m} \\ \vdots & & \vdots \\ H_{m1} & \cdots & H_{mm} \end{bmatrix}, \quad (3.14)$$

and the $mJ \times 1$ vector

$$b = [b_1 \quad b_2 \quad \cdots \quad b_m]^T. \quad (3.15)$$

Observing the structure of A , we gain some knowledge about the singular values. We first note that for the diagonal blocks, that is, when $k = i$, we have $E^{-1} H_{kk} = [e^{i2\pi l j/N}]$, for

$l = 0, 1, \dots, N - 1$ and $j = 2, 3, \dots, J + 1 = N/2 + 1$, are $N \times J$ matrices with the nice form of J columns of the DFT matrix,

$$E^{-1}H_{kk} = \begin{bmatrix} e^{i2\theta_0} & \dots & e^{i(J+1)\theta_0} \\ \vdots & & \vdots \\ e^{i2\theta_{N-1}} & \dots & e^{i(J+1)\theta_{N-1}} \end{bmatrix} \quad (3.16)$$

Finally, we also note that

$$\frac{1}{N}H_{kk}^*H_{kk} = I_{N/2}, \quad (3.17)$$

the $N/2 \times N/2$ identity matrix, where $H_{kk}^* = [e^{-i2\pi lj/N}]$, is the Hermissian transpose. Consequently, the eigenvalues of H_{kk} are all 1. For the off-diagonal blocks, the H_{ik} , $k \neq i$, looking at matrix 3.12, we see that the entries decrease like powers of $r_k/|r_i + c_{ik}| < 1$. Therefore, the singular values of H_{ik} , $i \neq k$ decay to 0 as N increases. The singular values of the blocks of A/\sqrt{N} are analyzed and plotted for similar systems in [BD16].

Finally, we want to solve the system we just constructed so we denote the following; $A_R = \text{Re}\{A\}$, $A_I = \text{Im}\{A\}$, $b_R = \text{Re}\{b\}$, and $b_I = \text{Im}\{b\}$. We also define the two vectors

$$\underline{b} := \begin{bmatrix} b_R \\ b_I \end{bmatrix} \quad \text{and} \quad \underline{r} := \begin{bmatrix} r_1 \\ r_2 \\ \vdots \\ r_m \end{bmatrix} \quad \text{where} \quad \underline{r}_k = \begin{bmatrix} \text{Re} [Ue^{-i\theta_0}] \\ \text{Re} [Ue^{-i\theta_1}] \\ \vdots \\ \text{Re} [Ue^{-i\theta_{N-1}}] \end{bmatrix}. \quad (3.18)$$

Defining, $A_S := \begin{bmatrix} A_R & -A_I \end{bmatrix}$, we can then solve the $mN \times mN$ system

$$\text{Re}[Ab] = A_S \underline{b} = \begin{bmatrix} A_R & -A_I \end{bmatrix} \begin{bmatrix} b_R \\ b_I \end{bmatrix} = \underline{r} \quad (3.19)$$

using the MATLAB `backslash` operator or by conjugate gradient for the normal equations using `cgl`s from [Han98].

It follows from our analysis above and a discussion of similarly structured matrices in [BD16], that $A_S/\sqrt{N/2}$ has singular values well-grouped around one, as shown in Figure 3.5 for the full system. Therefore, $(A_S)^T(A_S)$ has the form of the identity plus a low

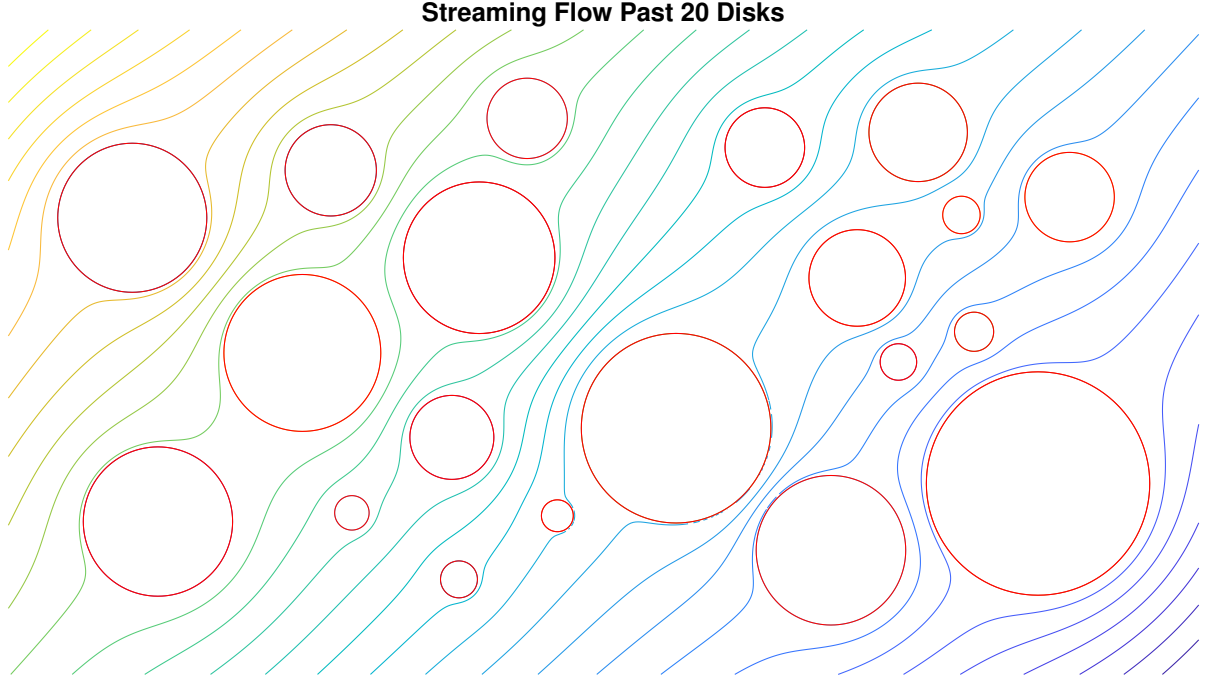


Figure 3.4: Contour plot of the streaming flow past $m = 20$ disks computed by our method.

rank matrix and so we will get rapid convergence to a solution using conjugate gradient for the normal equations. Figure 3.4 shows a contour plot of the streaming flow past $m = 20$ disks as computed using our method and plotted using the `contour` function in MATLAB.

3.2.2 Circulating or Vortex Flow for Multiple Disks

Next we consider the circulating flow potential around our m non-overlapping disks. Building upon the ideas from the single disk case, we can represent the vortex potential flow, $w_{\text{circ}}(z)$, as a Laurent series expansion satisfying the following boundary conditions:

- (1) $\Gamma_k = \text{a given constant} \neq 0$ and $\Gamma_j = 0$ for $j = 1, 2, \dots, m$ when $j \neq k$,
- (2) $\text{Im}\{w_{\text{circ}}(z)\} = \text{constant}$ for $z \in C_i$, with $i = 1, 2, \dots, m$ (3.20)
- (3) $\lim_{z \rightarrow \infty} w'_{\text{circ}}(z) \rightarrow 0$.

We can represent the vortex flow in the following form,

$$w_{\text{circ}}(z) = \sum_{k=1}^m \frac{i\Gamma_k}{2\pi} \ln(z - c_k) + \sum_{k=1}^m \sum_{j=1}^{\infty} \left(\frac{r_k}{z - c_k} \right)^j a_{kj} \quad (3.21)$$

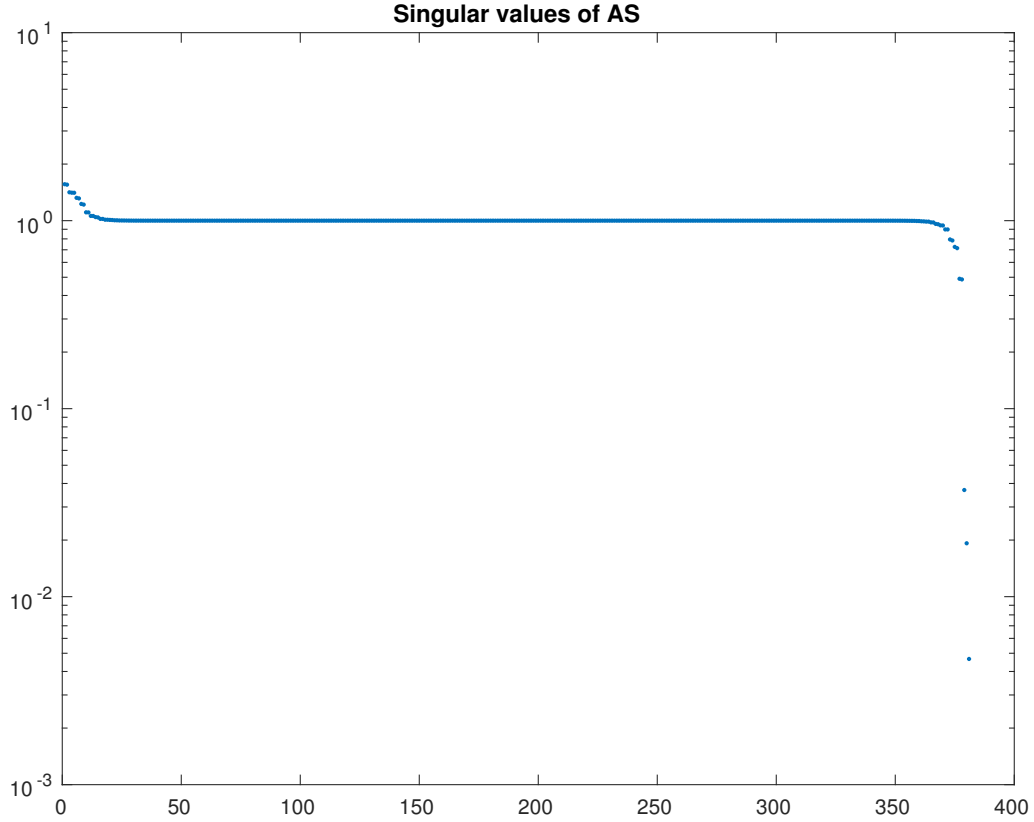


Figure 3.5: Singular values from a system computing the flow over $m = 3$ disks using our new series method with $N = 128$ and $J = 63$.

Because the C_i 's are streamlines, by Theorem 2.3, the fluxes $F_k = 0$, and we may assume that the circulations Γ_k around each circle are real. As before, $\text{Im}[w(z)]_{C_i} = \text{constant}$ on

$z \in C_i$, $z = c_i + r_i e^{-i\theta}$ gives

$$\begin{aligned}
0 &= \frac{\partial}{\partial \theta} \text{Im} [w_{\text{circ}}(c_i + r_i e^{-i\theta})] \\
&= \frac{\partial}{\partial \theta} \text{Im} \left[\sum_{k=1}^m \frac{i\Gamma_k}{2\pi} \log(c_i - c_k + r_i e^{-i\theta}) + \sum_{k=1}^m \sum_{j=1}^{\infty} \left(\frac{r_k}{c_i - c_k + r_i e^{-i\theta}} \right)^j a_{kj} \right] \\
&= \text{Im} \left[\frac{\partial}{\partial \theta} \sum_{k=1}^m \frac{i\Gamma_k}{2\pi} \log(c_i - c_k + r_i e^{-i\theta}) + \frac{\partial}{\partial \theta} \sum_{k=1}^m \sum_{j=1}^{\infty} \left(\frac{r_k}{c_i - c_k + r_i e^{-i\theta}} \right)^j a_{kj} \right] \\
&= \text{Im} \left[\sum_{k=1}^m \frac{i\Gamma_k}{2\pi} \left(\frac{-ir_i e^{-i\theta}}{c_i - c_k + r_i e^{-i\theta}} \right) + \sum_{k=1}^m \sum_{j=2}^{\infty} j \left(\frac{r_k}{c_i - c_k + r_i e^{-i\theta}} \right)^{j-1} \left(\frac{-r_k(-r_i e^{-i\theta})}{(c_i - c_k + r_i e^{-i\theta})^2} \right) a_{kj} \right] \\
&= \text{Im} \left[\sum_{k=1}^m \frac{i\Gamma_k}{2\pi} \left(\frac{-ir_i e^{-i\theta}}{c_i - c_k + r_i e^{-i\theta}} \right) \right] + \text{Im} \left[\sum_{k=1}^m \sum_{j=2}^{\infty} \left(\frac{r_k}{c_i - c_k + r_i e^{-i\theta}} \right)^{j-1} \left(\frac{j r_i r_k i e^{-i\theta}}{(c_i - c_k + r_i e^{-i\theta})^2} \right) a_{kj} \right] \\
&= \text{Im} \left[\sum_{k=1}^m \frac{\Gamma_k}{2\pi} \left(\frac{r_i}{(c_i - c_k) e^{i\theta} + r_i} \right) \right] + \text{Re} \left[\sum_{k=1}^m \sum_{j=1}^{\infty} e^{-i\theta} \left(\frac{r_i r_k}{c_i - c_k + r_i e^{-i\theta}} \right)^{j+1} \frac{j a_{kj}}{r_k} \right].
\end{aligned}$$

Canceling the r_i 's, yields,

$$\text{Re} \left[\sum_{k=1}^m \sum_{j=1}^{\infty} e^{-i\theta} \left(\frac{r_k}{c_i - c_k + r_i e^{-i\theta}} \right)^{j+1} \left(\frac{j a_{kj}}{r_k} \right) \right] = - \sum_{k=1}^m \text{Im} \left[\frac{1}{2\pi} \frac{1}{(c_i - c_k) e^{i\theta} + r_i} \right] \Gamma_k. \quad (3.22)$$

Given the Γ_k 's, with $\theta = \theta_n$, truncating the sum at $J = N/2$ and as before defining $c_{ik} := c_i - c_k$, we may consider this system for the $b_{jk} = j a_{jk} / r_k$. Define the $N \times m$ matrix,

$$L_i := \begin{bmatrix} \frac{1}{c_{i1} e^{i\theta_0} + r_i} & \frac{1}{c_{i2} e^{i\theta_0} + r_i} & \cdots & \frac{1}{c_{im} e^{i\theta_0} + r_i} \\ \frac{1}{c_{i1} e^{i\theta_1} + r_i} & \frac{1}{c_{i2} e^{i\theta_1} + r_i} & \cdots & \frac{1}{c_{im} e^{i\theta_1} + r_i} \\ \vdots & \vdots & \ddots & \vdots \\ \frac{1}{c_{i1} e^{i\theta_{N-1}} + r_i} & \frac{1}{c_{i2} e^{i\theta_{N-1}} + r_i} & \cdots & \frac{1}{c_{im} e^{i\theta_{N-1}} + r_i} \end{bmatrix}. \quad (3.23)$$

Then,

$$\text{Re} [A\mathbf{b}] = \begin{bmatrix} A_R & -A_I \end{bmatrix} \begin{bmatrix} b_R \\ b_I \end{bmatrix} = -L_I \underline{\Gamma}, \quad (3.24)$$

where $L_I = \text{Im } L$, and

$$L = \begin{bmatrix} L_1 & L_2 & \cdots & L_m \end{bmatrix}^T, \quad (3.25)$$

is an $Nm \times m$ matrix and

$$\underline{\Gamma} = \left[\Gamma_1 \quad \Gamma_2 \quad \dots \quad \Gamma_m \right]^T \quad (3.26)$$

We can see that the structure of this system is very similar to the streaming flow case, therefore we have the same nice behavior for the singular values and can solve the system efficiently using `cgl`s. Figure 3.6 demonstrates a contour plot of the vortex potential flow past $m = 10$ disks as computed using our method and presented using the `contour` function in MATLAB.

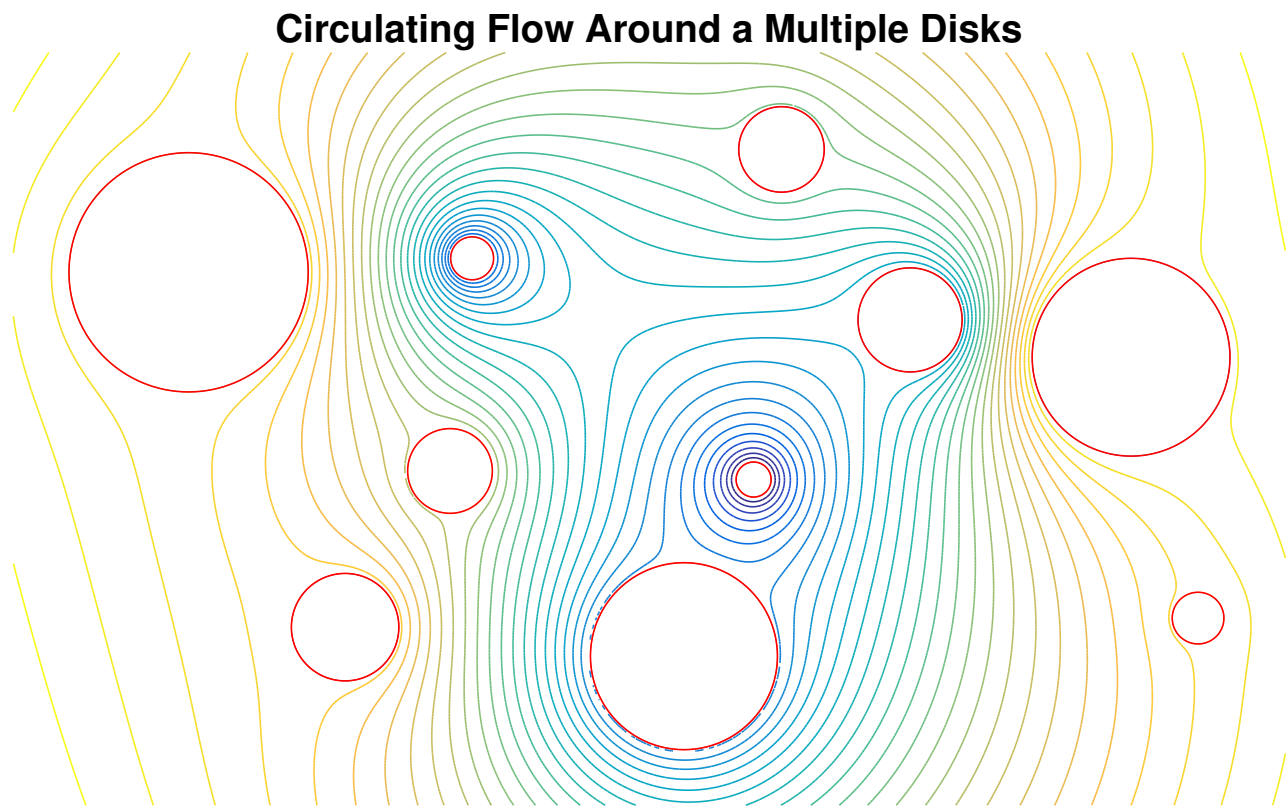


Figure 3.6: Contour plot of the circulating flow past $m = 10$ disks as computed using our method.

3.2.3 Total Flow for Multiple Disks

Finally, we must now combine the streaming and vortex velocity potentials to get the “total” flow potential over our assemblage of disks. We will represent this “total” flow in

the form,

$$w(z) = w_{\text{stream}}(z) + w_{\text{circ}}(z) = Uz + \sum_{k=1}^m \frac{i\Gamma_k}{2\pi} \ln(z - c_k) + \sum_{k=1}^m \sum_{j=1}^{\infty} \left(\frac{r_k}{z - c_k} \right)^j a_{jk}. \quad (3.27)$$

As before, applying the requirement that the circles be streamlines gives,

$$\begin{aligned} 0 &= \frac{\partial}{\partial \theta} \text{Im} [w(c_i + r_i e^{-i\theta})] \\ &= \frac{\partial}{\partial \theta} \text{Im} \left[U(c_i + r_i e^{-i\theta}) + \sum_{k=1}^m \frac{i\Gamma_k}{2\pi} \log(c_i - c_k + r_i e^{-i\theta}) + \sum_{k=1}^m \sum_{j=1}^{\infty} \left(\frac{r_k}{c_i - c_k + r_i e^{i\theta}} \right)^j a_{jk} \right] \\ &= -\text{Re} [Ur_i e^{-i\theta}] + \text{Im} \left[\sum_{k=1}^m \frac{\Gamma_k}{2\pi} \frac{r_i}{(c_i - c_k) e^{i\theta} + r_i} \right] + \text{Re} \left[\sum_{k=1}^m \sum_{j=1}^{\infty} e^{-i\theta} \left(\frac{r_i r_k}{c_i - c_k + r_i e^{-i\theta}} \right)^{j+1} \frac{j a_{jk}}{r_k} \right] \end{aligned}$$

Eliminating the r_i 's and rearranging yields,

$$\text{Re} \left[\sum_{k=1}^m \sum_{j=1}^{\infty} e^{-i\theta} \left(\frac{r_i r_k}{c_i - c_k + r_i e^{-i\theta}} \right)^{j+1} \frac{j a_{kj}}{r_k} \right] = \text{Re} [Ur_i e^{-i\theta}] - \text{Im} \left[\sum_{k=1}^m \frac{\Gamma_k}{2\pi} \frac{r_i}{(c_i - c_k) e^{i\theta} + r_i} \right].$$

As before, we truncate the series at $J = N/2 - 1$ and letting $\theta = \theta_n = 2\pi n/N$ for $n = 0, 1, \dots, N-1$ and $i = 1, 2, \dots, m$, the discrete system for the $j a_{kj}/r_k$'s is given by,

$$\text{Re} \left[\sum_{k=1}^m \sum_{j=1}^J e^{-i\theta_n} \left(\frac{r_i r_k}{c_i - c_k + r_i e^{-i\theta_n}} \right)^{j+1} \frac{j a_{kj}}{r_k} \right] = \text{Re} [Ur_i e^{-i\theta_n}] - \text{Im} \left[\sum_{k=1}^m \frac{\Gamma_k}{2\pi} \frac{r_i}{(c_i - c_k) e^{i\theta_n} + r_i} \right]$$

when the Γ_k 's are given. As in our previous two cases, the block matrix form can be written as

$$\text{Re} [Ab] = \underline{r} - \text{Im} [L] \underline{\Gamma}, \quad (3.28)$$

where \underline{r} and $\underline{\Gamma}$ are given. Since this system has a similar structure to our previous cases, we again have nicely behaved singular values, and can solve the system using **cgls**. Figures 3.7 and 3.8 consist of a contour plot of the potential flow for $m = 3$ disks with zero circulation and the associated singular values for those systems, respectively.

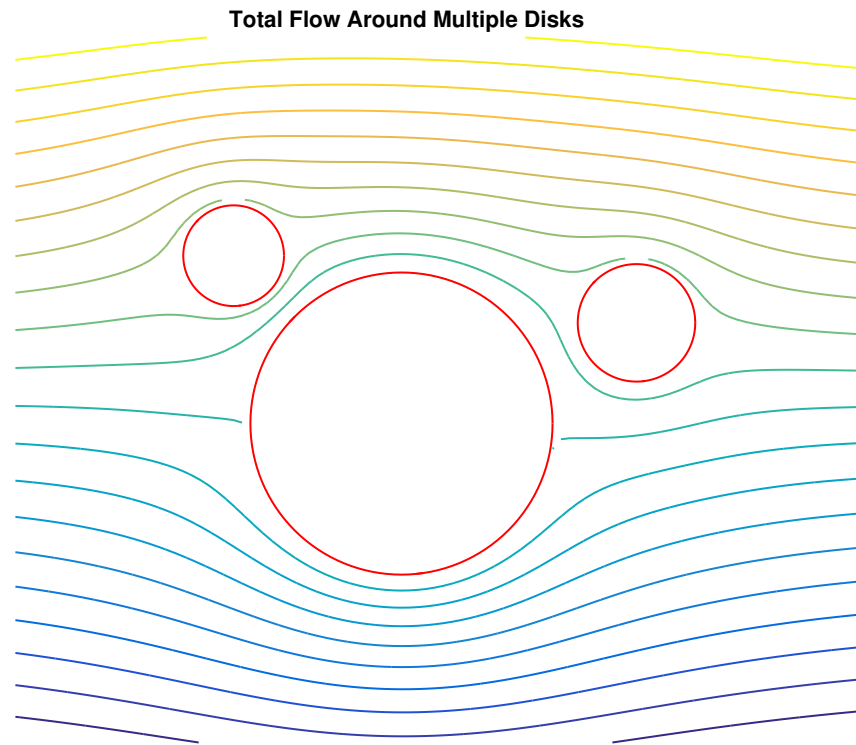


Figure 3.7: Contour lines for the “total” potential flow for three disks with no circulation.

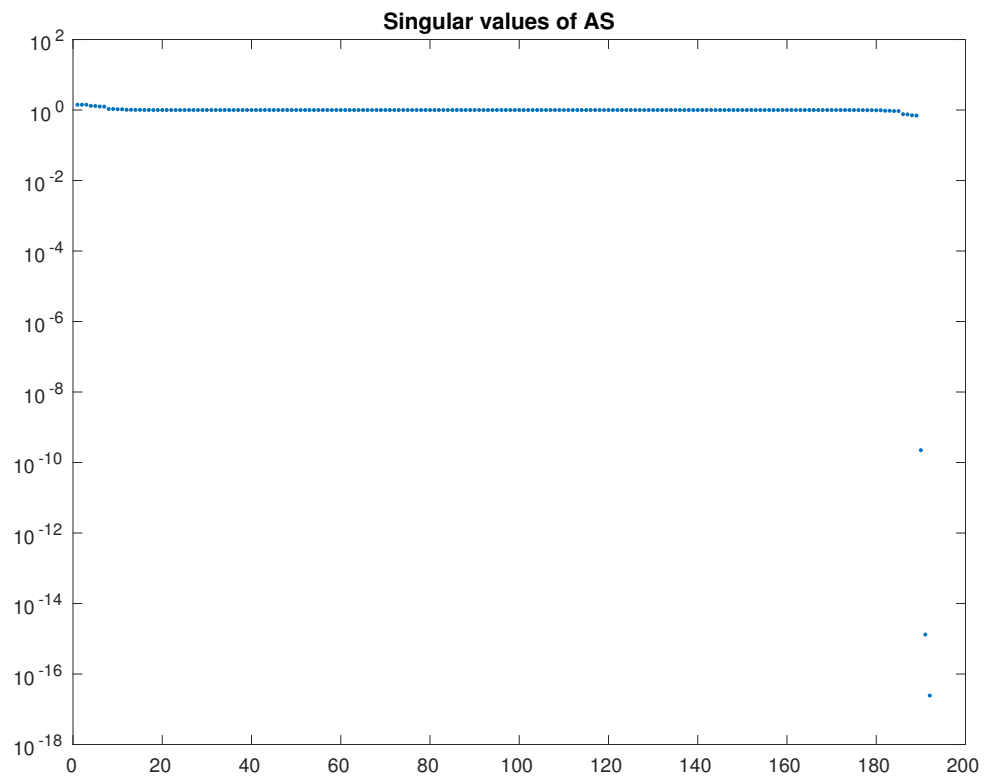


Figure 3.8: Singular values of A_S for the set of disks in Figure 3.7 from our the new method.

3.2.4 Applying the Kutta condition to solve for the Γ_k 's

We now suppose that the set of m non-overlapping circles are the images of a set of airfoils mapped by a conformal map, and that we know which points are the images of the stagnation points at the trailing edges of these airfoils. As we have seen in the previous section, the velocity V over the set of circles has the form

$$V = V_{\text{stream}} + \sum_{k=1}^m \Gamma_k V_k,$$

where V_k is the circulating velocity with circulation 1 around circle C_k and 0 on C_j with $j \neq k$, and V_{stream} is the uniform streaming flow with velocity U at infinity and the circles C_j as streamlines. Wanting to incorporate the Kutta condition into our system, we recall that this condition selects the unique physical solution by requiring that the velocities at all trailing edges are zero. We can achieve this by finding the Γ_k 's such that

$$V_{\text{stream}}(z_l) + \Gamma_1 V_1(z_l) + \cdots + \Gamma_m V_m(z_l) = 0$$

for $l = 1, 2, \dots, m$, where the z_l 's are the images of the trailing edges on the circles as in [SH85, eq.13]. That is, we want to solve the complex linear system

$$\begin{bmatrix} V_1(z_1) & V_2(z_1) & \cdots & V_m(z_1) \\ V_1(z_2) & V_2(z_2) & \cdots & V_m(z_2) \\ \vdots & \vdots & \vdots & \vdots \\ V_1(z_m) & V_2(z_m) & \cdots & V_m(z_m) \end{bmatrix} \begin{bmatrix} \Gamma_1 \\ \Gamma_2 \\ \vdots \\ \Gamma_m \end{bmatrix} = - \begin{bmatrix} V_{\text{stream}}(z_1) \\ V_{\text{stream}}(z_2) \\ \vdots \\ V_{\text{stream}}(z_m) \end{bmatrix} \quad (3.29)$$

for the real circulations Γ_k . Incorporating this system into the system we defined in the previous section introduces an additional m equations, which is comparatively a low rank perturbation which leaves the favorable grouping of the eigenvalues intact. So the full system, which we will develop and represent in block matrix form later in this section, can still be solved efficiently. Additionally, we can guarantee that the circulations are real through the following theorem.

Theorem 7. *The complex system given in 3.29 for the circulations satisfying the Kutta condition has a unique, real solution.*

Proof. For a given image z_l of a trailing edge, the velocities $V_{\text{stream}}(z_l)$ and $V_k(z_l)$ all have the same direction, since the circles are streamlines, that is, $V_k(z_l) = r_k e^{i\theta_l}$. Therefore, the complex system can be made real by multiplying each row l by $e^{-i\theta_l}$. \square

So, we want to compute the circulations, Γ_k , so that the velocities at the given stagnation points, given by $z_l = c_l + r_l e^{i\phi_l}$, for $l = 1, 2, \dots, m$, is 0, that is,

$$0 = v(z_l) = \overline{w'(z_l)}. \quad (3.30)$$

Substituting these values into Equations 3.27 and differentiating, we have

$$w'(z) = w'_{\text{stream}}(z_l) + w'_{\text{circ}}(z_l) = U + \sum_{k=1}^m \frac{i\Gamma_k}{2\pi(z_l - c_k)} - \sum_{k=1}^m \sum_{j=1}^{\infty} \left(\frac{r_k}{z_l - c_k} \right)^{j+1} \frac{ja_{kj}}{r_k} = 0.$$

So, we have the following $l = 1, 2, \dots, m$ complex-valued equations for the ja_{kj}/r_k and Γ_k 's

$$- \sum_{k=1}^m \sum_{j=1}^J \left(\frac{r_k}{c_l - c_k + r_l e^{i\phi_l}} \right)^{j+1} \left(\frac{ja_{kj}}{r_k} \right) + \sum_{k=1}^m \frac{i}{2\pi(c_l - c_k + r_l e^{i\phi_l})} \Gamma_k = -U \quad (3.31)$$

Recalling that $U = |U|e^{-i\alpha}$ and $c_{ik} = c_i - c_k$, to express these equations in block matrix form, we first define the $m \times J$ matrix,

$$B_k := \begin{bmatrix} \left(\frac{r_k}{r_1 e^{i\phi_1} + c_{1k}} \right)^2 & \left(\frac{r_k}{r_1 e^{i\phi_1} + c_{1k}} \right)^3 & \cdots & \left(\frac{r_k}{r_1 e^{i\phi_1} + c_{1k}} \right)^{J+1} \\ \left(\frac{r_k}{r_2 e^{i\phi_2} + c_{2k}} \right)^2 & \left(\frac{r_k}{r_2 e^{i\phi_2} + c_{2k}} \right)^3 & \cdots & \left(\frac{r_k}{r_2 e^{i\phi_2} + c_{2k}} \right)^{J+1} \\ \vdots & \vdots & & \vdots \\ \left(\frac{r_k}{r_m e^{i\phi_m} + c_{mk}} \right)^2 & \left(\frac{r_k}{r_m e^{i\phi_m} + c_{mk}} \right)^3 & \cdots & \left(\frac{r_k}{r_m e^{i\phi_m} + c_{mk}} \right)^{J+1} \end{bmatrix} e^{i\alpha}, \quad (3.32)$$

the $m \times m$ matrix,

$$C := \begin{bmatrix} \frac{i}{r_1 e^{i\phi_1} + c_{11}} & \frac{i}{r_1 e^{i\phi_1} + c_{12}} & \cdots & \frac{i}{r_1 e^{i\phi_1} + c_{1m}} \\ \frac{i}{r_2 e^{i\phi_2} + c_{21}} & \frac{i}{r_2 e^{i\phi_2} + c_{22}} & \cdots & \frac{i}{r_2 e^{i\phi_2} + c_{2m}} \\ \vdots & \vdots & & \vdots \\ \frac{i}{r_m e^{i\phi_m} + c_{m1}} & \frac{i}{r_m e^{i\phi_m} + c_{m2}} & \cdots & \frac{i}{r_m e^{i\phi_m} + c_{mm}} \end{bmatrix} \frac{e^{i\alpha}}{2\pi} \quad (3.33)$$

and the $m \times mJ$ matrix,

$$B := - \begin{bmatrix} B_1 & B_2 & \cdots & B_m \end{bmatrix}. \quad (3.34)$$

From these matrices we note that the sum for k in Equation 3.31 in matrix-vector form is $B_k b_k$, recalling from earlier that $b_k := [b_{1,k}, \dots, b_{J,k}]^T$ and $b_{jk} := ja_{jk}/r_k$. Also, all the elements c_{kk} in C are 0 since $c_{kk} = c_k - c_k$. So, the Kutta condition in matrix form is,

$$Bb + C\underline{\Gamma} = \underline{u}, \quad (3.35)$$

where \underline{u} is the $m \times 1$ vector, $\underline{u} = -|U| [1, 1, \dots, 1]^T$. Since the Γ_k 's are real, we can just take the imaginary part of this system, giving us

$$\begin{bmatrix} B_I & B_R \end{bmatrix} \begin{bmatrix} b_R \\ b_I \end{bmatrix} + C_I \underline{\Gamma} = \underline{0}, \quad (3.36)$$

where $\underline{0}$ is an $m \times 1$ vector of zeros. The rest of the system is a rearrangement of the system from Section 3.2.3,

$$\text{Re}[Ab] + \text{Im}[L]\underline{\Gamma} = \underline{r}. \quad (3.37)$$

Finally, defining the vectors

$$\underline{b}_\Gamma := \begin{bmatrix} b_R \\ b_I \\ \underline{\Gamma} \end{bmatrix}, \quad (3.38)$$

and

$$\underline{r} := \begin{bmatrix} r_1 & r_2 & \vdots & r_m \end{bmatrix}^T, \quad (3.39)$$

where $r_k = [\text{Re}[Ue^{-i\theta_0}], \text{Re}[Ue^{-i\theta_1}], \dots, \text{Re}[Ue^{-i\theta_{N-1}}]]^T$, and also redefining A_S , we can write our final system in block form as,

$$A_S \underline{b}_\Gamma = \begin{bmatrix} A_R & -A_I & L_I \\ B_I & B_R & C_I \end{bmatrix} \begin{bmatrix} b_R \\ b_I \\ \underline{\Gamma} \end{bmatrix} = \begin{bmatrix} \underline{r} \\ \underline{0} \end{bmatrix}, \quad (3.40)$$

Alternatively, we could have solved for the circulation using the real part of the Kutta condition. In this case, the system above would become

$$A_S \underline{b}_\Gamma = \begin{bmatrix} A_R & -A_I & L_I \\ B_R & -B_I & C_R \end{bmatrix} \begin{bmatrix} b_R \\ b_I \\ \underline{\Gamma} \end{bmatrix} = \begin{bmatrix} \underline{r} \\ \underline{u} \end{bmatrix}. \quad (3.41)$$

which has an advantage that is illustrated in Figure 4.1. Finally, we can solve the resulting $(Nm + m) \times (2Jm + m)$ system for the $(2J + 1)m$ unknowns, b_R , b_I , and Γ_k , using the MATLAB `backslash` operator or by conjugate gradient for the normal equations using `cgls` from [Han98]. Now, when $J = N/2$, there are m singular values equal to 0. This likely results from the fact that the flow is not unique if the m circulations are unspecified. There is some analysis of these zero-valued singular values for a matrix similar to A_S in [BD16] where the related singular values of diagonal blocks H_{kk} of A are calculated exactly. As we will discuss more in-depth in the next chapter, to avoid any problems, we take $J = N/2 - 1$ so that the singular values of the smaller system interlace those of the larger system with $J = N/2$ and the zero-valued singular values are perturbed to m small nonzero singular values.

In the remainder of this chapter, we will next discuss some numerical observations, several ways of measuring the accuracy of our method, and then present a convergence result relating our series-based solution to the exact potential function $w(z)$.

3.3 Some Numerical Observations

Before we can begin our discussion of accuracy or convergence, we make some observations upon which our estimates will depend. Following a discussion similar to that presented in [DMS23], we note that for $J = N/2$, there are exactly m singular values of A_s with values $\sigma_k \approx 10^{-15}$, as shown in Figure 3.9, resulting with iterations that initially converge but then diverge due to the presence of these nearly zero singular values. This type of semi-convergence is typical for ill-conditioned systems, such as those seen in inverse-problems.

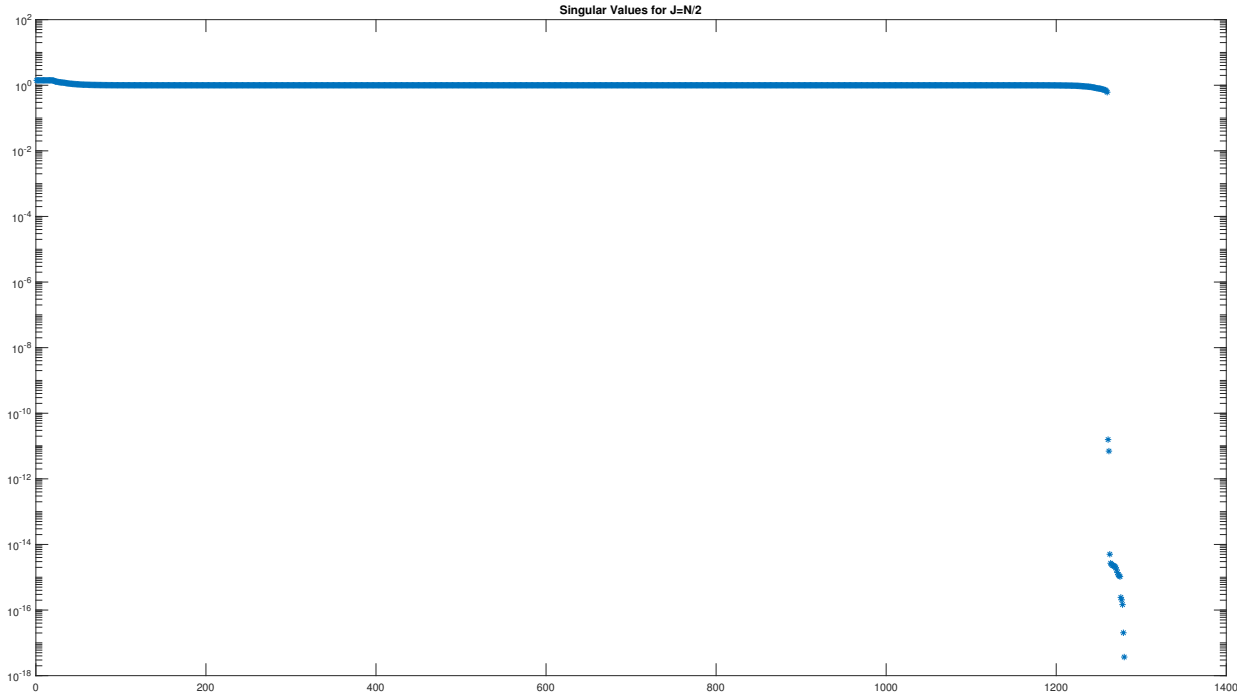


Figure 3.9: Singular values for a system with discretization of $J = N/2$ chosen.

Selecting $J = N/2 - 1$ perturbs these m near zero singular values to about $10^{-3} < \sigma_k < 1$, as is shown in Figure 3.10. One might assume that choosing smaller values for J , say $J < N/2 - 1$, might provide a better result, but in practice a smaller value does not change these observations. Additionally, these values mainly depend on the C_j 's and are independent of N and α . Balu and DeLillo provide an additional discussion about these effects for similar systems in [BD16]. Thus, $J = N/2 - 1$ is sufficient to ensure that the matrix A_S is full rank and by standard theorems, conjugate-gradient-like methods will converge. This convergence is super-linear because the eigenvalues of $A_S^T A_S$ are well-grouped around 1, with about $2m$ outliers having values slightly more or less than one.

Additionally, one could instead choose to regularize the system by dampening the higher-order Fourier coefficients, which has also been shown to handle the semi-convergence for similar problems in numerical conformal mapping, such as was shown by Wegmann in [Weg05, p 403].

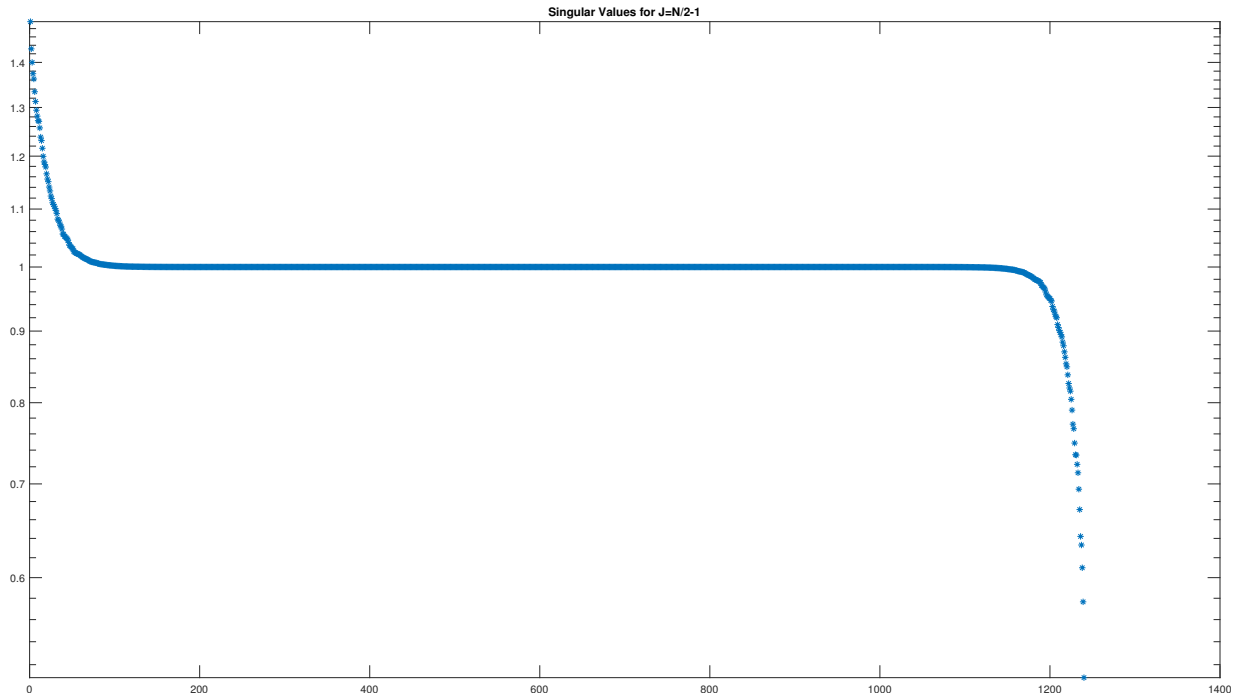


Figure 3.10: Singular values for a system with discretization of $J = N/2 - 1$ chosen.

3.4 Accuracy Estimates

Now following similar discussions presented in both [DMS21] and [DMS23], we recall the condition that $\text{Im} \{w(z)\}$ is constant on the boundary of the circles. We want to construct a way to measure how nearly-constant the imaginary values are on the boundary circles. An effective way to measure this error, ϵ , is by taking the difference of the imaginary parts of the potential $w(z)$ at $2N$ Fourier points with the average value at the N Fourier points used to solve the system. Let the $2N$ Fourier points be given by,

$$z_{k,n} = c_k + r_k e^{i\theta_n} \in C_k$$

where $\theta_n = 2\pi n/2N$ for $n = 0, 1, \dots, 2N - 1$ and N collocation points used for the construction of $w(z)$ be given by,

$$\zeta_{k,j} = c_k + r_k e^{it_j},$$

with $t_j = 2\pi j/N$ for $j = 0, 1, \dots, N - 1$. Then the difference described above is defined by

$$\epsilon_{k,n} := \left| \operatorname{Im} [w(z_{k,n})] - \frac{1}{2N} \sum_{j=0}^{N-1} \operatorname{Im} [w(\zeta_{k,j})] \right|.$$

Next define

$$\epsilon_k := \max_n \epsilon_{k,n}$$

and then the overall error ϵ is given by

$$\epsilon := \max_k \epsilon_k.$$

Through experimentation we found that increasing the number of error measurement points $z_{k,n}$ on each circle to $4N$ or greater gives the same order of magnitude of the error for a given N . Because $w(z)$ is analytic on the boundaries, the convergence of the ϵ of the conjugate-gradient iterates at the level of accuracy for a given N is superlinear in $O(2m)$ steps. Also, through the examples in Chapter 4 we will show that we get spectral accuracy for general smooth boundaries but an overall decrease in accuracy occurs when conformal mapping techniques for removing corners are used, which agrees with similar results from DeLillo and Sahraei in [DS18]. Finally, we note that using this estimate is reasonable to use in this situation as it was used by Balu and DeLillo in [BD16] where a similar calculation was used for conformal maps to multiply connected slit domains.

There are no nontrivial exact solutions to these problems with which to validate errors in our calculations, but the reflection calculations in Chapter 2 exhibit similar behavior, as was shown in Table 2.1. Additionally, the average constant values of the $w(z)$'s on the circle agree with the values computed by our series methods to the order of accuracy available using the reflection method. However, we remind the reader that in our discussion of the reflection method we mentioned that it converges much more slowly in the number of levels of reflection N_{refl} and it is difficult to generate solutions with more than 5 or 6 digit accuracy, shown in Figure 2.2. It is important to note and emphasize that both the series approximations and the reflection approximations to $w(z)$ are analytic, as is the exact $w(z)$, and the real and imaginary parts cannot be specified independently on the boundaries.

Another computationally inexpensive measure of the discretization error for each `cgls` iteration, is the size of the last Laurent coefficients,

$$\epsilon_{a_k} = \max_{k=1:m} |a_{kj}| \quad (3.42)$$

as shown in Figure 4.9. Although we did not implement this condition in our method, it would be possible to adaptively increase the number of Fourier points N independently on each circle until the ϵ_{a_k} 's are on the order of machine epsilon.

In general, the greatest determining factor in the rate of decrease for the errors on each circles is the distance into each circle $w(z)$ can be extended analytically. As one would expect, this distance is determined by the nearest inner singularity to each boundary. The reflection method gives us a way to measure this distance. Recalling that the reflection method extends $w(z)$ analytically by reflecting the centers, and their previous reflections, successively through the circles, for two circles C_j and C_k , the nearest singularity inside C_j to C_k is determined by the limit of the successive reflections of the centers c_j . This limit is a fixed point ζ_{kj} of the Moebius maps formed by reflection in C_j followed by reflection in C_k , which is given by

$$z_j = c_j + \frac{r_j^2}{\bar{z} - \bar{c}_j} \quad (3.43)$$

and

$$z_{jk} = T(z) := c_k + \frac{r_k^2}{\bar{z}_j - \bar{c}_k} = c_k + \frac{r_k^2(z - c_j)}{r_j^2 + (\bar{c}_j - \bar{c}_k)(z - c_j)} \quad (3.44)$$

The two fixed points of T are found by solving $z = T(z)$, which leads to a quadratic equation

$$0 = (\bar{c}_j - \bar{c}_k)z^2 + ((\bar{c}_k - \bar{c}_j)(c_j + c_k) + r_j^2 - r_k^2)z + ((\bar{c}_j - \bar{c}_k)c_j c_k + r_k^2 c_j - r_j^2 c_k) \quad (3.45)$$

The two solutions ζ_j and ζ_k inside C_j and C_k respectively determine the singularities nearest the boundaries for each pair of circles. Finally, the rate of decay of the Laurent coefficients for the series converging in the exterior of C_j is then determined by the maximum value of

$$R_j = \max_k \frac{|\zeta_j - c_j|}{r_j}. \quad (3.46)$$

That is, $|a_{kj}| \leq CR_j^k$, as can be seen from the definition of a_{kj} .

3.5 Convergence

Following similarly to the details presented in [DMS23], we know that the velocity potential function $w(z)$ describing a flow over a set of m non-overlapping disks exists and is uniquely determined if the velocity at infinity and the circulations around each circle are either given or determined to satisfy some condition, such as the Kutta condition. Determining if our (analytic) Laurent series converges to the exact analytic solution is our next concern. We begin this discussion by working with the exact series for $w'(z)$, which we recall was given as

$$w'(z) = U + \sum_{k=1}^m \frac{i\Gamma_k}{2\pi(z - c_k)} - \sum_{k=1}^m \sum_{j=1}^{\infty} \left(\frac{r_k}{z - c_k} \right)^{j+1} \frac{ja_{k,j}}{r_k}.$$

Defining $b_0 := U$, $b_{k,1} := i\Gamma_k/2\pi r_k$, and $b_{k,j} := -ja_{k,j}/r_k$, for $j = 2, 3, \dots, \infty$ and $k = 1, 2, \dots, m$, we can rewrite this derivative in a more succinct form,

$$w'(z) = b_0 + \sum_{k=1}^m \sum_{j=1}^{\infty} \left(\frac{r_k}{z - c_k} \right)^j b_{k,j}.$$

Since the solution to the potential flow problem for a given circle domain is unique as long as U is specified and the Γ_k 's are given, this series satisfies our boundary conditions,

$$\text{Im} \{w'(z)\} = 0, \quad \text{for } z \in C_k, \quad k = 1, 2, \dots, m.$$

We next note that $w'(z)$ extends analytically across the C_k 's up to the radius determined by the nearest singularities inside C_k . So, from the last section, we have $|a_{k,j}| \leq CR_j^k$. Taking $R = \max_j R_j < 1$, we then have

$$|b_{k,j}| \leq C_j R^j \rightarrow 0 \quad \text{as } j \rightarrow \infty \tag{3.47}$$

for all j, k and some $C > 0$. Next, we consider the truncated series,

$$w'_J(z) = b_0 + \sum_{k=1}^m \sum_{j=1}^J \left(\frac{r_k}{z - c_k} \right)^j b_{k,j}. \tag{3.48}$$

Then, because

$$\left| \frac{r_k}{z - c_k} \right| \leq 1 \tag{3.49}$$

for $z \in C_j$ with $j = 1, 2, \dots, m$,

$$\text{Im } |w'_j(z)| \leq CJR^J \rightarrow 0 \quad \text{for} \quad J \rightarrow \infty, \quad (3.50)$$

for some $C > 0$. Therefore, if b denotes the vector of real and imaginary parts of the $b_{k,j}$'s, then b satisfies a linear system, derived from discretizing in z at N Fourier points on each circle, of the form,

$$A_S b = r + e. \quad (3.51)$$

Here r denotes the right-hand side for the discrete system and the error vector e , due to truncating the infinite series, satisfies $\|e\|_\infty = O(JR^J)$. Recall from the previous chapter that A_S is a $(Nm + m) \times (2Jm + m)$ matrix of full rank $2Jm + m$ when $J = N/2 - 1$. For a given domain, we have found that the outlying singular values of A_s , σ_1 and $\sigma_{2Jm+m} > 0$, do not change much with N . Therefore, the condition number of A_S is

$$\kappa(A_S) = \frac{\sigma_1}{\sigma_{2Jm+m}}, \quad (3.52)$$

and it does not grow with N . Next, let the SVD of A_s be given by

$$A_S = \sum_{j=1}^{2Jm+m} \sigma_j u_j v_j^T, \quad (3.53)$$

and let \hat{b} be the solution to the discrete system from above, now written in a more convenient form as

$$A_S \hat{b} = r, \quad (3.54)$$

Then

$$A_S(b - \hat{b}) = e \quad (3.55)$$

and therefore

$$\begin{aligned} b - \hat{b} &= A_S^{-1} e \\ \hat{b} &= b - A_S^{-1} e \\ \hat{b} &= b - \sum_{j=1}^{2Jm+m} u_j \frac{v_j^T}{\sigma_j} e. \end{aligned}$$

Since $\|e\|_\infty$ converges to 0 like $O(JR^J)$ as $N \rightarrow \infty$, \hat{b} will converge to b . We have therefore proven the following theorem.

Theorem 8. *If the circle domain bounded by given C_j , $j = 1, 2, \dots, m$ is such that the condition numbers of the family of matrices A_S formed for each N and $J = N/2 - 1$ remain uniformly bounded, then the approximate velocity potentials will converge to the exact potential $w(z)$ as $N \rightarrow \infty$.*

Having introduced our new method, we will next apply it to many types of examples to demonstrate its efficiency and accuracy.

CHAPTER 4

EXAMPLES OF FLOW CALCULATIONS

With all necessary tools in place, we can now review several examples involving potential flow computations utilizing our new series method. We will begin by considering potential flow within simple circle domains where either the Kutta condition is satisfied or we have set the circulation. Then we will look at potential flow over multiply-connected regions with smooth boundaries which only require the use of Fornberg's multiply connected exterior method to map the flow from the circle domain to the smooth bounded domains. Finally, we will close the chapter by looking at various examples involving computing the potential flow over sets of airfoils, which will require a composition of conformal maps including Karman-Trefftz to smooth the corners. All of these examples and discussions follow examples and discussions presented in [DMS21] and [DMS23].

4.1 Potential Flow in the Circle Domain

In our first set of examples, we will look at using the combined series method for computing the potential flow satisfying the Kutta condition within simple circle domains.

4.1.1 Example 1: Single Disk Example From Acheson

The example, demonstrated in Figure 4.1, comes from [Ach05, Chapter 4] as presented in [DMS21], shows the potential flow calculations for $m = 1$. Here we have used $N = 32$ Fourier points on the boundary and set the argument ϕ_1 of the stagnation point as $\phi_1 = -0.999\pi/2$, and the parameter

$$B = -\frac{\Gamma}{2\pi}|U|r_1 = 1.999999975. \quad (4.1)$$

When we compute the error on the boundary, ϵ , we find to be 3.0×10^{-16} . Using the imaginary part of Kutta condition equation, this method fails for $\psi_1 = -\pi/2$ even though there should be a stagnation point at $B = 2$ as in [Ach05], because we have $L_I = \underline{0}$ and $C_I = 0$. Using the real equation for Γ_1 we get $B = 2$, as is expected.

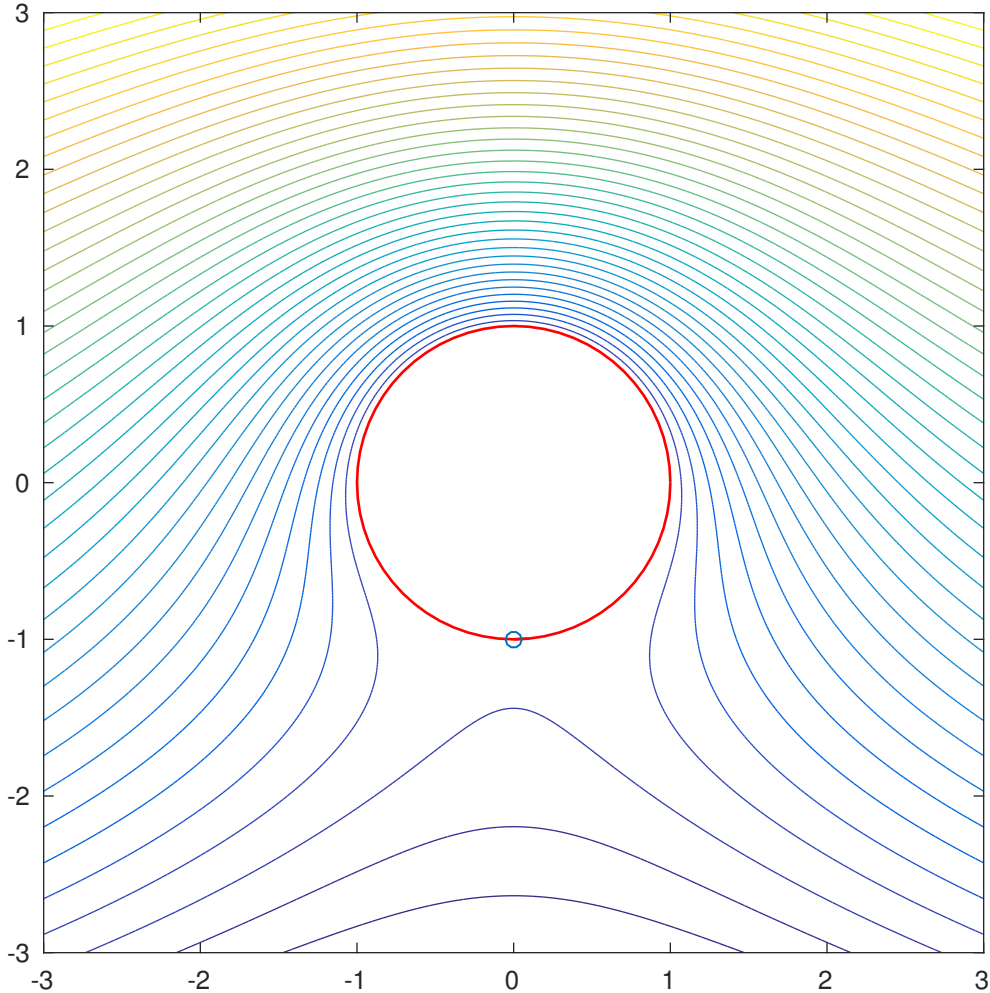


Figure 4.1: Test of Γ_1 calculation using series method and new system for $m = 1$.

4.1.2 Example 2: Flow Over a Set of Three Disks

The next example, as presented in [DMS21], we demonstrate the spectral accuracy of our combined system. The flow is computed using the full system, including solving for the Kutta condition, over a set of $m = 3$ disks as shown in Figure 4.2 computed with $N = 128$ and $J = 63$. Table 4.1, displays the spectral accuracy of our series method with increasing N . Figure 4.3 shows the nice grouping of the singular values. The rate of decrease of the errors of the boundary conditions for successive `cgls` iterates is shown in Figure 4.4. And finally, Figure 4.5 shows the decay of the magnitudes of the Laurent coefficients, $|a_{kj}|, j = 1, \dots, J$

for the $m = 3$ circles $C_k, k = 1, 2, 3$ numbered from left to right. The convergence of the successive iterates of the Γ_k 's is similar to that of the boundary conditions. We note that the rate of decrease of the errors for the cgl's iterates is independent of N until the level of discretization error is reached.

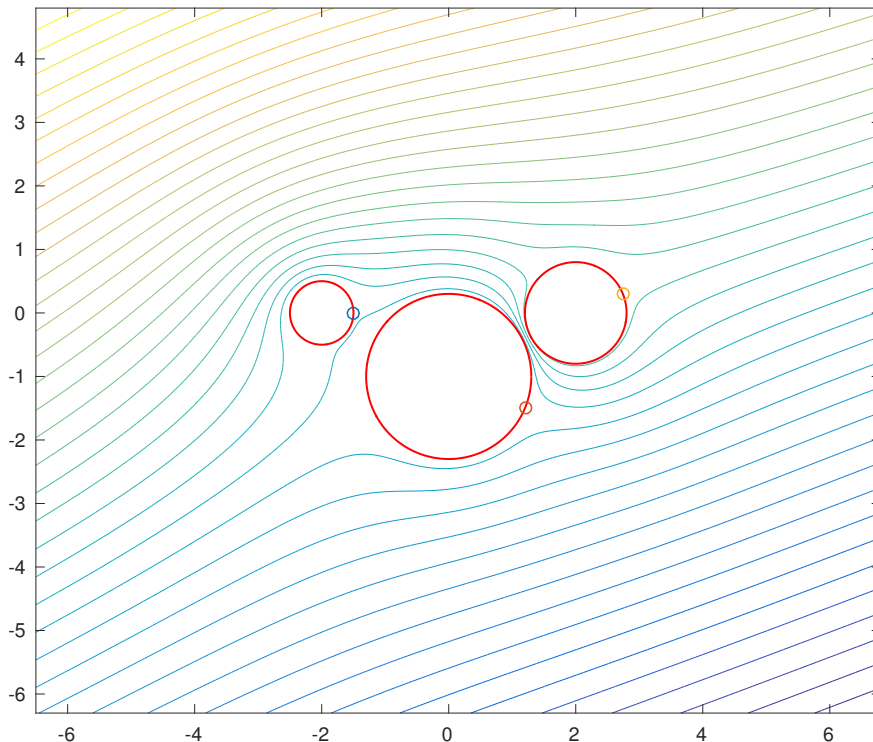


Figure 4.2: Flow over $m = 3$ disks using the new combined method solving for the Kutta condition using MATLAB contour plot.

Table 4.1: Comparison of typical timings in seconds on a laptop running MATLAB version R2012a, for $m = 3$ example, radius=[0.9 0.35 0.3], center=[0 1.4+0.6i -1+1i], $U = 1, \Gamma_i = 0$. We stop the cgl's iterations at k_ϵ , a few iterations after the error stops decreasing. The spectral accuracy with increasing N is clearly seen on each circle.

N	setup(sec)	cgl's(sec)(k_ϵ)	C_1 error	C_2 error	C_3 error
32	0.025	0.0046(20)	$.43 \cdot 10^{-3}$	$.16 \cdot 10^{-6}$	$.16 \cdot 10^{-6}$
64	0.053	0.0033(20)	$.51 \cdot 10^{-6}$	$.62 \cdot 10^{-11}$	$.11 \cdot 10^{-10}$
128	0.070	0.0067(25)	$.16 \cdot 10^{-11}$	$.16 \cdot 10^{-14}$	$.26 \cdot 10^{-14}$

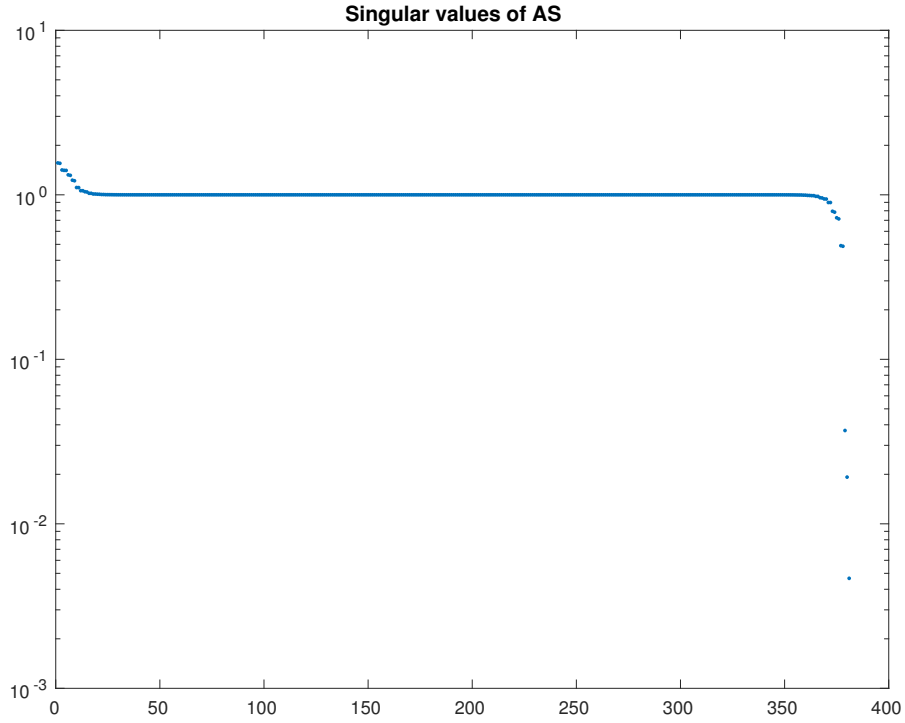


Figure 4.3: Singular values for system describing the flow shown in Figure 4.2.

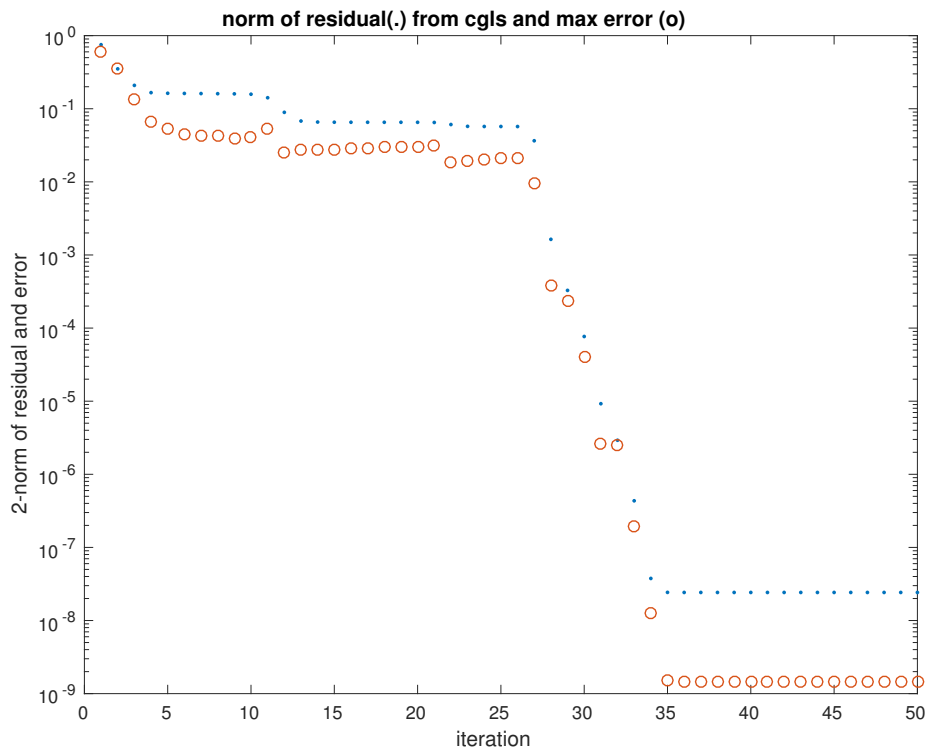


Figure 4.4: Boundary value error for successive cgls iterates.

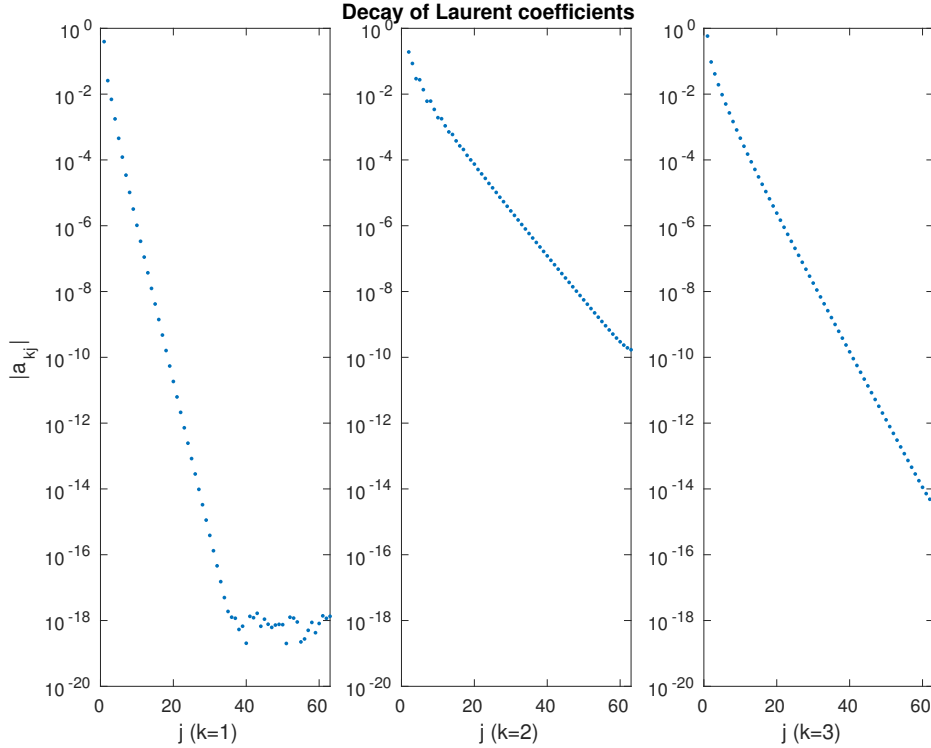


Figure 4.5: Log plot of the decay of the Laurent coefficients.

4.1.3 Example 3: Flow Over a Set of Eight Disks

In this example, as presented in [DMS23], we look at the flow computed using the full system, including solving for the Kutta condition, over a set of $m = 8$ disks as shown in Figure 4.6 using $N = 64$ and $J = 31$. The circulations were calculated so that the ‘O’s on the disks correspond to the stagnation points. Figure 4.7 shows the similar grouping of the singular values that we saw in the previous example. Figure 4.8 shows the error ϵ on the boundary, and Figure 4.9 shows the decay of the Laurent coefficients. As expected we have the same spectral accuracy that we saw in the previous example. In general, this holds for all flows computed in the circle domain.

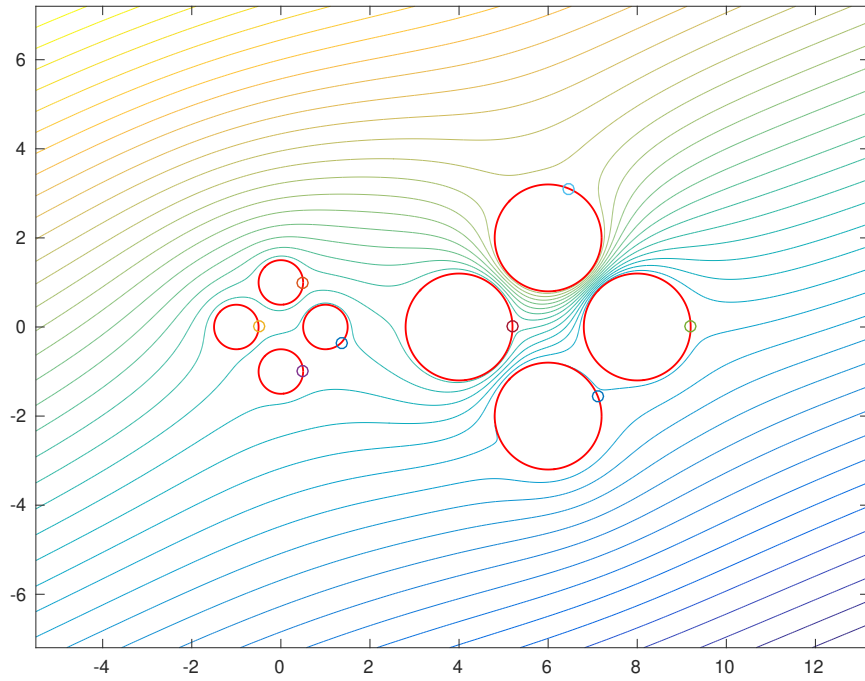


Figure 4.6: Contour plot of the flow over $m = 8$ disks using the new combined method solving for the Kutta condition using MATLAB contour plot.

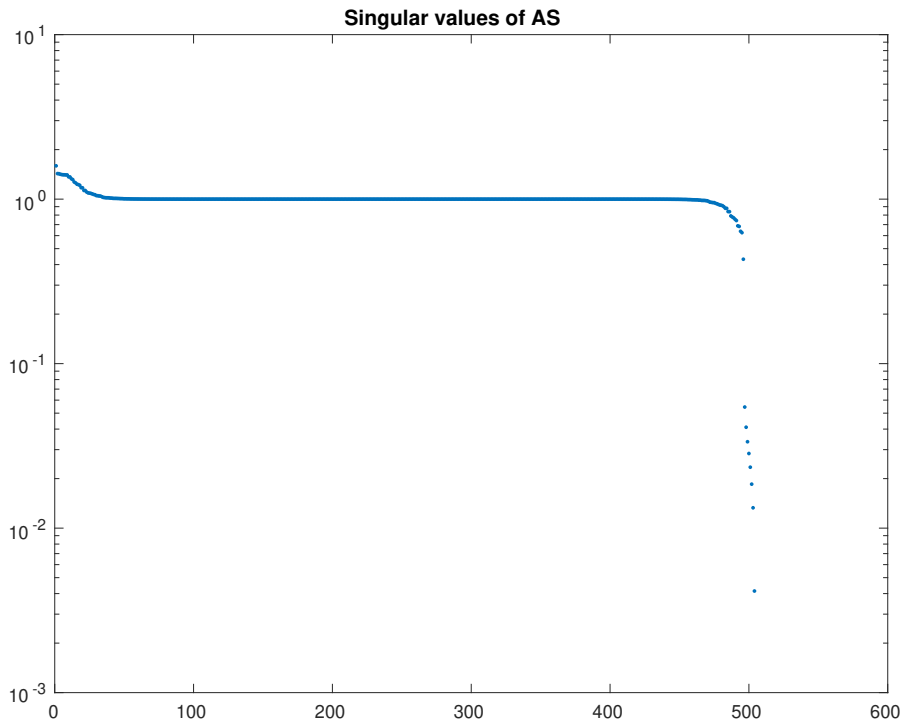


Figure 4.7: The singular values of the system for $m = 8$ circles.

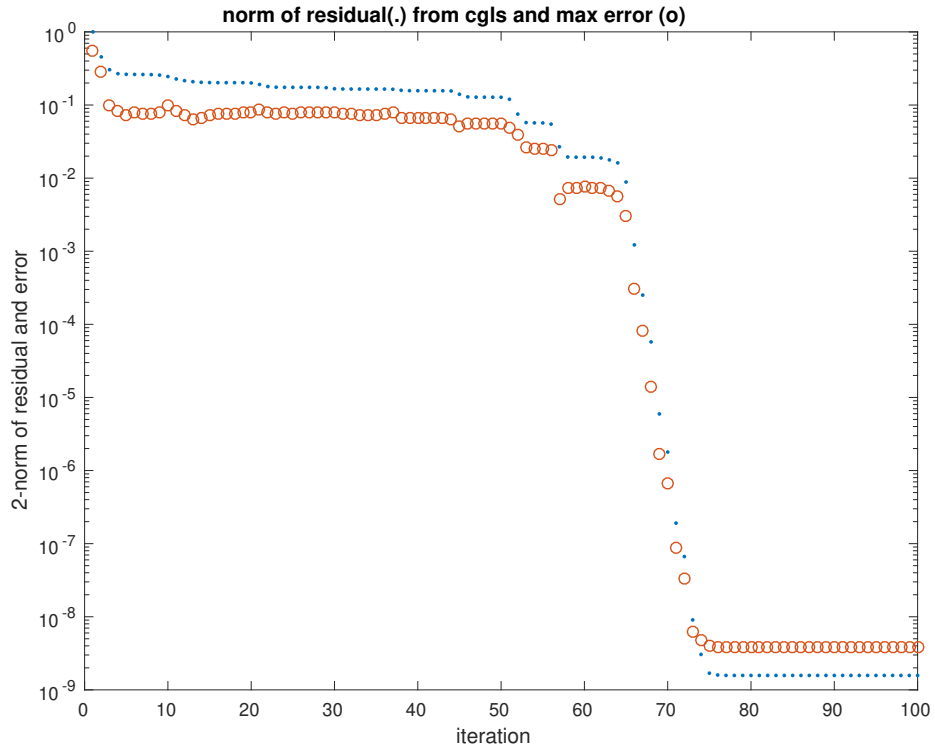


Figure 4.8: Boundary error ϵ of the system for $m = 8$ circles.

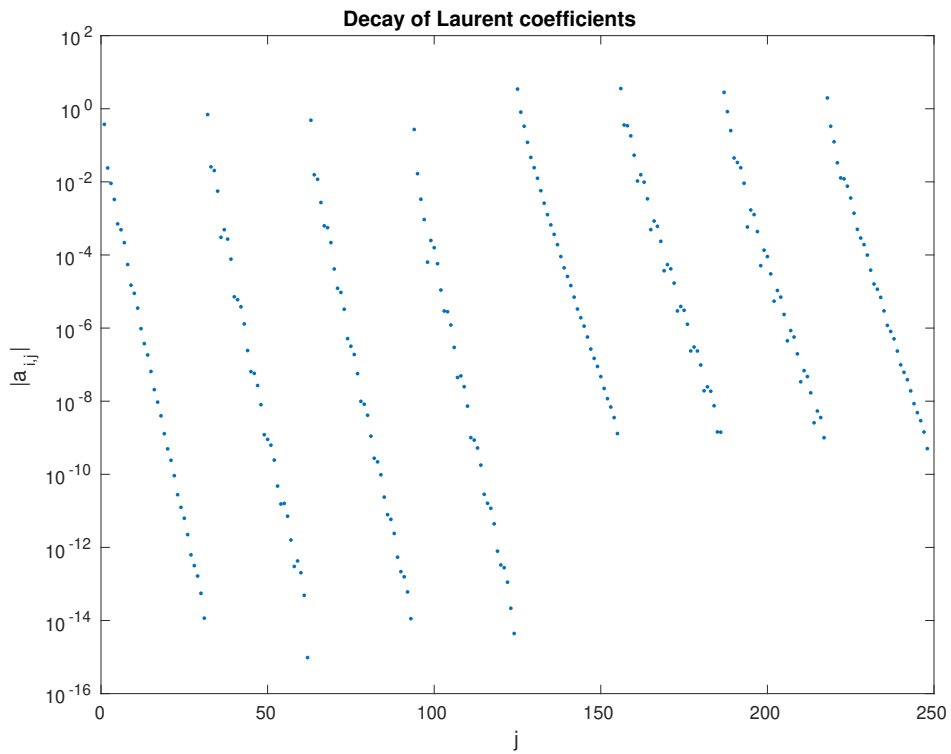


Figure 4.9: Log plot of the decay of the Laurent coefficients for each of the $m = 8$ circles.

4.1.4 Example 4: Efficiency for High Connectivity

In our final example of this section, as presented in [DMS21], we address the efficiency of our method for regions with high connectivity. In Figure 4.10 we have the contour plot for the potential flow over a set of $m = 16$ disks as computed by our combined system with stagnation points at the ‘O’s. Table 4.2 gives a comparison of the efficiency between the new method and the least squares method in terms of operation counts. We see that the new method, with an operation count of $O(mN)^2$ is faster than the least squares method, with an operation count of $O(mN)^3$. In Figure 4.11 we have plotted the norm of the residual and the error for 200 `cgl`s iterations.

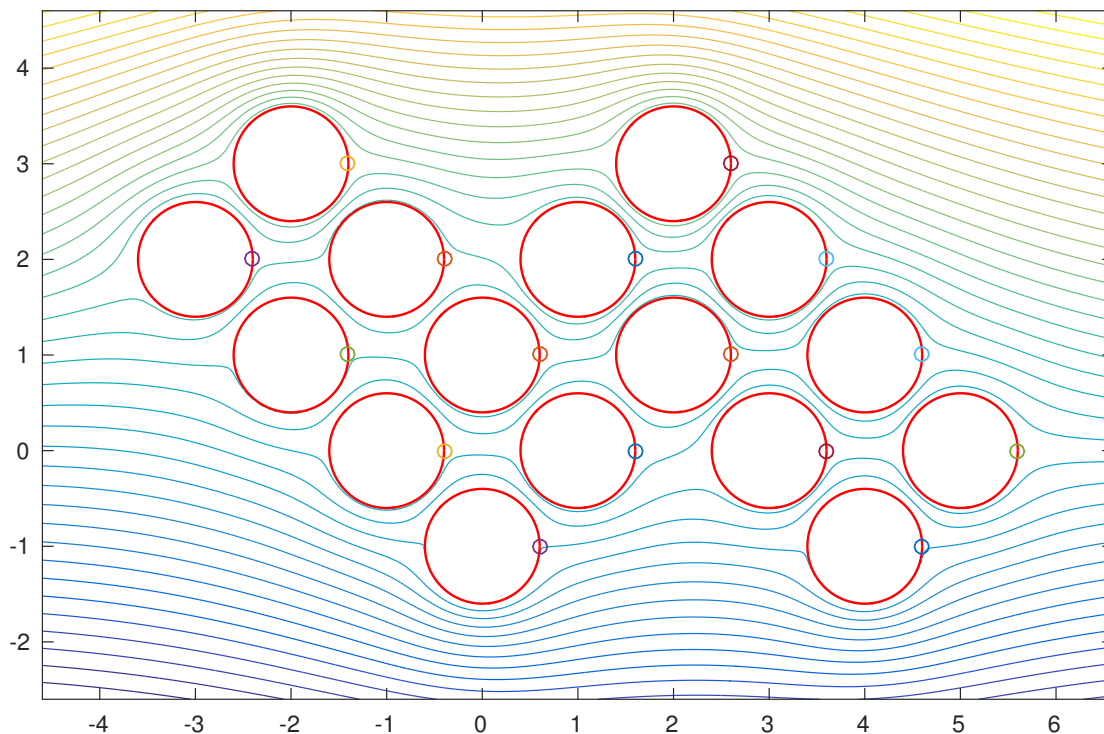


Figure 4.10: Flow over $m = 16$ disks using the new method with $N = 64, J = 31$.

Table 4.2: Comparison of typical timings in seconds on a laptop running MATLAB version R2012a, for $m = 16$ example, using least squares/backslash (left) and cgls (right). cgls is iterated iter. steps—slightly more than the number of steps needed to achieve the minimum error.

least squares			new method		
N	error	backslash(sec)	N	error	cgls(iter.)
33	$.77 \cdot 10^{-5}$	0.04	32	$.89 \cdot 10^{-5}$	0.03 (100)
65	$.30 \cdot 10^{-9}$	0.47	64	$.36 \cdot 10^{-9}$	0.42 (200)
129	$.78 \cdot 10^{-15}$	3.34	128	$.10 \cdot 10^{-13}$	1.85 (250)
257	$.16 \cdot 10^{-14}$	26.03	256	$.24 \cdot 10^{-13}$	1.89 (300)

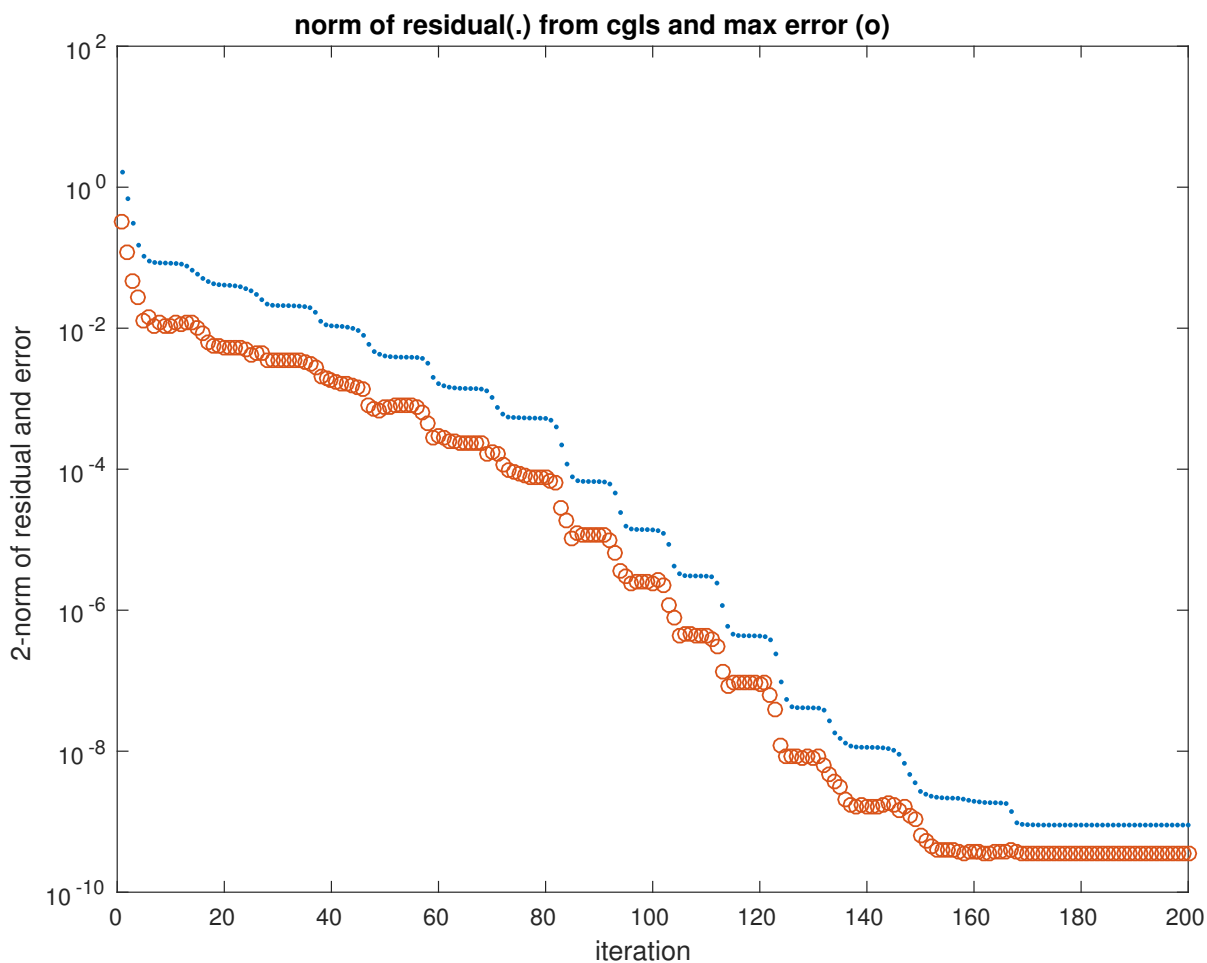


Figure 4.11: Errors and residuals for 200 cgls iterations of flow in Figure 4.10.

4.2 Flow Over Multiply Connected Smooth Domains

In our second set of examples we will look at applying the new series method for computing the potential flow in the exterior circle domain and mapping it to the exterior of smooth boundaries. In these cases the circulations have been chosen arbitrarily.

4.2.1 Example 5: Flow Over Two Smooth Boundaries

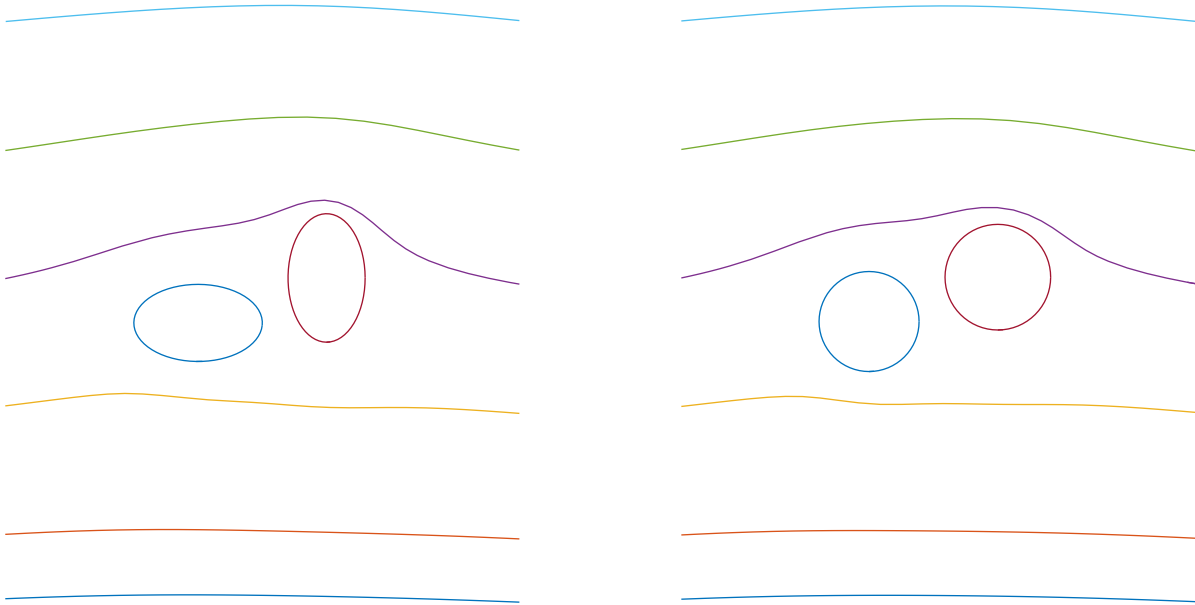


Figure 4.12: Streamlines for flow exterior to $m = 2$ ellipses with $N = 6, \Gamma_1 = \Gamma_2 = 2, U = 1$.

Our first example of this section was presented in [DMS23] and it addresses the accuracy associated with conformally mapping the computed potential from the circle domain into domains with smooth boundaries. In Figure 4.12 we have computed the flow over $m = 2$ ellipses. The circulations were given by $\Gamma_1 = \Gamma_2 = 2$, and we've chosen $J = N/2 - 1$ for our discretization resulting with $\sigma_{min}(A_S) \approx 0.8$ for all N . For the conformal mapping code, we have used $N_s = 8000$ knots in the periodic cubic spline used to fit the ellipse boundary. The errors for the average values of $\text{Im}\{w(z)\}$, list in Table 4.3, evaluated at $2N$ Fourier points converge roughly quadratically as N is doubled. Table 4.3 also lists the error for the

conformal mapping function $f(z)$. This error is estimated by how closely the map's real and imaginary parts, evaluated at $2N$ Fourier points on the circles, satisfy the equations for the elliptical boundaries. As one would expect for analytic boundaries, these errors also converge quadratically in N . We get similar accuracy using the analytic parameterization for the elliptical boundaries.

Table 4.3: Average values of $\text{Im } w(z), z \in C_1, C_2$, for $m = 2$ smooth boundaries and overall accuracy of conformal map in Figure 4.12.

N	$\text{Im } w(z), z \in C_1$	$\text{Im } w(z), z \in C_2$	map accuracy
16	0.114391338010714	-0.350081754431789	$1.1 \cdot 10^{-02}$
32	0.114295133088431	-0.349692481939068	$5.6 \cdot 10^{-05}$
64	0.114295784168430	-0.349691589528057	$9.1 \cdot 10^{-09}$
128	0.114295784171233	-0.349691589519629	$1.6 \cdot 10^{-14}$
256	0.114295784171233	-0.349691589519634	$1.6 \cdot 10^{-14}$

4.2.2 Example 6: Flow Over Four Smooth Boundaries

In another example from [DMS23], we consider the flow over $m = 4$ smooth boundaries with $N = 256$ Fourier points on each boundary and circulations of 2 around the smaller circles and -2 around the larger one. The contour plot for the potential flow is shown in the respective domains by the top two images. As we noted in the Chapter 3, the decay of the Laurent coefficients can give us a gauge of the level of accuracy of our computations. The bottom plots in Figure 4.13 show us this decay in terms of the log plots of the magnitude of the Laurent coefficients. The near-linear appearance to this decay suggest the spectral accuracy of our methods for smooth curves. In both cases we have discretized our system with $J = N/2$ coefficients.

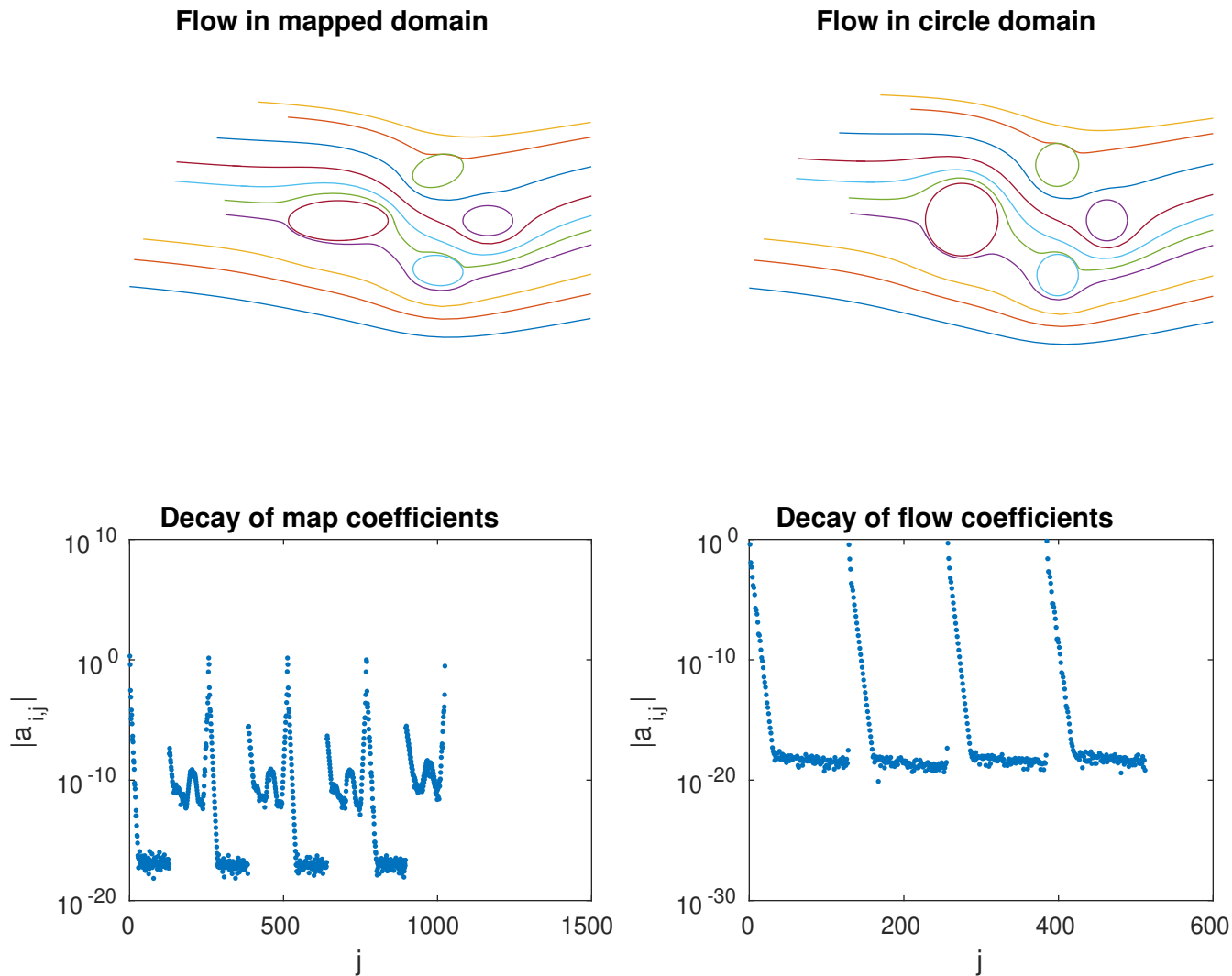


Figure 4.13: Potential flow over $m = 4$ smooth boundaries with $N = 256$.

4.2.3 Example 7: Flow Over Five Smooth Boundaries

The next example, presented in [DMS23] and shown in Figure 4.14, is computing the potential flow over $m = 5$ smooth boundaries with $N = 128$ Fourier points on each boundary. The flow is uniform at ∞ with $U = 1$ and the circulations have been specified around each of the circles. The target boundaries, or “physical” boundaries when we talk about airfoils later, are given and Fornberg’s conformal mapping method is used to compute the Laurent

series $f(z)$ for the map and the centers and radii of the unique, conformally equivalent circles with $f(z)$ normalized by $f(z) \approx z$ for $z \rightarrow \infty$.

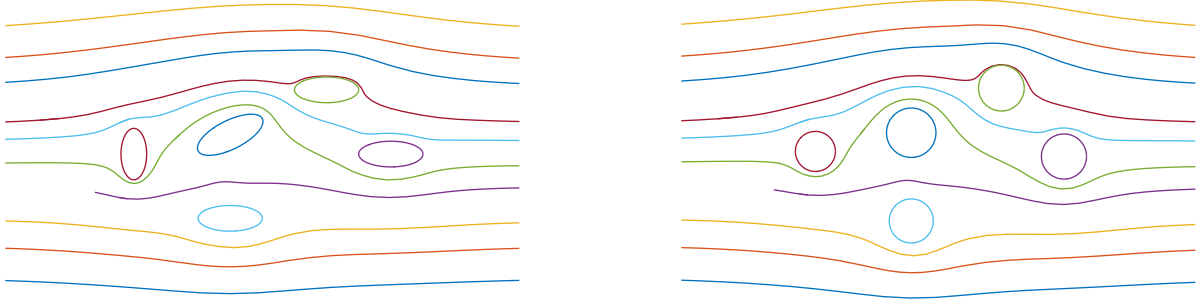


Figure 4.14: Potential flow over $m = 5$ smooth boundaries with $N = 128$.

4.2.4 Example 8: Flow Over Regions of Increasing Multiplicity with Smooth Boundaries

For our final example, as presented in [DMS23], we look at the timings, shown in Table 4.4 for computing the map and potential flow over smooth regions in Figure 4.15 with connectivities $m = 2, 4, 8$ computed in MATLAB on a laptop. For the conformal map computations we have fixed number of Newton iterations at 10 and the number of conjugate gradient iterations at 30. For the potential flow computations we have fixed the number of `cgl`s iterations at 20. This results in an accuracy of about 10^{-14} for all cases. The dominant operation count in these computations is the $O((mN)^2)$ matrix-vector multiplications for solving the conjugate gradient solutions. We note that the timings here are similar for airfoils where the circulations and preliminary Karman-Trefftz maps have to be computed.

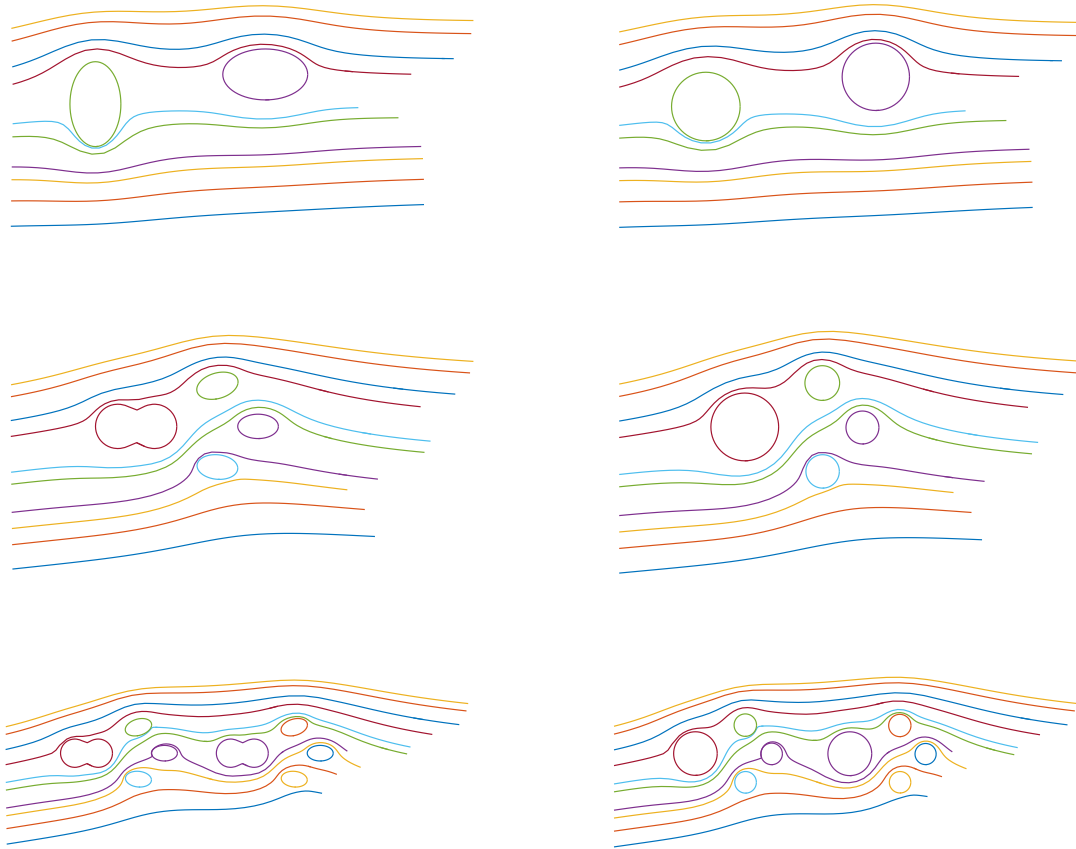


Figure 4.15: Potential flow over $m = 2, 4, 8$ smooth boundaries with $N = 64$ for timings in Table 4.4. The circulations are given.

Table 4.4: Sample timings for domains in Figure 4.15.

N	$m = 2$		$m = 4$		$m = 8$	
	map	sec flow	map	sec flow	map	sec flow
64	0.07	0.54	0.20	0.82	0.58	1.95
128	0.15	0.82	0.49	1.86	1.98	6.55
256	0.50	1.44	2.05	4.60	7.96	20.09
512	2.54	4.67	9.69	19.98	79.23	101.97
1024	38.19	22.23	104.69	105.71	603.35	601.68

4.3 Flow Over Multi-Element Airfoils

In our third and final set of examples we look at computing the potential flow over sets of airfoils. We will briefly explain the process of mapping between the “physical” airfoil domain and the computational circle domain. We will also set up the calculations for the pressure curves of the airfoils using our computed potential flows, and then apply these to compute and plot the pressure curves in each example.

4.3.1 Mapping from the Airfoil Domain to the Circle Domain

For regions that do not necessarily have smooth boundaries, such as airfoils, we need to use maps such as Karman-Trefftz to remove any corners. Indeed, suppose that we now have m airfoils defined by boundaries $\partial\Omega_i$ for $i = 1, 2, \dots, m$. We begin by smoothing the trailing edge corners of the $\partial\Omega_i$ by successively applying the Karman-Trefftz transformation k_i to each of the airfoils. This produces a multiply connected region with nearly circular, smooth boundaries. We can then use Fornberg’s method, as in the previous section, to find the Laurent coefficients of the mapping function h from a domain exterior to nonoverlapping disks to the exterior of a domain with smooth boundaries. Inverting the Karman-Trefftz maps to produces the composite map,

$$Z = f(z) = k_1^{-1} \circ k_2^{-1} \circ \dots \circ k_m^{-1} \circ h(z), \quad (4.2)$$

from the circle domain to the airfoil domain. The potential flow is computed in the circle domain using the series method developed in Chapter 3, with circulations computed to satisfy the Kutta condition, and mapped back to the airfoil domain.

This procedure is illustrated in Figure 4.16 for the map exterior of $m = 4$ cosine airfoils, on the left, with the center image showing the four smooth regions resulting from applying four successive Karman-Trefftz maps to smooth the trailing edges and the method from [BDHW07] to compute the map from the exterior of the circles on the right to the smooth domain in the center. The X’s mark the images of the trailing edges which are computed on the circles by interpolating the boundary correspondences so that the Kutta

condition can be applied. As we have noted in the previous chapter, it is necessary to continuously track the roots for the Karman-Trefftz maps to ensure we are always on the appropriate complex branch. So, we will use such a function in all of our examples involving the Karman-Trefftz map.

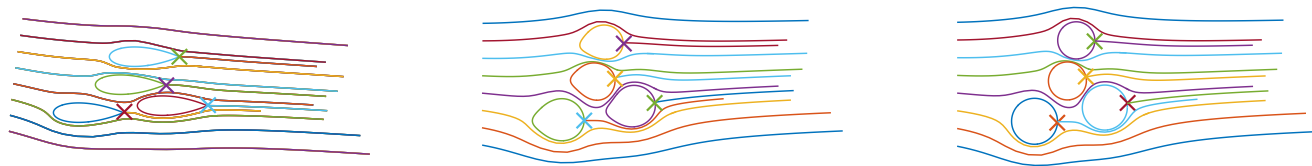


Figure 4.16: Conformal map $f = k^{-1} \circ h$, where composition of Karman-Trefftz maps $k = k_1 \circ k_2 \circ k_3 \circ k_4$ successively, smoothing corners (left), Laurent series map h maps from circle domain (right) to smooth domain (center), and potential flow with Kutta condition at trailing edges (X) is computed in circle domain by Laurent series and $N = 128$ Fourier points on each circle.

The cosine airfoils in this example are given by

$$\gamma(\sigma) = -\cos(K\sigma)e^{i\sigma}, \quad -\frac{\pi}{2K} \leq \sigma \leq \frac{\pi}{2K},$$

with the trailing edge interior angle π/K and $K = 4$. We can then calculate the exterior angle by

$$\beta\pi = 2\pi - \frac{\pi}{4} = \frac{7\pi}{4},$$

which is then removed by the Karman-Trefftz with

$$\delta = \frac{1}{\beta} = \frac{K}{2K-1} = \frac{4}{7}.$$

Of course the β need not be the same on each airfoil, but this example at least illustrates the process we will be using to compute the potential flow. In order to plot streamlines originating near the stagnation points at the trailing edges, we use that fact that since $w'(z) = u - iv$, we need only solve the following system numerically with MATLAB `ode45`,

$$\frac{dx}{dt} = u = \text{Re}\{w'(z)\} \quad \text{and} \quad \frac{dy}{dt} = v = -\text{Im}\{w'(z)\}.$$

The streamlines in the circle domain are then mapped to the airfoil domain.

4.3.2 Calculating Pressures

Pressure on the exterior of an airfoil is one of the important values that can be calculated once the velocity potential has been computed. We will calculate the pressure p around the boundaries of the airfoils using Bernoulli's law,

$$p = 1 - |V|^2,$$

where V is the velocity. Letting Z be the physical plane containing the airfoils Ω_i , the velocity potential $W(Z)$ in the airfoil domain in terms of the velocity potential $w(z)$ in the circle domain and the conformal map $Z = f(z)$ is given by

$$W(Z) = W(f(z)) = w(z) = w(f^{-1}(Z)).$$

Then, the velocity V is given by,

$$\bar{V} = \frac{dW}{dZ} = \frac{d}{dZ}w(f^{-1}(Z)) = w'(z)\frac{dz}{dZ} = \frac{w'(z)}{dZ/dz} = \frac{w'(z)}{f'(z)}.$$

At ∞ we need the uniform velocity in the physical Z -plane, U_Z to satisfy

$$\bar{U}_Z = \frac{w'(\infty)}{f'(\infty)} = \frac{\bar{U}}{f'(\infty)},$$

where U is the uniform velocity in the circle z -plane. Next, because we know that $f(z) = k^{-1}(h(z))$, by the chain rule we have

$$f'(z) = (k^{-1})'(h(z))h'(z).$$

Next, we know that for the Fornberg map $h(z)$, $h(\infty) = \infty$ and $h'(\infty) = 1$, based on the normalization condition $f(z) = z + O(1/z)$ for $z \approx \infty$. Also, for a single inverse Karman-Trefftz map, $k_i^{-1}(\zeta)$, a calculation gives

$$(k_i^{-1})'(\infty) = \frac{1}{\beta} \left(\frac{z_2 - z_1}{\zeta_2 - \zeta_1} \right).$$

Putting these all together, we need

$$\bar{U} = \bar{U}_Z f'(\infty) = \frac{\bar{U}_Z}{\beta} \left(\frac{z_2 - z_1}{\zeta_2 - \zeta_1} \right)$$

4.3.3 Example 9: Three Cosine Airfoils

Presented in [DMS23] and shown in Figure 4.17 we display example of the mapping and potential flow calculations for $m = 3$ cosine airfoils along with the pressure curves for the airfoils shown respectively from left to right. The cosine airfoils are constructed using the same formula as before with $K = 4$. For this case we have with $U = e^{i\pi/16}$ and $N_s = 100$. The potential flow with the Kutta condition at the trailing edges, X's is computed in the circle domain by the series method with $n = 128$ Fourier points on each circle.

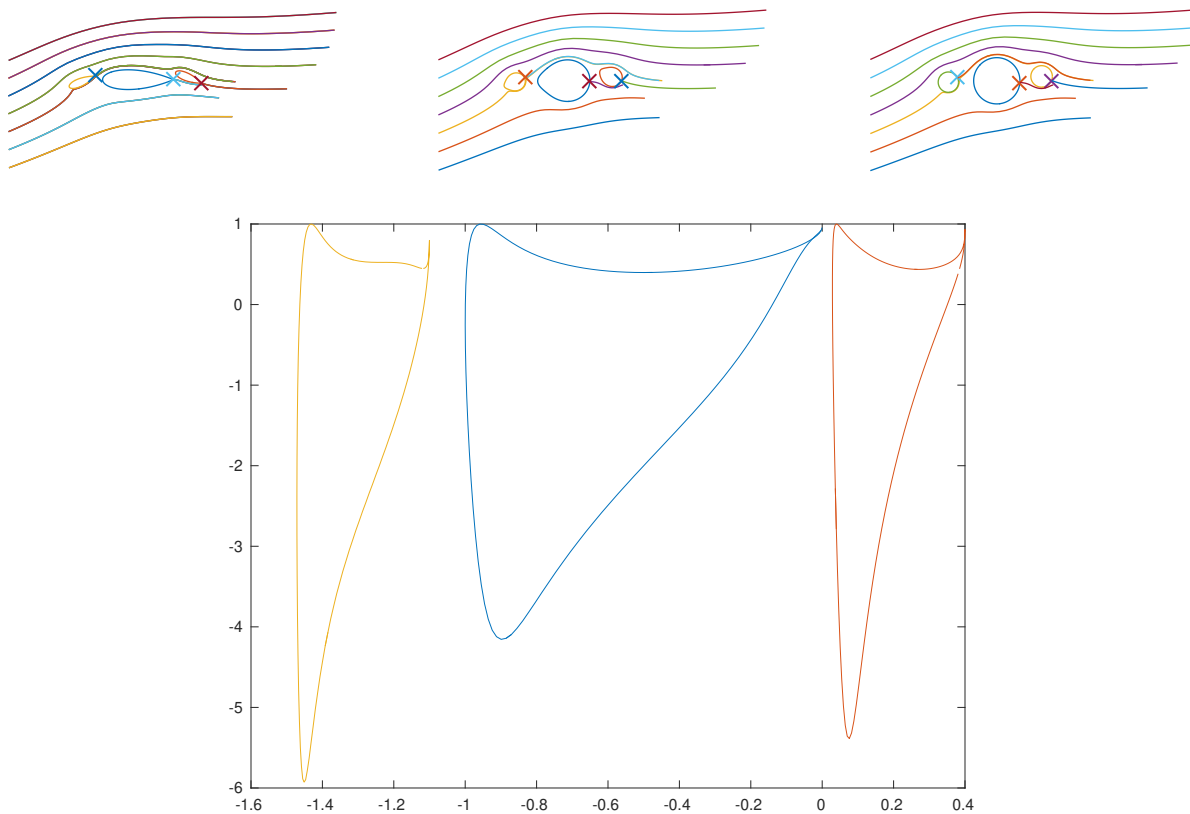


Figure 4.17: Conformal map between airfoil domain and circle domain along with potential flow. Pressures on the upper and lower portion of each airfoil are plotted in the lower figure. The horizontal axis is the real part of the points on the airfoil.

For this example, we solved the full system to find the Laurent coefficients and the circulations satisfying the Kutta condition, with our computed errors given in Table 4.5

below. We list the values for the circulation Γ_1 , the $\text{Im}\{w(z)\}$ at $2N$ Fourier points, and the argument ϕ_1 of the stagnation point for the larger(middle) circle C_1 . With this data we see much slower convergence rates and little improvement in accuracy with increasing N . In fact, the values do not improve much beyond 6 digits of accuracy. This limitation is a result of the accuracy of the conformal map as it is computationally difficult to locate the preimages, with arguments ϕ_k , of the trailing edges of the airfoils. In general, they do not fall on Fourier points on the circles, and consequently their locations must be computed through interpolation. This interpolation process begins with approximating the inverse of the boundary correspondence $\theta_k = \theta_k(S)$ by interpolation of the mesh points with a cubic spline. Then the images of trailing edges on the smooth boundaries will be either $\phi_k = \theta_k(0)$ or $\theta_k(2\pi)$. The limiting accuracy is that of the cubic spline interpolation, which is roughly third order, as can be seen in the table. In general, it is difficult to compute conformal maps to domains with corners accurately to more than a few digits using Fourier series based methods. A more in-depth discussion about these properties is available in [DS18].

Table 4.5: Accuracy of Γ_1 , $\text{Im } w(z)$, $z \in C_1$, and ϕ_1 for middle circle and overall accuracy ε in Figure 4.17, $m = 3$, $Ns = 8000$, $J = N/2 - 1$. The accuracies for C_2 and C_3 are similar. $\sigma_{\min}(AS) \approx 10^{-2}$ for all N .

N	Γ_1	$\text{Im } w(z), z \in C_1$	ϕ_1	ε
32	1.0958944619	-0.0700282779	6.2698640405	$9.8 \cdot 10^{-07}$
64	1.3914187475	-0.0733887932	6.2113250060	$4.3 \cdot 10^{-11}$
128	1.3905777394	-0.0733406660	6.2102720760	$5.4 \cdot 10^{-16}$
256	1.3905512683	-0.0733404812	6.2102694711	$6.4 \cdot 10^{-16}$
512	1.3906294182	-0.0733411579	6.2102693434	$1.0 \cdot 10^{-15}$
1024	1.3906293929	-0.0733411724	6.2102699099	$3.1 \cdot 10^{-15}$

4.3.4 Example 10: Two-Airfoils From Williams

The next example we include, was presented in [DMS23] but originates from a paper by Williams [Wil73, Config.A]. This example involves two airfoils with a specific geometric setup, see [Wil73, Fig 8] where, one of the airfoils is larger, acting as the “main” airfoil, while the second is much smaller and is positioned behind the main airfoil, and rotated down by 30° to act as a “flap”. The geometric information and parameters for this setup can be found in [Wil73, Tables 1 and 2, pp. 19 - 21], but an example of it, with the computed potential flow, is shown in Figure 4.18.

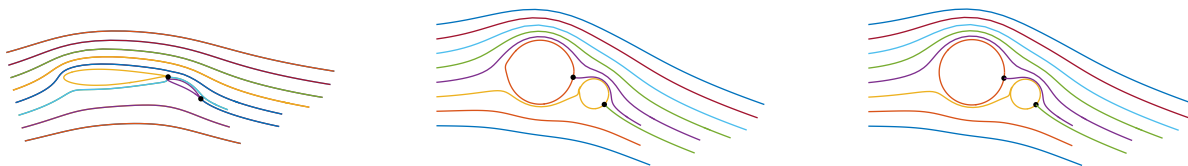


Figure 4.18: Flow for configuration A from [Wil73] using the full series with $N = 128$.

We have computed the conformal mapping and potential flow with the Kutta condition using the combined linear system 3.40 to solve for the Laurent coefficients and circulations. The angle of attack $\alpha = 0$ and we have chosen $N = 128$ Fourier points on the boundary and $k_{steps} = 25$ conjugate gradient iterations. Also, we have smoothed the Fornberg map iterations by zeroing the three highest-order Fourier coefficients.

Table 4.6: Computed circulation comparison from [Wil73] between the reflection method and our new method using $N = 128$ Fourier points on the boundary.

Source	Main Airfoil	Flap
	Γ_1	Γ_2
Williams Paper	1.3909	0.4784
New Method	1.3889486...	0.4773498...

Table 4.6 contains a comparison between the computed circulations from [Wil73] and our new method. Williams used the reflection method discussed in Chapter 2 to compute the potential flows, as in [DS18], which is generally less accurate than the series method unless many levels of reflection are used. Furthermore, one typically only expect 2 to 4 digit accuracy when composing Fourier series conformal mapping methods with methods to smooth corners, see [BDS19] for more information on this limitation. Though, in practice, airfoil shapes are not defined more accurately, so this is not a serious limitation.

Finally, we have plotted the pressure curves in Figure 4.19 for the setup. Comparing these pressure curves computed by our method with those in [Wil73, Tables 9 and 10, pp.32-33] we see that the shapes and ranges are similar.

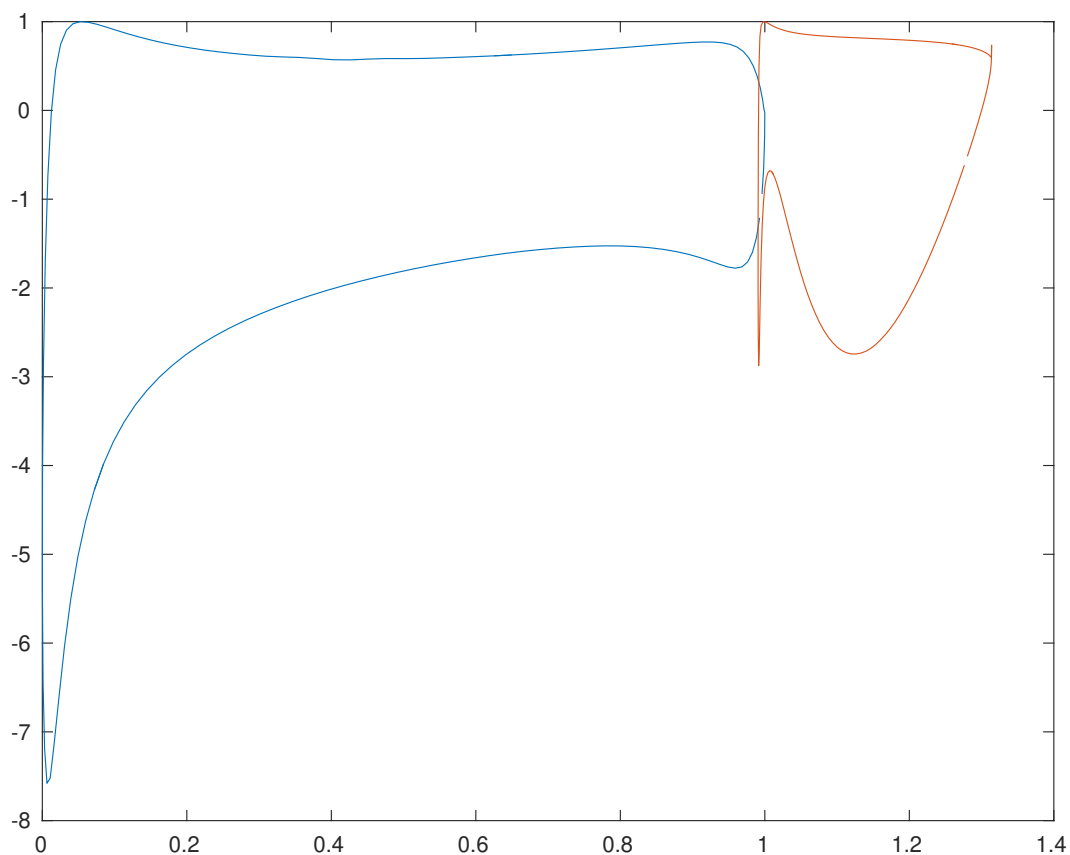


Figure 4.19: Pressure curves for configuration A from [Wil73] using the full series with $N = 128$.

4.3.5 Example 11: Three-Airfoils from Suddhoo and Hall

In our penultimate example, we look at Configuration B from Suddhoo and Hall [SH85], originally presented in [DMS23] and shown here in Figure 4.20. The airfoil setup is constructed by applying $m = 3$ inverse Karman-Trefftz transformations successively to chosen circles. We then use a different sequence of Karmann-Trefftz maps to smooth the corners and compose with the Laurent series maps in order to apply the combined linear system 3.40 to compute the Laurent coefficients and the circulations with $N = 128$ Fourier points on each boundary.

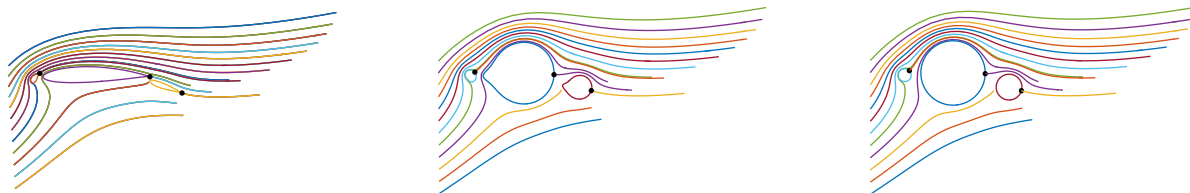


Figure 4.20: Flow for configuration B from [SH85] using the full series method with $N = 128$ and angle of attack $\alpha = 20^\circ$ using $k_{steps} = 35$ cg iterations. Operation counts for the flow and the map are $O((mN)^2 \times k_{steps})$.

Sample Timings, Circulation values, and boundary value error are provided in Table 4.7 for various values of N Fourier points.

Table 4.7: Sample timings (sec), circulations, Γ_i , and accuracy of the MATLAB code on a laptop for a set of airfoils from [SH85] for $m = 3$ configuration B with angle of attack $\alpha = 20^\circ$.

N	map	flow	Γ_1	Γ_2	Γ_3	ϵ
32	0.12	0.30	1.46716332	0.8929293	6.4021316	$1.4 \cdot 10^{-04}$
64	0.23	0.34	1.46893074	0.8825023	6.4254065	$1.8 \cdot 10^{-07}$
128	0.77	0.55	1.46857660	0.8840742	6.4221982	$9.9 \cdot 10^{-13}$
256	3.37	1.08	1.46856840	0.8841090	6.4221244	$1.2 \cdot 10^{-14}$

Comparing the $N = 128$ values with those from [SH85, Table 5] given by

$$\Gamma_1 = 1.4747 \quad \Gamma_2 = 0.8849, \quad \Gamma_3 = 6.4355$$

we see that our values are pretty similar. Additionally, the increase in accuracy shown in the table of about one decimal place for each doubling of N illustrates the roughly third-order accuracy due to the spline interpolation used in finding the preimages of the trailing edges. The error of the boundary points, defined in Chapter 3, is roughly spectral. Finally, we have pressure curves plotted in Figure 4.21 for the three airfoils in Figure 4.20. These curves are similar to [SH85, Figure 10].

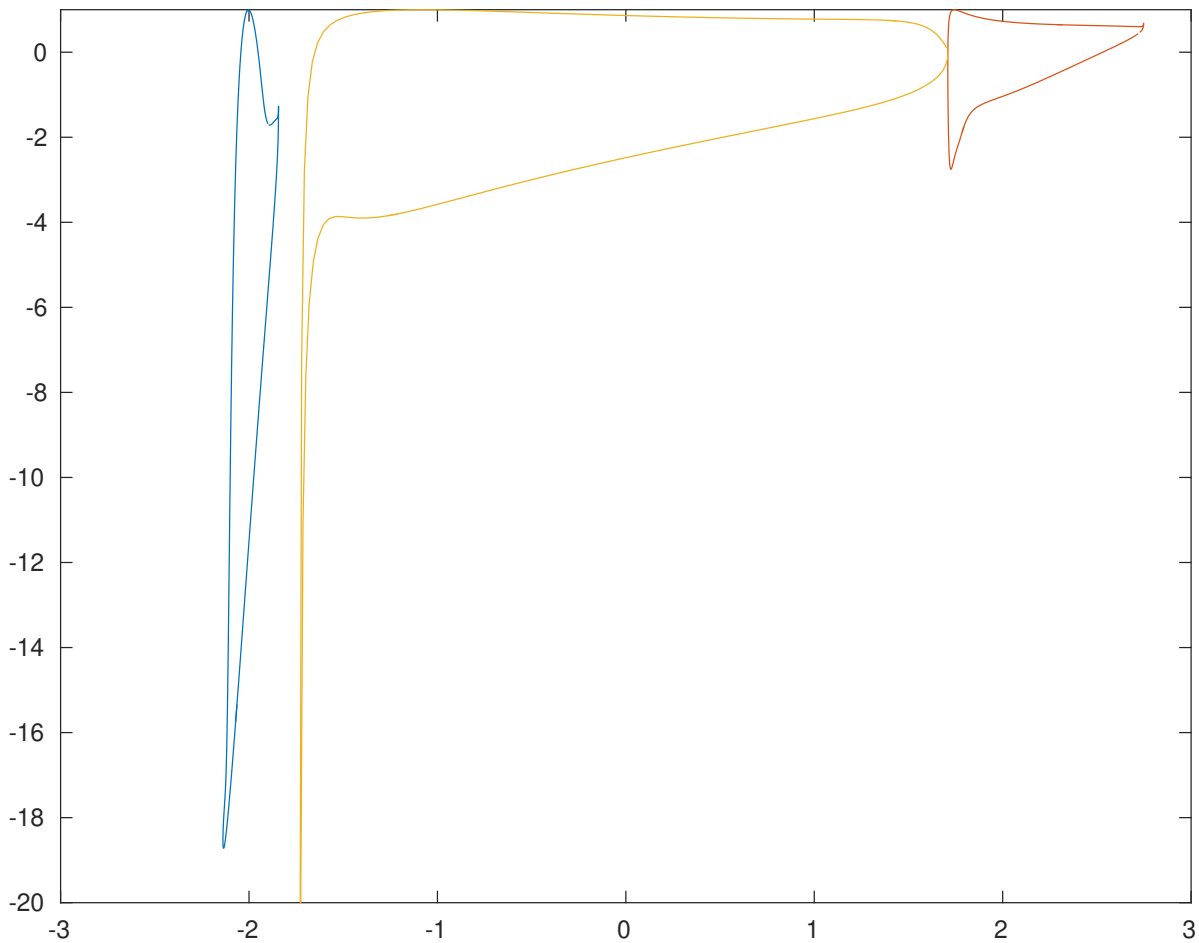


Figure 4.21: Pressure curves for the airfoils in configuration B from [SH85] computed using our methods demonstrated in Figure 4.20.

4.3.6 Example 12: Four-Airfoil from Suddhoo and Hall

In our final example of this section, we look at configuration A from Suddhoo and Hall [SH85] and originally presented in [DMS23]. Configuration A from Suddhoo and Hall is an exact test case generated by applying $m = 4$ inverse Karman-Trefftz transformations successively to chosen circles. The exact map from the exterior of 4 disks is produced by the sequence of map shown in Figure 4.22.

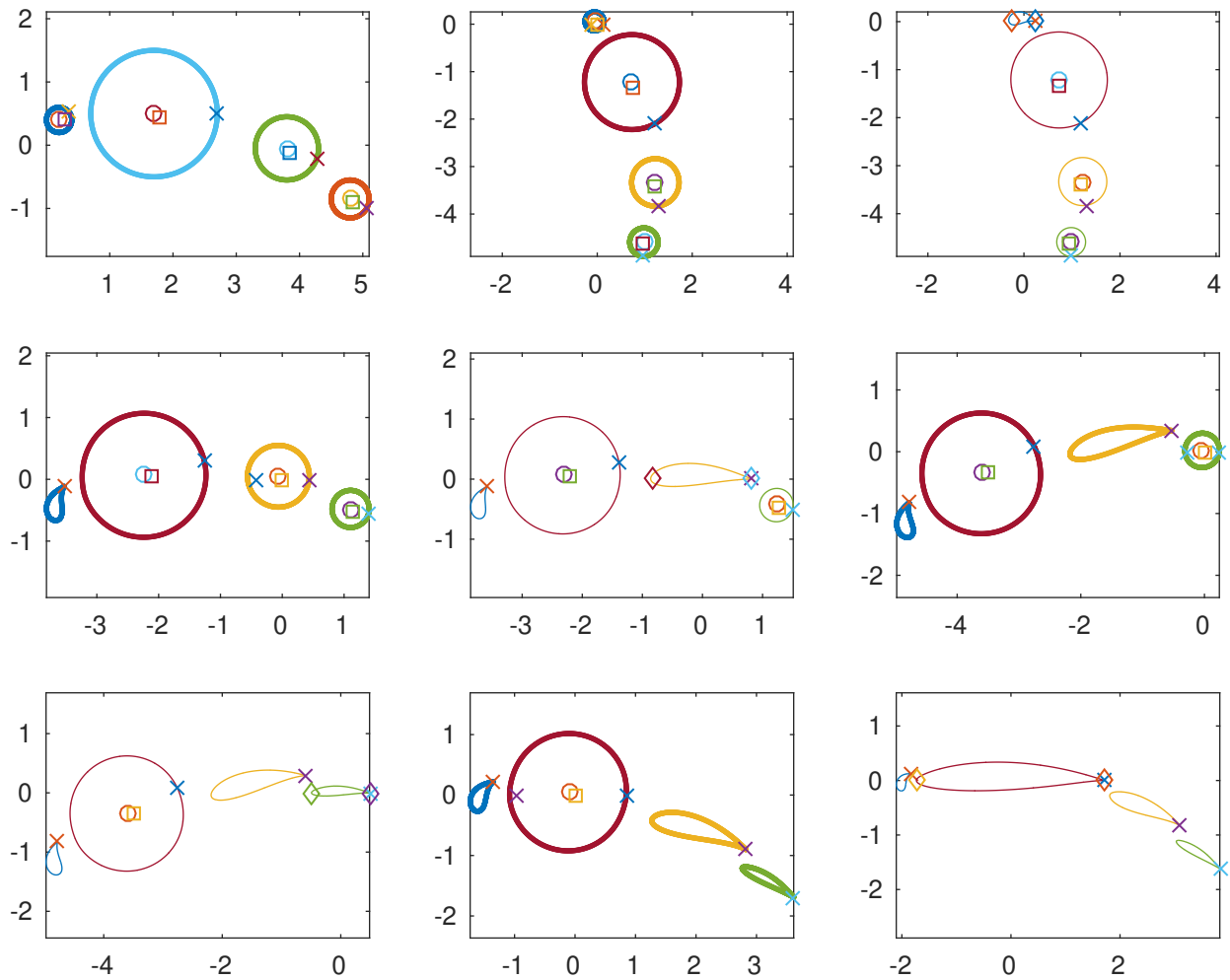


Figure 4.22: Exact map given by successive Karman-Trefftz transformations applied to four circles to produce the four-airfoil setup.

The flow for this case, shown in Figure 4.23, was computed using the combined system 3.40 and Fornberg map with $N = 128$ Fourier points and an angle of attack $\alpha = 0$.

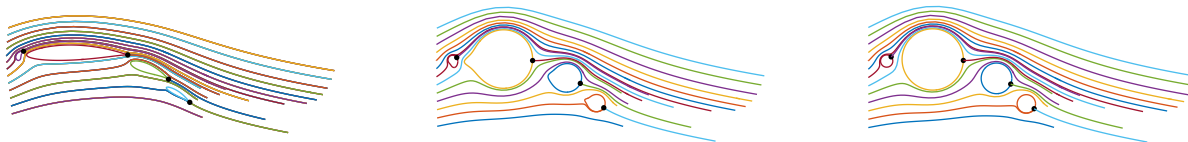


Figure 4.23: Flow for configuration A from [SH85] using the full series with $N = 128$ and angle of attack $\alpha = 0$ and $k_{steps} = 40$ cg iterations. Operation counts for the flow and the map are $O((mN)^2 \times k_{steps})$.

Table 4.8 contains some timings, circulation calculations, and accuracy estimates for various values of N .

Table 4.8: Sample timings (sec), circulations, Γ_i , and accuracy of the MATLAB code on a laptop for a set of airfoils from [SH85] for $m = 4$ configuration A with angle of attack $\alpha = 0^\circ$.

N	map	flow	Γ_1	Γ_2	Γ_3	Γ_4	ϵ
64	0.37	0.38	0.522048	2.07908	0.72162	4.71769	$1.3 \cdot 10^{-07}$
128	1.39	0.87	0.521940	2.07956	0.72166	4.71673	$4.8 \cdot 10^{-13}$
256	7.16	1.91	0.521939	2.07957	0.72167	4.71672	$7.5 \cdot 10^{-15}$

Similarly to the previous example, comparing the circulation values for $N = 128$ to those from from [SH85, Table 5], which are given by,

$$\Gamma_1 = 0.5215 \quad \Gamma_2 = 2.0794 \quad \Gamma_3 = 0.7216 \quad \Gamma_4 = 4.7157$$

we get about the accuracy we would expect. Finally, we have plotted the pressure curves in Figure 4.24 which look similar to those given in [SH85, Figure 9].

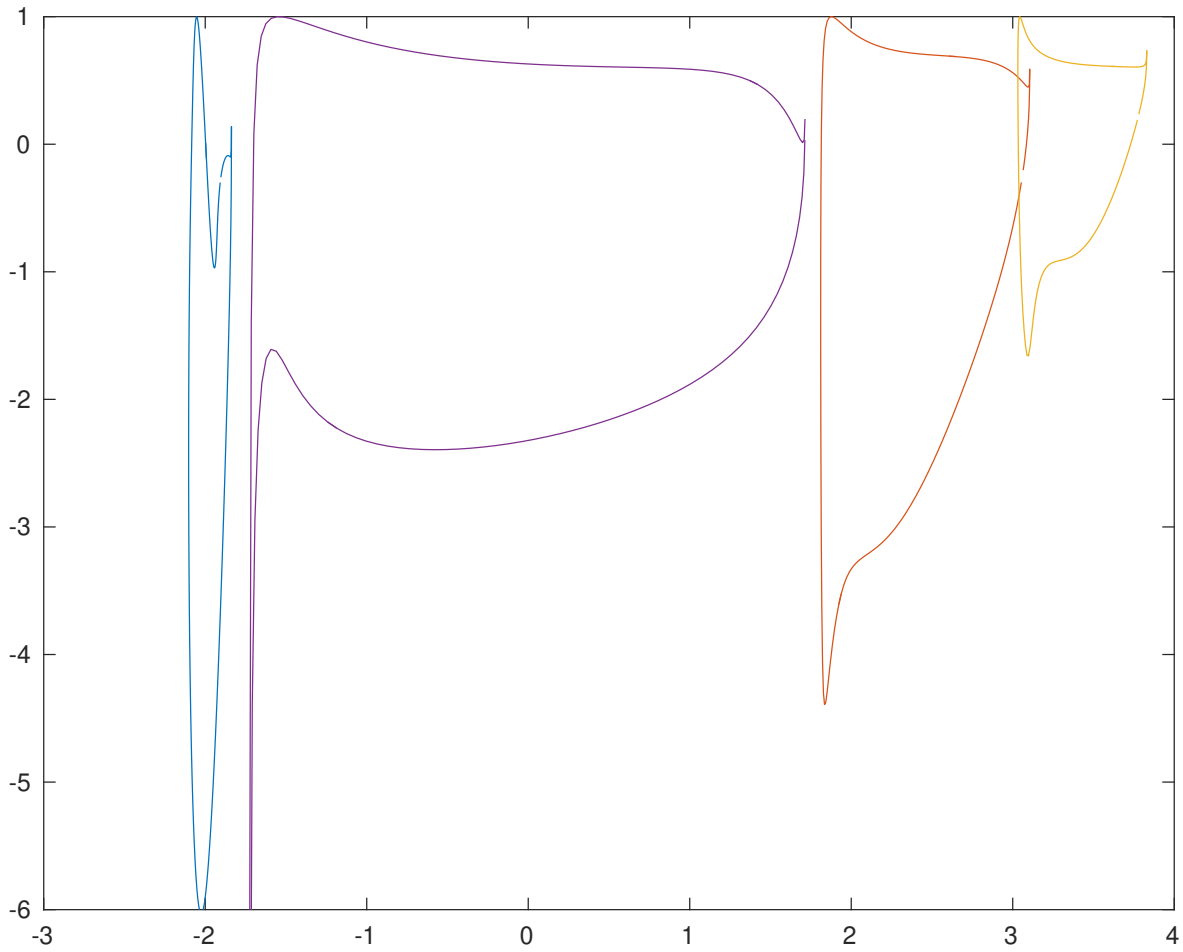


Figure 4.24: Pressure curves for the airfoils in configuration A from [SH85] computed using our methods demonstrated in Figure 4.23.

CHAPTER 5

CONCLUSION AND FUTURE WORK

We have presented an efficient method for computing potential flow in the plane using a Laurent series expansion. We showed that this system has the special “Identity plus a low-rank operator” structure allowing us to efficiently solve for the Laurent series coefficients using conjugate-gradient like methods. We also established the conditions necessary to guarantee that the our discretized series converges to the exact solution. Additionally, we compared our method with alternative processes for computing potential flow, showing that our method is at least as accurate and more efficient. Finally, we provided many examples involving regions with both smooth non-smooth boundaries.

In the future, we could replace the Fornberg-like method with Wegmann’s similar Newton-like method. Alternatively, Wegmann’s [Weg05] version of Prosnak’s projection method from [Pros87] can be used to map directly to the airfoil domain, not necessitating a corner-removing method. Although this projection method does not require smooth boundaries, it is only lineary convergent, making it less operationally efficient. Additionally, the Schottky-Klein prime function based formulation, presented by Crowdy in [Crow18] can be used to compute the potential flow in the circle domain instead of our series method. Finally, as was proposed by Trefethen in [Tref18], it should be possible to solve the flow problems directly in the physical domain efficiently using series methods, therefore avoiding the computation of the conformal maps. We plan to make comparisons of these alternatives, along with more traditional methods based on integral equations, in future work.

REFERENCES

LIST OF REFERENCES

- [Child09] S. CHILDRESS, *An Introduction to Theoretical Fluid Mechanics*, Courant Lecture Notes 19, AMS, 2009.
- [Crow18] D. CROWDY, *Solving Problems in Multiply Connected Domains*, NSF CBMS Conference, June 2018, UC Irvine.
- [Tref18] L. N. TREFETHEN, *Series solution of Laplace problems*, ANZIAM J. (2018).
- [BD16] R. BALU AND T. K. DELILLO, *Numerical methods for Riemann-Hilbert problems in multiply connected circle domains*, Journal of Computational and Applied Mathematics, 307 (2016), pp. 248–261.
- [DS18] T. K. DELILLO AND S. SAHRAEI, *Computation of plane potential flow past multi-element airfoils using conformal mapping, revisited*, Journal of Computational and Applied Mathematics, <https://doi.org/10.1016/j.cam.2018.08.031>.
- [Pros87] W. J. PROSNAK, *Computation of Fluid Motions in Multiply Connected Domains*, G. Braun, 1987.
- [Ach05] D. J. ACHESON, *Elementary Fluid Dynamics*, Oxford, 2005.
- [AF97] M. J. ABLOWITZ AND A. S. FOKAS, *Complex Variables - Introduction and Applications*, Cambridge, 1997.
- [Wil73] B. R. WILLIAMS, *An exact test case for the plane potential flow about two adjacent lifting airfoils*, RAE Technical Report No. 3717, London (1973).
- [ZMH18] A. ZEMLYANOVA, I. MANLY, AND D. HANDLEY, *Vortex generated fluid flows in multiply connected domains*, *Complex Variables and Elliptic Eqs.*, 63 (2018) 151–170.
- [AS07] Y. A. ANTIPOV AND A. V. SILVESTROV, *Method of automorphic functions in the study of flow around a stack of porous cylinders*, *Quart. J. Mech. Appl. Math.*, 60 (2007) 337–366.
- [DMS21] T.K. DELILLO, J. MEARS, AND A. SILVA-TRUJILLO, *Potential flow in a multiply connected circle domain using series methods*, *Journal of Computational and Applied Mathematics*, 391 (2021), 113445.
- [Hal79] N. D. HALSEY, *Potential flow analysis of multielement airfoils using conformal mapping*, *AIAA J.*, 17 (1979) 1281–1288.
- [SH85] A. SUDDHOO AND I. M. HALL, *Test cases for the plane potential flow past a multi-element airfoil*, *Aeronaut. J.*, 89 (1985) 403–414.

LIST OF REFERENCES

- [Burn91] W. BURNSIDE, *On functions determined from their discontinuities and a certain form of boundary condition*, Proc. London Math. Soc., 22 (1891) 346–358.
- [Tref05] L. N. TREFETHEN, *2005 Ten Digit Algorithms*, Report No. 05/13. Oxford, UK: Oxford University Computing Laboratory, 2005.
- [DDEP08] T. K. DELILLO, T. A. DRISCOLL, A. R. ELCRAT, AND J. A. PFALTZGRAFF, *Radial and circular slit maps of unbounded multiply circle connected domains*, Proc. R. Soc. A, 464 (2008) 1719–1737.
- [Weg01] R. WEGMANN, *Constructive solution of a certain class of Riemann-Hilbert problems on multiply connected circular domains*, J. Comput. Appl. Math., 130 (2001) 139–161.
- [Weg05] R. WEGMANN, *Methods for Numerical Conformal Mapping*, in R. Kuehnau, ed., Handbook of Complex Analysis, Geometric Function Theory, vol. 2, Elsevier (2005) 351–477.
- [DMS23] T.K. DELILLO, J. MEARS, AND S. SAHRAEI, *Computation of potential flow in multiply connected domains using conformal mapping*, to appear in Electr. Trans. Numer. Anal. (2023)
- [Han98] P.-C. HANSEN, *Regularization Tools: A Matlab Package for Analysis and Solution of Discrete Ill-Posed Problems*, version 2.0 for Matlab 4.0 (1992, revised 1998); see Numer. Algor. 6 (1994) 1–35; software available via netlib@research.att.com from directory NUMERALGO.
- [Ahl79] L. V. AHLFORS, *Complex Analysis: An Introduction to the Theory of Analytic Functions of One Complex Variable*, McGraw-Hill, New York, 1979. pp. 229–230
- [Hen86] P. HENRICI, *Applied and Computational Complex Analysis, vol. III*, Wiley, New York, 1986.
- [BDHW07] N. BENCHAMA, T. DELILLO, T. HRYCAK, AND L. WANG, *A simplified Fornberg-like method for the conformal mapping of multiply connected regions—comparisons and crowding*, J. Comput. Appl. Math., 209 (2007), pp. 1–21.
- [For80] B. FORNBERG, *A numerical method for conformal mappings*, SIAM J. Sci. Stat. Comput., 1 (1980), pp. 386–400.
- [BDS19] M. BADREDDINE, T. K. DELILLO AND S. SAHRAEI, *A comparison of some numerical conformal mapping methods for simply and multiply connected domains*, Discrete and Continuous Dynamical Systems - B, 24 (2019), pp. 55–82.

LIST OF REFERENCES

- [DP98] T. K. DELILLO AND J. A. PFALTZGRAFF, *Numerical conformal mapping methods for simply and doubly connected regions*, SIAM J. Sci. Comput., 19 (1998), pp. 155–171.
- [HK72] W. D. HOSKINS AND P. R. KING, *Periodic cubic spline interpolation using parametric splines*, The Computer Journal, 15 (1972), pp. 282–283.